NONLINEAR ESTIMATION AND CONTROL WITH APPLICATION TO UPSTREAM PROCESSES

Reza Asgharzadeh Shishavan

A dissertation submitted to the faculty of
Brigham Young University
in partial fulfillment of the requirements for the degree of

Doctor of Philosophy

John D. Hedengren, Chair
Randy Beard
David Lignell
Michael Nikolaou
William Hecker
Brad Bundy

Department of Chemical Engineering

Brigham Young University

March 2015

ABSTRACT

NONLINEAR ESTIMATION AND CONTROL WITH
APPLICATION TO UPSTREAM PROCESSES

Reza Asgharzadeh Shishavan
Department of Chemical Engineering, BYU
Doctor of Philosophy

Subsea development and production of hydrocarbons is challenging due to remote and harsh conditions. Recent technology development with high speed communication to subsea and downhole equipment has created a new opportunity to both monitor and control abnormal or undesirable events with a proactive and preventative approach rather than a reactive approach. Two specific technology developments are high speed, long-distance fiber optic sensing for production and completion systems and wired pipe for drilling communications. Both of these communication systems offer unprecedented high speed and accurate sensing of equipment and processes that are susceptible to uncontrolled well situations, leaks, issues with flow assurance, structural integrity, and platform stability, as well as other critical monitoring and control issues. The scope of this dissertation is to design monitoring and control systems with new theoretical developments and practical applications. For estimators, a novel ℓ_1-norm method is proposed that is less sensitive to data with outliers, noise, and drift in recovering the true value of unmeasured parameters. For controllers, a similar ℓ_1-norm strategy is used to design optimal control strategies that utilize a comprehensive design with multivariate control and nonlinear dynamic optimization. A framework for solving large scale dynamic optimization problems with differential and algebraic equations is detailed for estimation and control. A first area of application is in fiber optic sensing and automation for subsea equipment. A post-installable fiber optic clamp is used to transmit structural information for a tension leg platform. A proposed controller automatically performs ballast operations that both stabilize the floating structure and minimize fatigue damage to the tendons that hold the structure in place. A second area of application is with managed pressure drilling with moving horizon estimation and nonlinear model predictive control. The purpose of this application is to maximize rate of drilling penetration, maintain pressure in the borehole, respond to unexpected gas influx, detect cuttings loading and pack-off, and better manage abnormal events with the drilling process through automation. The benefit of high speed data accessibility is quantified as well as the potential benefit from a combined control strategy versus separate controllers.

Keywords: high speed data, managed pressure drilling, nonlinear model predictive control, online estimation and control, subsea flow assurance, subsea structural monitoring

ACKNOWLEDGMENTS

I would like to express appreciation to the management at National Oilwell Varco, Astro Technology, Inc. and Hess Corporation for supporting this work. I would aso like to express my appreciation to Dr. Hedengren. This work would not have been possible without his guidance and help. I also appreciate the involvement of my Ph.D. committee for invaluable advice and direction. Hector Perez, Kristie Moffat, Logan Beal, Casey Hubbell, Spencer Christiansen, Landen Blackburn, Minee Ryum, David Pixton have contributed in significant ways to this work and I appreciate the long hours and dedication to the research.

TABLE OF CONTENTS

LIST OF TABLES

LIST OF FIGURES

NOMENCLATURE

$A_a(x)$	Annulus cross sectional area
$A_d(x)$	Drill string cross sectional area
$a_1 - a_8$	Constants that must be chosen based on local drilling conditions
BHA	Bottom Hole Assembly
$cos(\alpha)$	Cosine of the platform angle with vertical direction
$cos(\beta)$	Cosine of the platform angle with horizontal direction
CV	Controlled Variable
D	True vertical depth of drilling
d_b	Bit diameter
D_o	Outer pipe diameter
D_i	Inner pipe diameter
F_d	Friction factor in the drill string
F_{a_i}	Friction factor between the locations of i and (i-1) pressure sensors
FBG	Fiber Bragg Grating
F_j	Hydraulic impact force beneath the bit
g_p	Pore pressure gradient
g	Gravity constant
h	Fractional tooth dullness
h_{bit}	Vertical depth of the bit
K	Stiffness factor of tendons
K_c	Valve flow constant
L_{Total}	Total load on each leg
L_{Wave}	Load on each leg caused by tide action
L_{Wave}	Load on each leg caused by wave action
L_P	Load on each leg caused by platform weight
L_{Tank}	Load on each leg caused by ballast tank water weight
L_{T12}	Lengths of Tendon 12
L_{T21}	Lengths of Tendon 21
L_{T32}	Lengths of Tendon 32
L_{T41}	Lengths of Tendon 41
M	Lumped density per length parameter for drill string and annulus
M_a	Lumped density per length parameter for the annulus
M_d	Lumped density per length parameter for the drill string
MHE	Moving Horizon Estimation
MPC	Model Predictive Control
MPD	Managed Pressure Drilling
MV	Manipulated Variable
N	Drill string rotation speed
NLP	Nonlinear Programming
N_{Re_a}	Reynolds number in axial direction
N_{Re_r}	Reynolds number caused by rotation
n	Number of annulus pressure sensors
P_0	Atmospheric pressure

P_{bit}	Pressure at the drill bit
P_{ai}	Pressures along the annulus
P_p	Mud pump pressure
P_c	Choke valve pressure
$PRBS$	Pseudo-random binary signals
QP	Quadratic Programming
q_{pump}	Mud pump flow rate
q_{bit}	Flow rate through the drill bit
q_{back}	Flow rate of back pump
q_{res}	Reservoir influx flow rate
q_{choke}	Flow rate through the choke valve
ROP	Rate of Penetration
dF/dt	Rate of Penetration
RPM	Revolutions Per Minute
TLP	Tension Leg Platform
V_a	Volumes of the annulus
V_d	Volumes of the drill string
$V_{Platform}$	total volume of the platform
W	Bit weight
WDP	Wired Drill Pipes
WOB	Weight on Bit
x_B	Fraction of the platform that is under water
z_{choke}	Choke valve opening
$Beta_a$	Bulk modulus in the annulus
$Beta_d$	Bulk modulus in the drill string
ρ_d	Fluid density in the drill string
ρ_a	Fluid density in the annulus
ρ_c	Equivalent circulating density

CHAPTER 1. INTRODUCTION

Safe and environmentally responsible practices and equipment have been developed over many years to extract reserves and bring those reserves to market. Subsea development and production of hydrocarbon reserves is often challenging because of remote and harsh environmental conditions. As the demand for hydrocarbons continues to expand, additional opportunities for expansion of production are increasing in deep offshore waters, Arctic regions, or in land-based shale plays that require horizontal drilling and hydraulic fracture for economical production. These challenges are met with several new opportunities that have been created by a simultaneous development of high speed communication networks and an increase in computing power. The high speed communication networks discussed in this dissertation provide data along production flowlines or deep underground along a drillstring.

The data delivery rate and resolution of sensors are continuing to improve at an unprecedented pace. However, with this increase in data quality there is a need to turn this raw information into actionable content either by an operator or automated computer control system. Without this digital digestion process, the increased data may overwhelm or distract from key early warning signs and signals that may otherwise be noticed without the data overload.

The focus of this dissertation is the coupling of high speed communication networks with control system design for two key areas of upstream development and production. The first area is in Tension Leg Platform (TLP) stabilization with automated ballast operations for structural integrity management. This work includes development of a novel post-installed and non-penetrating fiber optic monitoring system coupled with a control system. The second high speed communication network is wired drillpipe consisting of an embedded co-axial cable in drillpipe that is retrofitted with this communication network. The specific application to Managed Pressure Drilling (MPD) is explored to quantify the potential benefit from a multi-variate and nonlinear model predictive controller.

The overall objective of this work is to apply the latest developments from estimation and control systems theory to the upstream industry in order to reduce risk and improve economics for exploration and production. Two specific applications are presented in this work but the foundational framework is applicable to a much wider range of potential applications. The monitoring and control systems are envisioned to create a network of sensors and automated decision agents that communicate to detect and respond to early warning signs of fatigue, flow assurance issues, or drilling disruptions. This system can be considered as analogous to the central nervous system for the body that can sense and respond to prevent damage and optimize a particular outcome. This intelligent sensing system is often classified as an Intelli-field network for subsea and subsurface assets.

1.1 Nonlinear Modeling, Estimation and Predictive Control

As mentioned in the previous section, the objective of this dissertation is designing advanced controllers and estimators and applying them to the subsea structures where there is available high speed communication. The new techniques in control and estimation includes model predictive control and moving horizon estimation which have better performance compared with the conventional controllers and estimators when applied to nonlinear processes. Further improvement is shown with noise, drift and outliers in the sensor data. These nonlinear techniques are inspired by researchers and motivated by industrial applications. Using the ℓ_1-norm objective with a dead-band for estimation and control improves the performance of these techniques. The dead-band in the objective is desirable for noise rejection, minimizing unnecessary parameter adjustments and movement of manipulated variables. The novel forms of the objective function are applied to estimation and control with industrial application to floating platform structures and drilling automation. A small and well-known nonlinear multivariable level control problem is detailed in chapter 2 that has a number of common characteristics to larger controllers seen in practice. The methods are also demonstrated on larger problems to reveal algorithmic scaling with sparse methods.Benchmark problems determine the algorithmic performance of the new techniques and give insight into the model predictive controller and with the ℓ_1-norm moving horizon estimator. The advanced estimation and control applications have never been applied previously and achieve

improved results for a variety of case scenarios and applications. Chapter 2 details all of these methods and is the algorithmic foundation for following applications in the dissertation.

1.2 Advanced Deepwater Monitoring

One of the novel applications of this advanced monitoring and control system is in balancing offshore platforms such as Tension Leg Platforms (TLPs). An overview of fiber optic sensors for temperature, pressure, strain, and fatigue of subsea structures is provided in this work. This overview is used to investigate new methods to improve deepwater monitoring by developing a monitoring and control system using advanced fiber optic sensors on already deployed risers, flowlines, trees, and other deepwater devices. Fiber optic technology in subsea monitoring began over 20 years ago. The first installations were included on newly installed subsea pipelines, production risers, and drilling risers to measure strain and vibration for fatigue life monitoring. Of particular interest for these systems were detecting riser vortex induced vibration and strain throughout the touchdown zone (the location where riser touches the ocean floor). A prior limitation was that sensors were only installed top-side on new subsea equipment. Recently a new technology has been developed to deploy fiber optic sensors on existing subsea equipment. However, there are some problems associated with post installed monitoring systems including poor coupling between the sensor and structure, temperature effects on the sensor results, and the need for calibration.

A monitoring device using fiber optic technology resulting from this work can be installed in-situ on underwater structures to enhance productivity and improve safety of offshore operations. Developments from this work include sensor calibration and temperature compensation to overcome the weaknesses inherent to these sensors in a subsea environment. The calibration and testing mentioned in this dissertation are part of the Clear Gulf study, a collaboration formed in 2010 between the offshore energy industry and NASA.

This work provides valuable data for assessing the feasibility of developing the next generation fiber optic sensor system that could be retrofitted onto existing subsea pipeline structures. The purpose of reliable post-installed advanced sensors is not only to detect failures of subsea infrastructure but also to warn of signs of fatigue or hydrate formation that contribute to catastrophic failures. The study continues to make advances in highly sensitive monitoring systems that antici-

pate failures, catastrophic events, and flow assurance issues. The novel contributions of this work are:

- Monitoring system and calibration on the post installed sensor stations and TLPs is developed for the first time. This leads to a system that is very sensitive to subtle load changes and enables fast detection of abnormal events. The high speed fiber optic system enables ballast operations.

- A control system for automatic balancing of the TLPs is developed for the first time. This leads to fast reaction to changes and decreases fatigue of the TLP tendons. Additionally, automatic balancing leads to reduced drilling time because adjustments are faster and automated to coordinate with the drilling activities instead of ballast operations that are performed manually and the industrial implementation is future work.

The monitoring system has actually been implemented on two TLP platforms in west Africa and is currently operating, verifying the success of the approach. However the control system has been designed and implemented in a simulated environment using a lower order model of the TLP platform.

1.3 Managed Pressure Drilling Automation

Drilling in the upstream oil and gas industry includes exploration of reserves, creation of injection wells that increase reservoir pressure, and formation of relief wells when the pressure cannot be controlled. Currently, drilling in the upstream industry is mostly done manually by trained technicians with experience in maintaining key operational parameters. Catastrophic events in the past have moved the attention of academic and industrial researchers into automating the control of this process, especially through managed pressure drilling [1, 2]. Managed pressure drilling is a relatively new type of drilling method where the pressure of the drilling mud is kept at the reservoir pressure. Automation is needed to avoid low mud pressure that can induce kicks or unexpected gas influx. Pressure that exceeds a certain limit can fracture or otherwise damage the reservoir. As a second novel application of nonlinear model predictive control and estimation, they are applied to a managed pressure drilling process.

1.3.1 Significance of Drilling Automation

While process automation and control has found many applications in the downstream industry, it is still immature in the upstream processes. One of the principle reasons that automation has not been progressed in the drilling industry is a lack of a high speed data communication network. Mud pulse telemetry has been the dominant technology available to send the data from sensors to topside equipment. However, mud pulse telemetry has limited bandwidth that is not capable, in many circumstances, to be used for high-speed automated control systems.

Recently, a new high speed technology system has been developed and introduced that sends data to the surface with a high bandwidth (57,600 bits/sec). In this technology, electrical wires and conductors are used to transfer signals through drill pipe and across each threaded pipe to the next segment. The increased data speeds make automation systems more practical and effective. The controller designed in this work is based on the wired pipe technology [3].

The two main goals in most drilling operations are safety and economics. In relation to safety, kick attenuation is vital to minimize operational risks. Kicks are the unexpected intrusion of formation gas into the void area between the drill pipe and well bore (annulus) due to a higher formation pressure. Kick attenuation can be achieved through annulus pressure regulation [2]. In relation to economics, a higher Rate of Penetration (ROP, which is the speed at which a drill bit breaks the rock and penetrates the formation) will lower the drilling cost. Therefore, ROP maximization is a motivating factor [4]. Automating the drilling process can improve kick attenuation and result in more consistent ROP.

There is economic incentive to increase the rate of penetration and have more precise directional drilling. Economic costs include raw materials such as mud, additives, hydraulic fracturing proppants, and other resources. Personnel and equipment costs add to the financial incentives to complete wells quickly within safe operating constraints. Maximizing the rate of penetration (ROP) is an aspect of drilling which significantly improves the completion time and reduces the drilling cost.

1.3.2 Description of Managed Pressure Drilling Process

In the drilling process a rotating drill string is placed into the well. The annulus is the void volume around the drill string that is the result of the drill bit creating a bore that is larger than the drill string pipe radius. During drilling, mud is pumped into the drill string, through the drill bit (located on the bottom of drillstring), and upwards through the annulus and choke valve into the mud pit. The purpose of drilling mud is to cool the bit, maintain hydrostatic pressure to balance reservoir pressure, suspend cuttings in case the mud stops flowing, and transport the cuttings resulting from drilling up to the surface. Figure 1.1 shows a simplified schematic of a drilling process with the basic elements found in many drilling operations.

Controlling the well pressure within a window is crucial during drilling operation to avoid formation damage, mud loss, and prevent blowouts. If the well pressure lies below the reservoir pore pressure, reservoir fluid enters the annulus. As reservoir gas displaces the mud, the hydrostatic force of the mud is further decreased, leading to increased flow from the formation. If left uncontrolled this positive feedback of mud displacement leading to more gas release leads to unexpected gas influx (referred to as a kick), and finally blowout. On the other hand, if the well pressure rises higher than the reservoir pressure, the mud migrates into the reservoir formation and damages the reservoir. In practice, there is not a single acceptable pressure for the well; the acceptable range varies along the entire drill string with different rock formations and depths. At times, the acceptable pressures along the drill sting create an infeasible situation where there is not a single pressure that can satisfy all constraints. In this case, the annulus pressure is purposefully higher than some upper limits leading to unintended formation damage and excessive mud loss.

1.3.3 Novel Contributions

Currently pressure control is mostly done manually in the upstream industry mainly due to the lack of a high bandwidth borehole pressure sensing system. The lack of a high speed communication system has makes it very challenging to send the measured borehole pressure values (thousands of feet under ground) to the surface. There have been attempts among upstream control studies in designing the automation system to indirectly control the borehole pressure through estimating its value using surface measurements (mud pump flow rate and choke valve opening). The

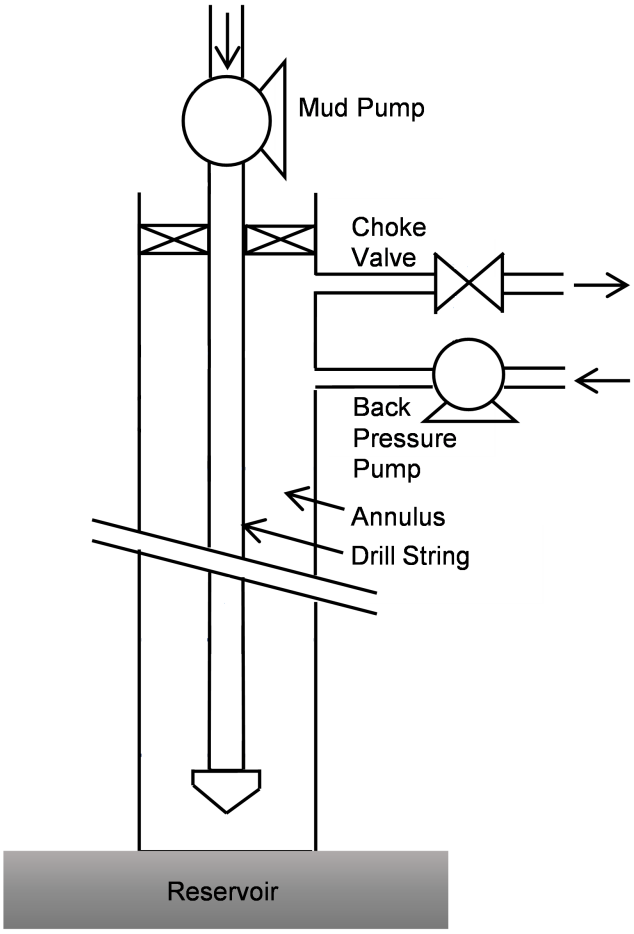

Figure 1.1: Schematic of managed pressure drilling process.

recent invention of new wired pipe technology has made it possible to directly measure and control the borehole pressure. Therefore a control system is designed based on this technology to control the borehole pressure. The control system is required to do fast control calculations (fractions of a second) to be able to fully utilize the benefit of wired pipe telemetry data.

There are several parameters that affect the borehole pressure. Among them only mud pump flow rate and choke valve opening have been used as manipulated variables in literature, but borehole pressure also depends on the friction factor, which is a function of drill string rotation speed.

On the other hand, rate of penetration (another important factor in drilling which determines drilling cost), is a function of drill string rotation speed (N), weight on the bit (WOB),

borehole pressure, and environmental variables. Real time optimization studies on ROP have only considered N and WOB as the manipulated variables and dismissed the effect of borehole pressure.

Previous research includes a separate optimizer for ROP and pressure control. A single comprehensive control system that can simultaneously control both the borehole pressure and ROP together is designed to improve both control responses. In order to do this, the interaction between the drill string and drilling hydraulics is considered. It was found that rotation speed of drill string affects friction factor. Friction factor changes the pressure drop along the annulus and therefore affects the pressure. The effect of drill string rotation speed of the drill string on the hydraulics is included in a controller for the first time. This innovative control system improves the controller performance. Another improvement is using the manipulated variables that were formerly decoupled in a coordinated fashion that both maintains pressure and maximizes ROP. This comprehensive controller leads to tighter control precision and fewer undesirable events such as kick. Another improvement is also during transient responses where ROP maximization is temporarily disregarded in favor of rejecting a pressure disturbance.

An advanced model predictive control system is used to design the comprehensive controller. Standard methods such as a linear quadratic regulator (LQR) have fast but limited performance in the drilling process because they do not consider constraints on process output variables as model predictive control. Another unexplored problem is how to design a control system that optimizes not only pressure at the Bottom Hole Assembly (BHA), but also along the drill string. This distributed pressure control problem must consider geological and formation information, rheological properties of the mud and tailings, drill string dynamics, and drill bit heat transfer and penetration rate.

Another proposed innovation of this research is an optimization based observer. In process control, an observer is used along with a controller when there are some parameters required by the controller that cannot be measured. The observer therefore attempts to estimate the unknown variable values using the known and measured parameters. One advantage of an optimization based observer over other observer types is that it does not need to be customized for specific applications. It is a general purpose technique that seeks to optimize the information content in the measurements to reconstruct true values of unmeasured parameters or variables.

A lower order model was used which includes the effect of hydraulics, rotation speed, friction factor and weight on bit and is a combination of first principles and empirical equations. The individual models are mostly from the work of other researchers. The goal of this project is to design the controllers based on consolidated model, not necessarily to improve the modeling accuracy.

In summary, the results of this project are development of a theoretical and practical foundation for a comprehensive controller which controls the ROP and borehole pressure simultaneously. To achieve this, a controller and observer is designed with new capabilities of wired pipe technology. The observer (estimator) utilizes a distributed dynamic model of the drill string, BHA, mud pump, choke valve, and other measured or manipulated variables. An analysis of measurement location also reveals the types and number of drill string measurements that meet acceptable control requirements.

1.4 Outline

This section gives a brief outline about the contents of the following chapters. Chapter 2 describes applications of nonlinear methods in model building, dynamic data reconciliation, and dynamic optimization that are inspired by researchers and motivated by industrial applications. A novel contribution of this work is an $\ell 1$-norm objective for estimation and control that includes a dead-band. The dead-band improves noise rejection, minimizing unnecessary parameter adjustments and movement of manipulated variables. As a motivating example, a small and well-known nonlinear multivariable level control problem is detailed that has a number of common characteristics to larger controllers seen in practice. The methods are also demonstrated on larger problems to reveal algorithmic scaling with sparse methods. The implementation details reveal capabilities of employing nonlinear methods in dynamic applications.

Chapter 3 details the development of a high speed fiber optic network to monitor and control subsea tensions on structures that stabilize an offshore oil and gas production platform. The data acquisition is accomplished with post-installed clamps that retrofit existing systems with a non-penetrating measurement device.

Chapter 4 combines ROP and borehole pressure into a single comprehensive controller for a managed pressure drilling (MPD) application. The controller adjusts mud pump flow rate, choke

valve position, drill string rotation rate, and weight-on-bit (WOB) simultaneously and with coordinated actions. The automated operations are guided by an objective function that includes factors relevant to both borehole pressure stabilization and ROP maximization. A preliminary MPD case study is used to assess the performance during different drilling events, including transition into varying formations causing an unexpected gas influx. For the unwanted gas influx case, the controller better stabilizes the pressure when there are low latency communications by simultaneously adjusting ROP. With wired drill pipe and the optimizing controller, there is substantial decrease in the time required to control influx events as compared to earlier controllers or manual methods. The high speed data availability affects both the pressure control reaction time and the resulting severity of the kick. When encountering different formations, there is also noticeable benefit of allowing pressure to fluctuate within an acceptable range to optimize ROP.

Chapter 5 investigates the controller performance in the case of multiple pressure sensors along the annulus and it includes a quantification of potential benefit during both kick attenuation and cuttings build. The further resolution provided by multiple sensor locations within a drillstring increases the speed of detection of a downhole influx event, providing a net improvement in the effectiveness of control over the kick and reducing the size of the influx. Further, data collected by distributed sensors is able to detect and accommodate kicks all along the drill string, not just at critical locations. Having such detailed relationships factored into the modeling process generates more consistent results that can quickly achieve target pressures and rates of penetration.

CHAPTER 2. NONLINEAR MODELING, ESTIMATION AND PREDICTIVE CONTROL FRAMEWORK

Much of the content of this chapter is taken from reference [5]:

- Hedengren, J. D., Asgharzadeh Shishavan, R., Powell, K., and Edgar, T., 2014. Nonlinear modeling, estimation and predictive control in APMonitor. Computers and Chemical Engineering, 70(5), November, pp. 133148.

2.1 Introduction

Applications of Model Predictive Control (MPC) are ubiquitous in a number of industries such as refining and petrochemicals [6]. Applications are also somewhat common in chemicals, food manufacture, mining, and other manufacturing industries [1]. Contributions by Morari and others have extended the MPC applications to building climate control [7, 8], stochastic systems [9, 10], induction motors [11], and other fast processes with explicit MPC [12–17]. However MPC applications are very new in the upstream industry and there is a large opportunity for improvement. A majority of the before mentioned applications employ linear models that are constructed from empirical model identification, however, some of these processes have either semi-batch characteristics or nonlinear behavior. To ensure that the linear models are applicable over a wider range of operating conditions and disturbances, the linear models are retrofitted with elements that approximate nonlinear control characteristics. Some of the nonlinear process is captured by including gain scheduling (using different controller gains in different operating regions), switching between multiple models depending on operating conditions, and other logical programming when certain events or conditions are present. The art of using linear models to perform nonlinear control has been refined by a number of control experts to extend linear MPC to a wider range of applications. While this approach is beneficial in deploying applications, main-

tenance costs are increased and sustainability is decreased due to the complexity of the heuristic rules and configuration.

A purpose of this chapter is to give implementation details on using nonlinear models in the typical steps of dynamic optimization including (1) model construction, (2) fitting parameters to data, (3) optimizing over a future predictive horizon, and (4) transforming differential equations into sets of algebraic equations. The predictive horizon is a specified sequence of time steps in future over which control calculations are performed. These techniques are used in the controller and estimator designs in the rest of the dissertation. Recent advancements in numerical techniques have permitted the direct application of nonlinear models in control applications [18]; however, many nonlinear MPC applications require advanced training to build and sustain an application. Perhaps the one remaining obstacle to further utilization of nonlinear technology is the ease of deploying and sustaining applications by researchers and practitioners. Up to this point, there remain relatively few actual applications of control based on nonlinear models in the oil and energy industry. An objective of this chapter is to reduce the barriers to implementation of nonlinear advanced control applications which helps in implementing these advanced controllers in different applications including drilling which is considered a nonlinear process. This is attempted by giving implementation details on the following topics:

- nonlinear model development.
- parameter estimation from dynamic data.
- model predictive control with large-scale models.
- direct transcription for solution of dynamic models.

In addition to the theoretical underpinnings of the techniques, a practical application with process data is used to demonstrate model identification and control. The application used in this chapter is a simple level control system that was selected to demonstrate the concepts without burdening the reader with model complexity. An illustration of scale-up to larger problems gives an indication of the size that can be solved with current computational resources. The example problems are demonstrated with the APMonitor Optimization Suite [19, 20], freely available software for solution of linear programming (LP), quadratic programming (QP), nonlinear programming

(NLP), and mixed-integer (MILP and MINLP) problems. Several other software platforms can also solve dynamic optimization problems with a variety of modeling systems, solution strategies, and solvers [21–26].

Of particular interest for this overview is the transformation of the differential and algebraic equation (DAE) systems into equivalent NLP or MINLP problems that can be solved by large-scale optimizers such as the active set solver APOPT [27] and the interior point solver IPOPT [28].

This chapter includes a number of innovative techniques for formulating large-scale control and optimization problems. A dead-band is added to well-known ℓ_1-norm objective forms for estimation and optimization. This form is different than the forms previously proposed [29, 30] in that it specifies a dead-band for noise rejection and move suppression. The formulation allows for batch or periodic control and avoids a separate steady-state target calculation. Similar characteristics to prior work [31] include tuning for speed of response, ranked utilization of manipulated variables (MVs), treatment of controlled variables (CVs) with equal concern, and prioritization among separate sets of MVs and CVs.

The objective form presented here for estimation and control is compared to squared-error or ℓ_2-norm objectives that are reported in the literature.

2.2 Chapter Overview

The following sections detail the different steps used in designing a model predictive controller and a moving horizon estimator. Steps include modeling, orthogonal collocation, control calculations and dynamic optimization using the determined objective function (ℓ_1 norm or squared error). Figure 2.1 shows a schematic representation of both MPC and MHE. A model consists of differential equations and represents the dynamics of the process. Next, orthogonal calculation is used to convert the differential equations into a set of linear equations. Finally, control or estimation calculations are performed and an objective function is determined and is given to an optimizer to find the desired variable values.

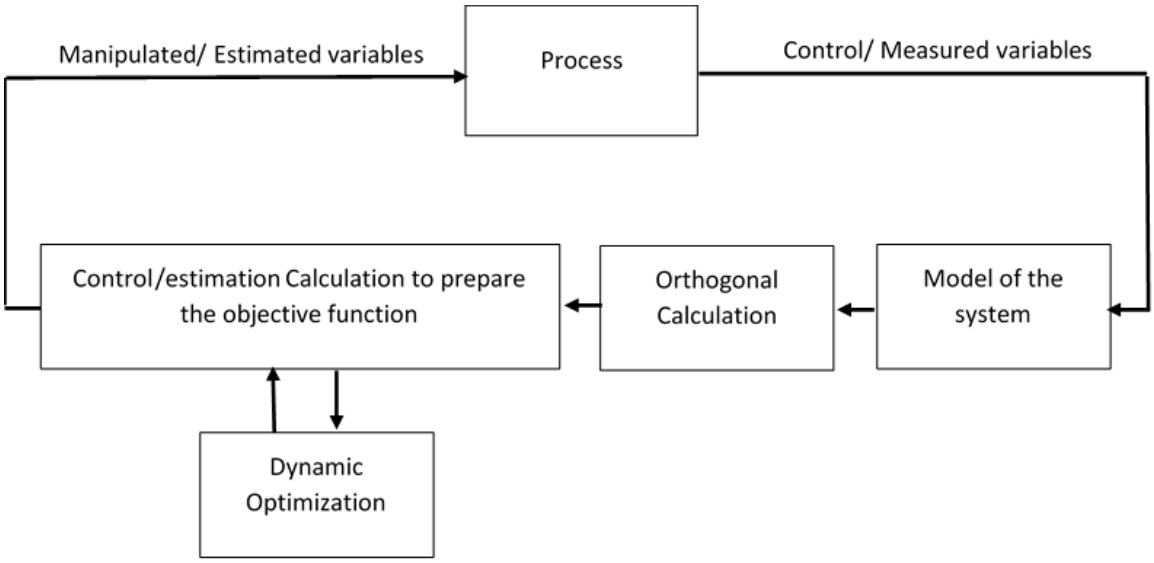

Figure 2.1: Overall overview of the steps used in model predictive controller and moving horizon estimator.

2.3 Nonlinear Modeling

A critical aspect of any controller is obtaining a sufficiently correct model form. The model form may include adjustable parameters that are not directly measurable but can be tuned to match both steady-state and dynamic data. Model identification involves adjustment of parameters to fit process data. Models may be linear or nonlinear, empirical or based on fundamental forms that results from material and energy balances, reaction kinetic mechanisms, or other pre-defined model structure. The foundation of many of these correlations is on equations of motion, individual reaction expressions, or balance equations around a control volume such as $accumulation = inlet - outlet + generation - consumption$. In the case of a mole balance, for example, this includes molar flows, reactions, and an accumulation term $\left(\frac{dn_i}{dt} = (n_i)_{in} - (n_i)_{out} - (n_i)_{rxn}\right)$. Model structure may also include constraints such as fixed gain ratios, constraints on compositions, or other bounds that reflect physical reality. Detailing the full range of potential model structures is outside the scope of this document. Equation 2.1 is a statement of a general model form that may include differential, algebraic, continuous, binary, and integer variables.

$$0 = f\left(\frac{dx}{dt}, x, y, p, d, u\right) \tag{2.1a}$$

$$0 = g(x, y, p, d, u) \tag{2.1b}$$

$$0 \leq h(x, y, p, d, u) \tag{2.1c}$$

The solution of Equation 2.1 is determined by the initial state x_0, a set of parameters p, a trajectory of disturbance values $d = (d_0, d_1, \ldots, d_{n-1})$, and a sequence of control moves $u = (u_0, u_1, \ldots, u_{n-1})$. Likewise, the variables values may be determined from the equations such as differential x or algebraic equations y. The equations include differential f, algebraic g, and inequality constraints h. The inequality constraints are included to model physical phenomena where complementarity conditions are required. It is important that the differential terms $\frac{dx}{dt}$ be expressed in implicit form as shown in 2.1a because some models cannot be rearranged into semi-explicit form such as $\frac{dx}{dt} = f(x, y, p, d, u)$. With the methods for solving DAEs demonstrated in Section 2.6, consistent initial conditions are not required and higher index DAEs are solvable without differentiating the high index algebraic expressions [32]. DAE index is the number of times required to differentiate the DAE to convert DAE into a set of ordinary differential equations An example of this capability for both inconsistent initial conditions and high index DAEs is given by a pendulum application [33]. The pendulum equations of motion are written as index-0 (ODE), index-1, index-2, and index-3 DAEs and solvable with this approach. The drawback of this approach is that the problem size is generally large, requiring the use of sparse methods and highly efficient solvers. Also, a suitable initial guess for the state trajectories is often required for solver convergence.

2.4 Nonlinear Dynamic Estimation

Nonlinear dynamic estimation (moving horizon estimation) is an optimization approach that uses a series of measurements observed over time (moving horizon) and produces estimates of unknown variables or parameters by minimizing the error between measurements and the associated modeled variables in the objective function.

Along with model form, the objective function is important to ensure desirable results. A common objective form is the least squares form: $(y_{model} - y_{measured})^2$ (see Equation 2.2). Although intuitive and simple to implement, the squared error form has a number of challenges such as sensitivity to bad data or outliers. An outlier is an observation point that is distant from other

observations. The sensitivity to outliers is exacerbated by the squared error objective, commonly proposed for dynamic data reconciliation [34–38].

Table 2.1 details the equations of the typical squared error norm and the ℓ_1-norm objective. The equations are used to calculate the objective function in designing the controllers throughout the dissertation. In optimization based on a squared error objective function, the summation of the squared difference between modeled y and measured y variables ($(y_x - y^T W_m (y_x - y)$), modeled variables and prior model values ($\hat{y}$) and also the change in estimated parameter values (Δp) is minimized. Each one of these terms has a penalty factor that can be tuned by adjusting the relative magnitude.

The ℓ_1-norm formulation in Equation 2.3 is less sensitive to data outliers and adjusts parameter values only when measurements are outside of a noise dead-band. In optimization using the ℓ_1-norm, the summation of slack variables associated with below and above the measurement dead band (e_U, e_L) , previous model values (c_U, c_L) and change in estimated parameters Δp are minimized. Dead band is an interval of a signal domain where no action occurs (the error term is zero). A small penalty on Δp (change in the parameter values) also discourages parameter movement without sufficient improvement in the model predictions. The change can be from an initial guess or the prior estimates from a Moving Horizon Estimation (MHE) approach. The ℓ_1-norm is similar to an absolute value function but is instead formulated with inequality constraints and slack variables. The reason that slack variables are used is that the absolute value operator is not continuously differentiable which can cause convergence problems for Nonlinear Programming (NLP) solvers. On the other hand, the ℓ_1-norm slack variables and inequalities create an objective function that is smooth and continuously differentiable. Without the dead-band ($db = 0$) in Equation 2.3, the equations for c_U, c_L are not required and the form reduces to the commonly known ℓ_1-norm for estimation that has desirable performance for outlier elimination [39–44].

Using dynamic data to fit nonlinear dynamic models has a number of challenges. One of the challenges with the simultaneous solution approach is that the data reconciliation problem can be very large. The data reconciliation problem is large because a discretization point of the DAE model must be calculated at every time instant where a measurement is available. Using the simultaneous optimization of model and objective function, the number of model states at a particular time is multiplied by the number of time steps in the prediction horizon. On the other hand, the se-

Table 2.1: Estimation: two forms for dynamic data reconciliation

Estimation with a Squared Error Objective

$$\begin{aligned}\min_{x,y,p,d}\ & \Phi = (y_x - y)^T W_m (y_x - y) + (y - \hat{y})^T W_p (y - \hat{y}) + \Delta p^T c_{\Delta p} \\ \text{s.t.}\quad & 0 = f\left(\tfrac{dx}{dt}, x, y, p, d, u\right) \\ & 0 = g(x, y, p, d, u) \\ & 0 \le h(x, y, p, d, u)\end{aligned} \tag{2.2}$$

Estimation with an ℓ_1-norm Objective with Dead-band

$$\begin{aligned}\min_{x,y,p,d}\ & \Phi = w_m^T (e_U + e_L) + w_p^T (c_U + c_L) + \Delta p^T c_{\Delta p} \\ \text{s.t.}\quad & 0 = f\left(\tfrac{dx}{dt}, x, y, p, d, u\right) \\ & 0 = g(x, y, p, d, u) \\ & 0 \le h(x, y, p, d, u) \\ & \\ & e_U \ge y - y_x + \tfrac{db}{2} \\ & e_L \ge y_x - \tfrac{db}{2} - y \\ & c_U \ge y - \hat{y} \\ & c_L \ge \hat{y} - y \\ & e_U, e_L, c_U, c_L \ge 0\end{aligned} \tag{2.3}$$

Nomenclature for Equations 2.2 and 2.3

Φ	objective function
y_x	measurements $(y_{x,0}, \ldots, y_{x,n})^T$
y	model values $(y_0, \ldots, y_n)^T$
$\hat{y}$	prior model values $(\hat{y}_0, \ldots, \hat{y}_n)^T$
w_m, W_m	measurement deviation penalty
w_p, W_p	penalty from the prior solution
$c_{\Delta p}$	penalty from the prior parameter values
db	dead-band for noise rejection
x, u, p, d	states (x), inputs (u), parameters (p), or unmeasured disturbances (d)
Δp	change in parameters
f, g, h	equation residuals, output function, and inequality constraints
e_U, e_L	slack variable above and below the measurement dead-band
c_U, c_L	slack variable above and below a previous model value

quential solution approach (solving objective function and model equations successively) reduces the number of variables that must be solved simultaneously [45]. This approach is better suited to systems that have a small number of decision variables yet large number of model variables or a long time horizon.

Other challenges in aligning the model to measured values include lack of data diversity to obtain certain constants or co-linearity of parameters. The sensitivity of parameters to the objective function can help guide which parameters have a significant effect on the outcome [46]. One solution to automatically eliminate parameters with little sensitivity to the objective is to impose a small penalty on parameter movement from a nominal value [47]. This approach automatically prevents unnecessary movement of parameter values that have little effect on the results of the parameter estimation.

2.5 Nonlinear Control and Optimization

This section details design of objective functions that are used in optimization calculations of MPC. MPC is an advanced method of process control which uses the process model to hold the control variables close to a set point while maintaining the constraints by minimizing the error between set point and a control variable (objective function) in a series of time points in future (predictive horizon). MPC only sends out the first change in each manipulated variable within the predictive horizon to be implemented, and repeats the calculation during the next cycle.

There are many challenges to the application of DAEs directly in nonlinear control and optimization [48]. Recent advances include simultaneous methods [45], decomposition methods [49, 50], efficient nonlinear programming solvers [28], improved estimation techniques [51–54], and experience with applications to industrial systems [47, 55]. In particular, applications require high service availability, reasonable extrapolation to operating conditions outside the original training set, and explanatory tools that reveal the rationale of the optimization results. Other motivating factors include consideration of lost opportunity during application development, sustainability of the solution, and ease of development and maintenance by engineers without an advanced training. In many instances non-technical challenges such as equipment and base-control reliability, operator training, and management support are critical factors in the success of an application [56].

A common objective function form is the squared error or ℓ_2-norm objective (see Equation 2.4). In this form, there is a squared penalty for deviation from a setpoint or desired trajectory. The squared error objective is simple to implement, has a relatively intuitive solution, and is well suited for Quadratic Programming (QP) or Nonlinear Programming (NLP) solvers. Control calculations using a squared error includes minimizing the summation of the squared error between the controlled variable (y) and the set point trajectory (y_t), change in the manipulated variable (Δu) and also terms that push values to a minimum or maximum limit.

An alternative form of the objective function is the ℓ_1-norm objective (see Equation 2.5) that has a number of advantages over the squared error form similar to those discussed for the estimation case. For control problems, the advantage is not in rejection of outliers but in the explicit prioritization of control objectives. The difference between the ℓ_1-norm and squared error is that the ℓ_1-norm uses slack variables below or above the trajectory dead band. The ℓ_1-norm simultaneously optimizes multiple objectives in one optimization problem as the solver manipulates the degrees of freedom selectively for the objective function contributions that have the highest sensitivity. Lower ranking objectives are met as degrees of freedom remain. However, the best objective function will always be met by minimizing the error associated with high ranking objectives. For problems that have safety, environmental, economic, and other competing priorities, the ℓ_1-norm with a dead-band gives an intuitive form that manages these trade-offs. This dead-band also gives flexibility to have non-symmetric objective functions in cases where an upper or lower limit is more important. Table 2.2 details the square error and ℓ_1-norm objective functions.

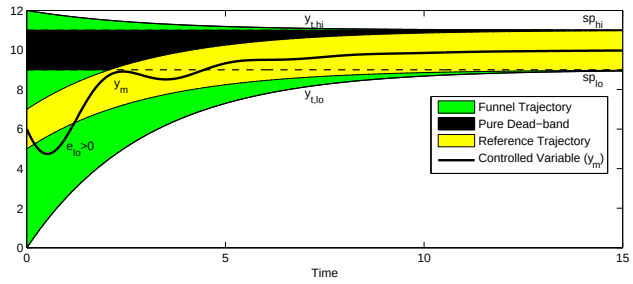

Figure 2.2: Three examples of ℓ_1-norm dead-band trajectory regions for model predictive control.

Table 2.2: Control: two objective forms for nonlinear dynamic optimization

Control Squared Error Objective

$$\begin{aligned}
&\min_{x,y,u} \Phi = (y-y_t)^T W_t (y-y_t) + y^T c_y + u^T c_u + \Delta u^T c_{\Delta u} \\
&\text{s.t.} \quad 0 = f\left(\tfrac{dx}{dt}, x, y, p, d, u\right) \\
&\qquad 0 = g(x, y, p, d, u) \\
&\qquad 0 \le h(x, y, p, d, u) \\
&\qquad \\
&\qquad \tau_c \tfrac{dy_t}{dt} + y_t = sp
\end{aligned} \tag{2.4}$$

Control ℓ_1-norm Objective

$$\begin{aligned}
&\min_{x,y,u} \Phi = w_{hi}^T e_{hi} + w_{lo}^T e_{lo} + y^T c_y + u^T c_u + \Delta u^T c_{\Delta u} \\
&\text{s.t.} \quad 0 = f\left(\tfrac{dx}{dt}, x, y, p, d, u\right) \\
&\qquad 0 = g(x, y, p, d, u) \\
&\qquad 0 \le h(x, y, p, d, u) \\
&\qquad \\
&\qquad \tau_c \tfrac{dy_{t,hi}}{dt} + y_{t,hi} = sp_{hi} \\
&\qquad \tau_c \tfrac{dy_{t,lo}}{dt} + y_{t,lo} = sp_{lo} \\
&\qquad e_{hi} \ge y - y_{t,hi} \\
&\qquad e_{lo} \ge y_{t,lo} - y
\end{aligned} \tag{2.5}$$

Nomenclature for Equations 2.4 and 2.5

Φ	objective function
y	model values $(y_0, \ldots, y_n)^T$
$y_t, y_{t,hi}, y_{t,lo}$	desired trajectory target or dead-band
w_{hi}, w_{lo}	penalty outside trajectory dead-band
c_y, c_u, $c_{\Delta u}$	cost of y, u and Δu, respectively
u, x, p, d	inputs (u), states (x), parameters (p), and disturbances (d)
f, g, h	equation residuals (f), output function (g), and inequality constraints (h)
τ_c	time constant of desired controlled variable response
e_{lo}, e_{hi}	slack variable below or above the trajectory dead-band
sp, sp_{lo}, sp_{hi}	target, lower, and upper bounds to final setpoint dead-band

The reference trajectories in both the squared-error and ℓ_1-norm moderate the speed at which the controller attempts to reach the desired setpoint sp or reach the desired range sp_{lo}, sp_{hi} as shown in Figure 2.2. Three different ℓ_1-norm trajectories are shown with varying initial conditions and are classified as a reference trajectory (inner-most), a pure dead-band (constant band), and a funnel trajectory (widest at the beginning). The initial conditions for $y_{t,hi}$ and $y_{t,lo}$ adjust the starting positions of the reference trajectory region of no penalty. For dead-band control, the initial conditions are set to the final target values with $y_{t,hi} = sp_{hi}$ and $y_{t,lo} = sp_{lo}$. If restrictions on near-term dynamics are less important than reaching a target steady-state value, the gap between $y_{t,hi}$ and $y_{t,lo}$ can be made large relative to the range of the final dead-band sp_{hi} and sp_{lo} as shown by the funnel trajectory in Figure 2.2.

2.6 Numerical Solution of DAE Systems

Both model predictive control and moving horizon estimation require dynamic optimization in which problems are solved over a time horizon. In predictive control, the horizon is the sequence of future time steps in which control calculations are performed. In moving horizon estimation, the horizon is a sequence of time points in the past where estimation calculations are performed.

Two types of methods for solving nonlinear MPC and dynamic optimization problems include sequential methods and simultaneous methods [45]. With the more compact sequential approach, the model equations are repeatedly solved to convergence tolerance to provide an objective function and gradient. The supervisory layer then proposes new decision variables and the simulation process is repeated. Conversely, the simultaneous approach involves solving the model equations and optimizing the objective function in parallel.

Sequential methods are easier to implement, but may fail to converge in a reasonable time for problems with a large number of degrees of freedom, thus delivering sub-optimal solutions. However, because sequential methods solve the model equations by forward integration, the solutions are always feasible with respect to the dynamic model, if not optimal. The simultaneous solution approach may be advantageous for certain problems, especially boundary value problems, terminal time constraints, and systems with unstable modes [32]. Simultaneous optimization approaches generally have a computational advantage for control problems with many decision

variables but with a moderate number of state variables. Sequential approaches may have computational advantage for a small number of decision variables coupled with large-scale models. Typical cases of large-scale models are distributed parameter systems. In this case, the computational gain obtained through simultaneous methods from the elimination of repeated integration is overcome by the very large number of space and time discretized states.

A characteristic of the simultaneous problem formulation is that a general DAE model can be posed in open equation format (refer to Equation 2.1). In open equation format, DAE models of index-1 or higher are solved without rearrangement or differentiation. The values of certain parameters, disturbances, or decision variables are discrete values over the time horizon to make the problem tractable for numerical solution (e.g. MVs in Figure 2.3). On the other hand, integrated variables are determined from differential and algebraic equations and generally have a continuous profile (e.g. CVs in Figure 2.3). The solid nodes in Figure 2.3 depict starting and ending locations for local polynomial approximations that are pieced together over the time horizon. With one internal node for each segment, this example uses a 2nd order polynomial approximation for each step. One solution approach to this dynamic system is the conversion of the DAE system to algebraic

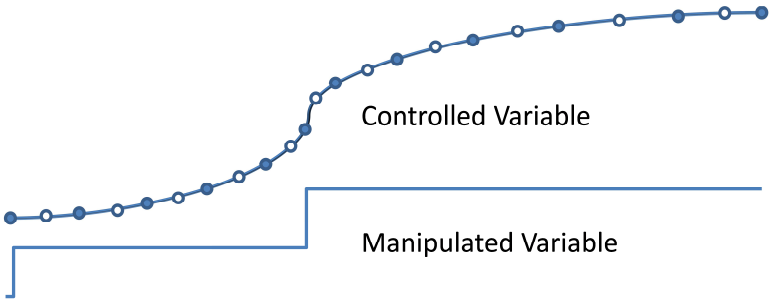

Figure 2.3: Dynamic discretization of equations over a time horizon.

equations through direct transcription [18]. This technique is also known as orthogonal collocation on finite elements [57]. Converting the DAE system to a Nonlinear Programming (NLP) problem permits the solution by large-scale solvers [35,58]. Additional details of the simultaneous approach are shown in Section 2.6.1 and an example problem in Section 2.6.2.

2.6.1 Weighting Matrices for Orthogonal Collocation

The objective is to determine a matrix M that relates the derivatives to the non-derivative values over a horizon at points 1,...n as shown in Equation 2.6. In order to do this, the differential equation solution is approximated as a polynomial function over the horizon time steps. In the case of Equation 2.6, four points are shown for the derivation. The initial value, x_0, is a fixed initial condition or otherwise equal to the final point from the prior interval. The value of M matrix is fixed and is based on a derivative that uses optimal time points given by Lobatto collocation. At every cycle time that control or estimation calculations are performed, the initial condition (x_0) represents the current time point.

$$\begin{bmatrix} \dot{x}_1 \\ \dot{x}_2 \\ \dot{x}_3 \end{bmatrix} = M \left(\begin{bmatrix} x_1 \\ x_2 \\ x_3 \end{bmatrix} - \begin{bmatrix} x_0 \\ x_0 \\ x_0 \end{bmatrix} \right) \tag{2.6}$$

The solution of the differential equations at discrete time points is approximated by a Lagrange interpolating polynomial as shown in Equation 2.7.

$$x(t) = A + Bt + Ct^2 + Dt^3 \tag{2.7}$$

Time points for each interval are chosen according to Lobatto quadrature. All time points are shifted to a reference time of zero ($t_0 = 0$) and a final time of $t_n = 1$ (general unit). For 3 nodes per horizon step, the one internal node is chosen at $t_1 = \frac{1}{2}$. An example of internal nodes are displayed in Figure 2.3 where the horizon is broken into multiple intervals of Lobatto quadrature with 3 nodes per horizon step (one internal node). In the case of 4 nodes per horizon step, the internal values are chosen at $t_1 = \frac{1}{2} - \frac{\sqrt{5}}{10}$ and $t_2 = \frac{1}{2} + \frac{\sqrt{5}}{10}$. With 5 nodes, time values are $\frac{1}{2} - \frac{\sqrt{21}}{14}$, $\frac{1}{2}$, and $\frac{1}{2} + \frac{\sqrt{21}}{14}$. At 6 nodes, time values are $\frac{1}{2} - \frac{\sqrt{7+2\sqrt{7}}}{42}$, $\frac{1}{2} - \frac{\sqrt{7-2\sqrt{7}}}{42}$, $\frac{1}{2} + \frac{\sqrt{7-2\sqrt{7}}}{42}$, and $\frac{1}{2} + \frac{\sqrt{7+2\sqrt{7}}}{42}$.

In this derivation, a third-order polynomial approximates the solution at the four points in the horizon. Increasing the number of collocation points increases the corresponding polynomial order. For initial value problems, the coefficient A is equal to x_0, when the initial time is arbitrarily defined as zero. To determine the coefficients B, C, and D, Equation 2.7 is differentiated and substituted into Equation 2.6 to give Equation 2.8. Note that the A coefficient from Equation 2.7 is

cancelled by x_0 on the right-hand side of Equation 2.8.

$$\begin{bmatrix} B+2Ct_1+3Dt_1^2 \\ B+2Ct_2+3Dt_2^2 \\ B+2Ct_3+3Dt_3^2 \end{bmatrix} = M \begin{bmatrix} Bt+Ct_1^2+Dt_1^3 \\ Bt+Ct_2^2+Dt_2^3 \\ Bt+Ct_3^2+Dt_3^3 \end{bmatrix}$$
$$\begin{bmatrix} 1 & 2t_1 & 3t_1^2 \\ 1 & 2t_2 & 3t_2^2 \\ 1 & 2t_3 & 3t_3^2 \end{bmatrix} \begin{bmatrix} B \\ C \\ D \end{bmatrix} = M \begin{bmatrix} t_1 & t_1^2 & t_1^3 \\ t_2 & t_2^2 & t_2^3 \\ t_3 & t_3^2 & t_3^3 \end{bmatrix} \begin{bmatrix} B \\ C \\ D \end{bmatrix} \tag{2.8}$$

Finally, rearranging and solving for M gives the solution shown in Equation 2.9.

$$M = \begin{bmatrix} 1 & 2t_1 & 3t_1^2 \\ 1 & 2t_2 & 3t_2^2 \\ 1 & 2t_3 & 3t_3^2 \end{bmatrix} \begin{bmatrix} t_1 & t_1^2 & t_1^3 \\ t_2 & t_2^2 & t_2^3 \\ t_3 & t_3^2 & t_3^3 \end{bmatrix}^{-1} \tag{2.9}$$

The final form that is implemented in practice is shown in Equation 2.10 by inverting M and factoring out the final time t_n $\left(t_n N = M^{-1}\right)$. This form improves the numerical characteristics of the solution, especially as the time step approaches zero ($t_n \to 0$).

$$t_n N \begin{bmatrix} \dot{x}_1 \\ \dot{x}_2 \\ \dot{x}_3 \end{bmatrix} = \begin{bmatrix} x_1 \\ x_2 \\ x_3 \end{bmatrix} - \begin{bmatrix} x_0 \\ x_0 \\ x_0 \end{bmatrix} \tag{2.10}$$

The matrices that relate $\frac{dx}{dt}$ to x are given in Tables 2.3 and 2.4 for intervals with 3 to 6 nodes. The formula for 2 nodes reduces to Euler's method for numerical integration differential equations. However, in this case the equations are not solved sequentially in time but simultaneously by an implicit solution method. Additional accuracy can be achieved over one interval with more nodes but more nodes also increases the number of equations and size of the problem. The time dynamic horizon is typically divided over a number of intervals where these equations are applied. An additional set of these equations must be included for every differential variable that appears in the model equations. In this case the differential variables are treated like regular

algebraic variables because there is an additional equation for every unknown derivative value at every time point.

Table 2.3: Direct transcription to solve differential equations as sets of algebraic equations

Orthogonal Collocation Equations	
$t_n N_{2x2} \begin{bmatrix} \dot{x}_1 \\ \dot{x}_2 \end{bmatrix} = \begin{bmatrix} x_1 \\ x_2 \end{bmatrix} - \begin{bmatrix} x_0 \\ x_0 \end{bmatrix}$	(2.11)
$t_n N_{3x3} \begin{bmatrix} \dot{x}_1 \\ \dot{x}_2 \\ \dot{x}_3 \end{bmatrix} = \begin{bmatrix} x_1 \\ x_2 \\ x_3 \end{bmatrix} - \begin{bmatrix} x_0 \\ x_0 \\ x_0 \end{bmatrix}$	(2.12)
$t_n N_{4x4} \begin{bmatrix} \dot{x}_1 \\ \dot{x}_2 \\ \dot{x}_3 \\ \dot{x}_4 \end{bmatrix} = \begin{bmatrix} x_1 \\ x_2 \\ x_3 \\ x_4 \end{bmatrix} - \begin{bmatrix} x_0 \\ x_0 \\ x_0 \\ x_0 \end{bmatrix}$	(2.13)
$t_n N_{5x5} \begin{bmatrix} \dot{x}_1 \\ \dot{x}_2 \\ \dot{x}_3 \\ \dot{x}_4 \\ \dot{x}_5 \end{bmatrix} = \begin{bmatrix} x_1 \\ x_2 \\ x_3 \\ x_4 \\ x_5 \end{bmatrix} - \begin{bmatrix} x_0 \\ x_0 \\ x_0 \\ x_0 \\ x_0 \end{bmatrix}$	(2.14)

2.6.2 Example Solution by Orthogonal Collocation

A simultaneous solution demonstrates the application of orthogonal collocation. In this case, the first order system $\tau \frac{dx}{dt} = -x$ is solved at 6 points from $t_0 = 0$ to $t_n = 10$ using Equation 2.14. In this case $\tau = 5$ and the initial condition is specified at $x_0 = 1$. For this problem, the time points for $\frac{dx}{dt}$ and x are selected as 0, 1.175, 3.574, 6.426, 8.825, and 10. The value of x is specified at $t_0 = 0$ due to the initial condition. As a first step, equations for $\frac{dx}{dt}$ are generated in Equation 2.19.

Table 2.4: Matrices for direct transcription

Orthogonal Collocation Matrices

$$N_{2x2} = \begin{bmatrix} 0.75 & -0.25 \\ 1.00 & 0.00 \end{bmatrix} \tag{2.15}$$

$$N_{3x3} = \begin{bmatrix} 0.436 & -0.281 & 0.121 \\ 0.614 & 0.064 & 0.046 \\ 0.603 & 0.230 & 0.167 \end{bmatrix} \tag{2.16}$$

$$N_{4x4} = \begin{bmatrix} 0.278 & -0.202 & 0.169 & -0.071 \\ 0.398 & 0.069 & 0.064 & -0.031 \\ 0.387 & 0.234 & 0.278 & -0.071 \\ 0.389 & 0.222 & 0.389 & 0.000 \end{bmatrix} \tag{2.17}$$

$$N_{5x5} = \begin{bmatrix} 0.191 & -0.147 & 0.139 & -0.113 & 0.047 \\ 0.276 & 0.059 & 0.051 & -0.050 & 0.022 \\ 0.267 & 0.193 & 0.251 & -0.114 & 0.045 \\ 0.269 & 0.178 & 0.384 & 0.032 & 0.019 \\ 0.269 & 0.181 & 0.374 & 0.110 & 0.067 \end{bmatrix} \tag{2.18}$$

$$\frac{dx}{dt} = \begin{bmatrix} \dot{x}_1 \\ \dot{x}_2 \\ \dot{x}_3 \\ \dot{x}_4 \\ \dot{x}_5 \end{bmatrix} = (t_n N_{5x5})^{-1} \left(\begin{bmatrix} x_1 \\ x_2 \\ x_3 \\ x_4 \\ x_5 \end{bmatrix} - \begin{bmatrix} x_0 \\ x_0 \\ x_0 \\ x_0 \\ x_0 \end{bmatrix} \right) \tag{2.19}$$

Substitution of Equation 2.19 into the derivatives of the model equation yields a linear system of equations as shown in Equation 2.20.

$$\tau\frac{dx}{dt} = -x$$

$$\tau\left(t_n N_{5x5}\right)^{-1}\left(\begin{bmatrix} x_1 \\ x_2 \\ x_3 \\ x_4 \\ x_5 \end{bmatrix} - \begin{bmatrix} x_0 \\ x_0 \\ x_0 \\ x_0 \\ x_0 \end{bmatrix}\right) = -\begin{bmatrix} x_1 \\ x_2 \\ x_3 \\ x_4 \\ x_5 \end{bmatrix} \tag{2.20}$$

Equation 2.20 is rearranged and solved with linear algebra as shown in Equation 2.21.

$$\begin{bmatrix} x_1 \\ x_2 \\ x_3 \\ x_4 \\ x_5 \end{bmatrix} = \left(\tau\left(t_n N_{5x5}\right)^{-1} + I\right)^{-1}\tau\left(t_n N_{5x5}\right)^{-1}\begin{bmatrix} x_0 \\ x_0 \\ x_0 \\ x_0 \\ x_0 \end{bmatrix} = \begin{bmatrix} 0.791 \\ 0.489 \\ 0.277 \\ 0.171 \\ 0.135 \end{bmatrix} \tag{2.21}$$

The numerical solution given in Equation 2.21 is within three significant figures of the analytical solution $x(t) = x_0 e^{-\frac{t}{\tau}}$, verifying that the numerical solution approximations are sufficiently accurate in this case. This is not always the case and discretization must sometimes be refined to reduce numerical error.

2.7 Application: Quadruple Tank Level Control

A quadruple tank process shown in Figure 2.4 has been the subject of theoretical [59] and practical demonstrations [60–63] of a multivariable and highly coupled system [61]. The four tank process has also been a test case for application of decentralized and coordinated control techniques [64, 65]. A number of other interesting characteristics of this process include configurations that cause the system to go unstable. This can be observed by showing that there are unstable poles in a transfer function representation of the system. Another challenge is the nonlinear tendency of the system. For example, this can be characterized by variable gains of the MVs to the CVs.

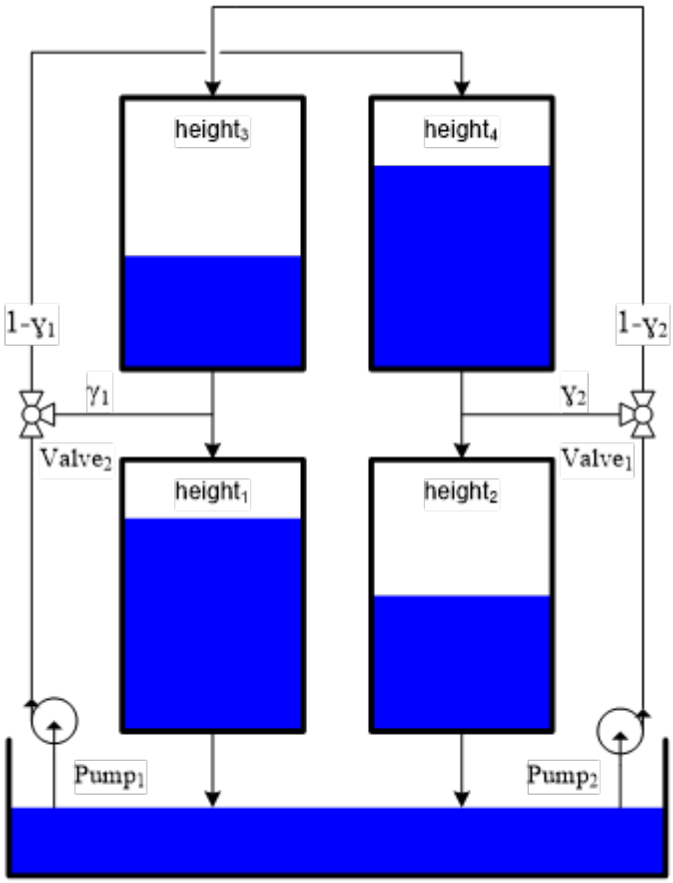

Figure 2.4: Diagram of the quadruple tank process. Pump 1 supplies tanks 1 and 4 while pump 2 supplies tanks 2 and 3.

The four tank process has two pumps that are adjusted with variable voltage to pump 1 (v_1) and pump 2 (v_2). A fraction of water from pump 1 is diverted to tank 1 proportional to γ_1 and to tank 4 proportional to $(1-\gamma_1)$. Similarly, a fraction of water from pump 2 is diverted to tank 2 proportional to γ_2 and to tank 3 proportional to $(1-\gamma_2)$. The valves that determine γ_1 and γ_2 are manually adjusted previous to the experiment and are held constant through-out a particular period of data collection. All tanks are gravity drained and tank 3 outlet enters tank 1. Tank 4 outlet enters tank 2, creating a coupled system of MVs and CVs. For $(\gamma_1+\gamma_2)\in(0,1)$, the linearized system has no RHP zeros but for $(\gamma_1+\gamma_2)\in(1,2)$, the linearized system has one RHP zero [59]. A RHP zero indicates that there may either be overshoot or an inverse response to a step change in the MV.

A combination of material balances and Bernoulli's law yields the process model for the four tank process as shown in Equation 2.22.

$$\begin{aligned} q_a &= k_m v_1 + k_b \\ q_b &= k_m v_2 + k_b \end{aligned} \tag{2.22a}$$

$$\begin{aligned} q_{1,in} &= \gamma_1 q_a + q_{3,out} \\ q_{2,in} &= \gamma_2 q_b + q_{4,out} \\ q_{3,in} &= (1-\gamma_2)\, q_b \\ q_{4,in} &= (1-\gamma_1)\, q_a \end{aligned} \tag{2.22b}$$

$$\begin{aligned} q_{1,out} &= c_1 \sqrt{2gh_1} \\ q_{2,out} &= c_2 \sqrt{2gh_2} \\ q_{3,out} &= c_3 \sqrt{2gh_3} \\ q_{4,out} &= c_4 \sqrt{2gh_4} \end{aligned} \tag{2.22c}$$

$$\begin{aligned} A_1 \frac{dh_1}{dt} &= q_{1,in} - q_{1_{out}} \\ A_2 \frac{dh_2}{dt} &= q_{2,in} - q_{2_{out}} \\ A_3 \frac{dh_3}{dt} &= q_{3,in} - q_{3_{out}} \\ A_4 \frac{dh_4}{dt} &= q_{4,in} - q_{4_{out}} \end{aligned} \tag{2.22d}$$

where γ_1 is the split factor for tanks 1 and 4 and γ_2 is the split factor leading to tanks 2 and 3 and the range of allowable values is $0 \leq \gamma_i \leq 1$. When $\gamma_i = 0$ all of the flow from the pumps enters the top tanks (3 or 4) and when $\gamma_i = 1$ all of the flow enters the lower tanks (1 or 2). The other parameters for this model include c_i as the outflow factor for tank i, k_m as the valve linearization slope, k_b as the valve linearization intercept, and A_i as the cross-sectional area of tank i. The variables include q_a as the flow from pump 1, q_b as the flow from pump 2, $q_{i,in}$ as the inlet flow to tank i, $q_{i,out}$ as the outlet flow from tank i, and h_i as the height of liquid in tank i.

Equation set 2.22a is the relationship between pump voltage and flow while Equation set 2.22b defines the inlet flow to each of the tanks. Equation set 2.22c is the outlet flow from each of the tanks with tanks 3 and 4 draining to tanks 1 and 2, respectively. Finally, equation set 2.22d

is a material balance around each tank with accumulation, inlet, and outlet terms. In this case, the density is assumed to be constant allowing a volumetric balance to be used instead.

The process model is nonlinear because the outlet flow is proportional to the square root of the liquid level. In this experiment, tanks 1 and 3 and tanks 2 and 4 have the same outlet diameter making $c_1 = c_3$ and $c_2 = c_4$. Additionally, tanks 1 and 3 have a cross-sectional area of 28 cm^2 while tanks 2 and 4 have a cross-sectional area of 32 cm^2. Unknown parameters include γ_1, γ_2, $c_{1,3}$, $c_{2,4}$, k_m, and k_b. The unknown parameters are determined from dynamic data.

2.7.1 Quadruple Tank Parameter Estimation

For the quadruple tank process, the model has only 14 differential or algebraic states. When calculated over the pseudo random binary sequence data horizon, the resulting optimization problem has 5766 to 11,526 variables, depending on the objective function form. There are additional equations for the differential states in the optimization problem from the orthogonal collocation transformation (see Section 2.6). Direct transcription by orthogonal collocation on finite elements is one of the methods to convert DAE systems into a Nonlinear Programming (NLP) problem [66]. This is accomplished by approximating time derivatives of the DAE system as algebraic relationships as discussed previously. Figure 2.5 shows the results of the reconciliation to the PRBS-generated data.

Only levels for tanks 1 and 2 are measured as shown in Figure 2.5. For the quadruple tank process 6 parameters were estimated, namely γ_1, γ_2, $c_{1,3}$, $c_{2,4}$, k_m, and k_b. The optimization solution overview is shown in Table 2.5 while initial and final values of the parameters are displayed in Table 2.6. MATLAB or Python scripts use the APMonitor Modeling Language [19] model to create the differential and algebraic (DAE) model. APMonitor translates the problem into an NLP and solves the equations with one of many large-scale solvers. The particular solver used in this study is IPOPT, an interior point large-scale nonlinear programming solver [28], for solving the resulting optimization problem. A summary of the optimization problem and the solution is shown in Table 2.5.

Using different objective function forms resulted in similar parameter estimates and comparable model predictions. As seen in Table 2.6, the optimal values for the parameters were well within the upper and lower constraints. These constraints were set for both ℓ_1-norm and squared-

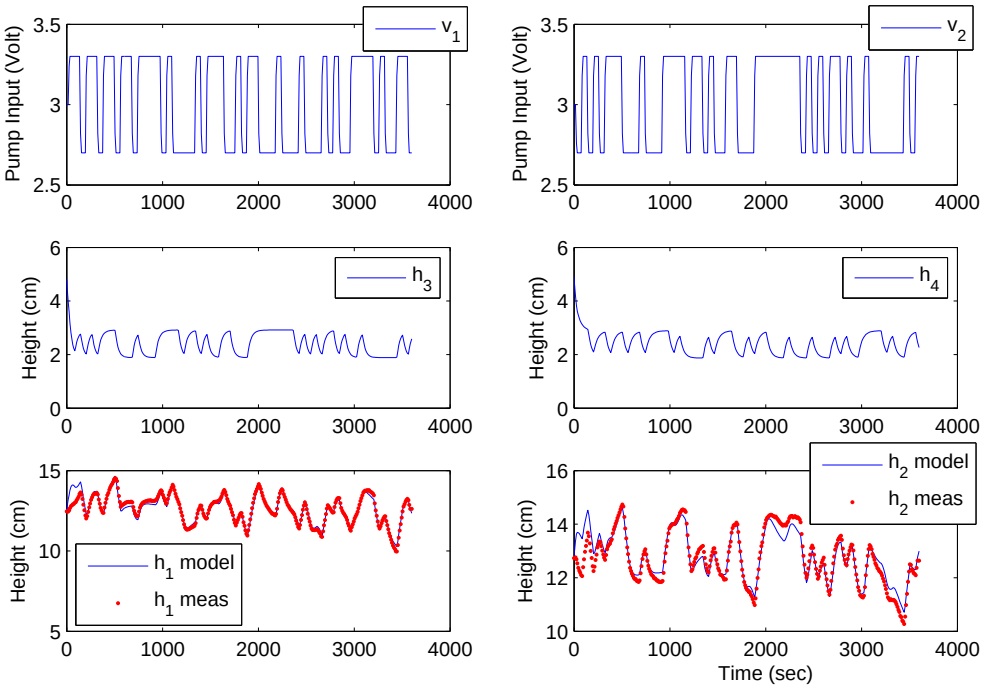

Figure 2.5: Results of the dynamic parameter estimation using PRBS generated data.

Table 2.5: Summary of the dynamic data reconciliation

Optimization Problem Overview		
Description	ℓ_1-Norm	Squared Error
Iterations	33	10
CPU Time (2.5 GHz Intel i7 Processor)	32.5 sec	10.3 sec
Number of Variables	11,526	5,766
Number of Equations	11,520	5,760
Degrees of Freedom	6	6
Number of Jacobian Non-zeros	40,312	28,792

error problems based on knowledge of the process; a violation of these constraints would indicate unreasonable parameter values. In this case, the ℓ_1-norm optimization problem had roughly twice the number of variables and required 3 times the amount of CPU time to find a solution. In this case, the increased computational time is an additional cost associated with ℓ_1-norm estimation.

Table 2.6: Results of the dynamic data reconciliation

Initial and Final Values of the Estimation Problem					
Parameter	Initial Value	Lower Bound	Upper Bound	ℓ_1-Norm Results	Squared Error Results
γ_1	0.43	0.20	0.80	0.627	0.585
γ_2	0.34	0.20	0.80	0.591	0.548
$c_{1,3}$	0.071	0.010	0.200	0.0592	0.0630
$c_{2,4}$	0.057	0.010	0.200	0.0548	0.0582
k_m	10.0	3.0	20.0	3.543	3.444
k_b	0.00	-2.00	2.00	-1.675	-0.810

Improved outlier rejection and parameter estimates are shown by purposefully introducing corrupted data. Three cases are shown in Figure 2.6 with the corrupted data being introduced at 1200 seconds.

The first case of corrupted data is a single outlier that is 10 cm higher than the actual measured value. While this specific outlier could easily be removed by automated outlier detection, it may not be possible to eliminate all outliers from data especially for real-time or large-scale systems. A second case involves measurement drift at a rate of +0.1 cm per second. After 550 seconds, the measurement drift is corrected and the measurement returns to actual measured values. A third case introduces normally distributed measurement noise with zero mean and standard deviation of one.

For all cases, it is desirable to retain original parameters even in the presence of corrupted data. The ℓ_1-norm form outperforms the squared-error form in two of the three cases and slightly better on the case with added noise. In the case of the single outlier, the ℓ_1-norm parameter values do not change, demonstrating the value in rejecting outlier values. In the case of measurement drift,

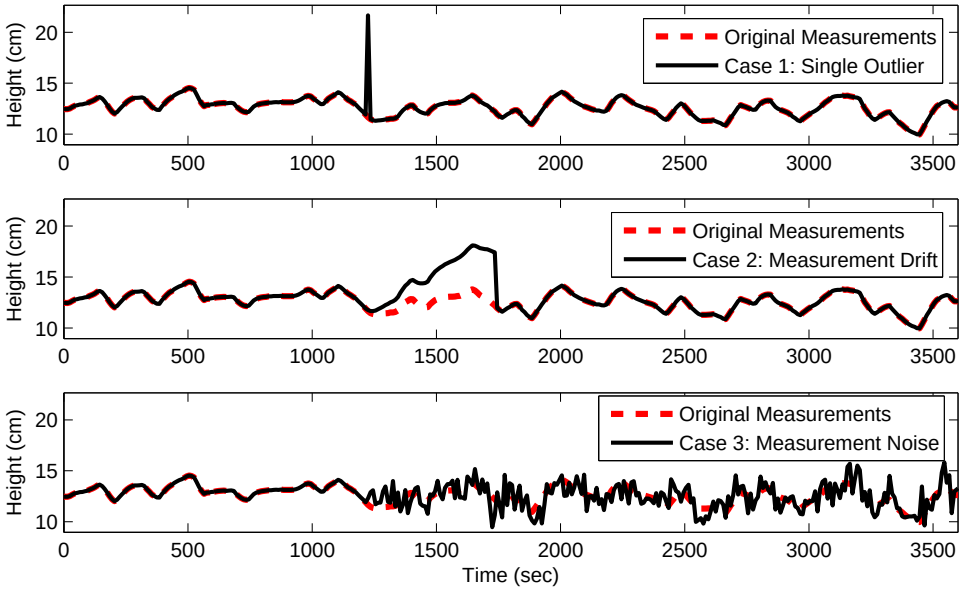

Figure 2.6: Three cases of corrupted data with (1) single outlier, (2) measurement drift, and (3) measurement noise.

Table 2.7: Changing parameter results with corrupted data

Parameter Value Change with ℓ_1-norm						
	γ_1	γ_2	$c_{1,3}$	$c_{2,4}$	k_m	k_b
Case 1 (Outlier)	0%	0%	0%	0%	0%	0%
Case 2 (Drift)	1%	1%	2%	0%	1%	0%
Case 3 (Noise)	5%	2%	8%	4%	2%	21%
Parameter Value Change with Squared Error						
	γ_1	γ_2	$c_{1,3}$	$c_{2,4}$	k_m	k_b
Case 1 (Outlier)	11%	6%	3%	4%	6%	42%
Case 2 (Drift)	3%	11%	15%	5%	3%	37%
Case 3 (Noise)	9%	4%	2%	9%	7%	72%

the ℓ_1-norm error parameters change by from 0-2% while the squared-error parameters change between 3-37%. Finally, for the measurement noise case, the ℓ_1-norm and squared-error parameters both change although the squared-error parameters change by roughly twice that of the ℓ_1-norm parameters. This corrupted data example demonstrates the ability of the ℓ_1-norm to better reject outliers, sensor drift, and noise.

2.7.2 Nonlinear Optimization of the Quadruple Tank System

Continuing with the quadruple tank example, the squared error model parameters from Section 2.7.1 are used to update the model. Either the squared-error or the ℓ_1-norm objective estimation values can be used because of nearly equivalent results. Data reconciliation can either be performed once or repeatedly as new measurements arrive in a receding horizon approach. As new measurements arrive, the model is readjusted to fit the data and continually refine the model predictions. These updated parameters can then be used in the NMPC application to better predict the future response.

Once the model is updated, nonlinear optimization calculates the optimal trajectory of the MV. In this case, a future move plan of the voltage to the two pumps is calculated as shown in Figure 2.7. MV moves are constrained by change, upper, and lower limits. The change constraints are set to limit the amount that the MV can move for each control action step and in this case the move limit is set to $|\Delta MV| \leq 1$. With a cycle time of 1 second, the rate that the voltage to the pump can change is $\pm 1 \frac{V}{sec}$. The control action is also constrained by absolute minimum $(MV_L = 1)$ and maximum $(MV_U = 6)$ limits. The lower limit is reached for the first pump ($v1$) and remains at the lower limit for 30 seconds before settling at the steady state value at $1.41V$. The upper limit is reached for second pump ($v2$) within two steps into the horizon and afterwards settles to a steady state value of $4.58V$. This over-shoot or under-shoot of MVs is typical for CV tuning that is faster than the natural process time constant. The natural process time constant is the speed of response due to a step change in a process input. When requesting a response that is faster than this nominal step change, the MVs must over-react to move the process faster. In most cases, steady state values of the MVs are independent of the controller tuning. CV tuning is a critical element to achieving desirable control performance. Aggressive CV tuning is shown in this example, giving over- or under-shoot of the MVs. For CV tuning that is equal to the natural process time constant, there

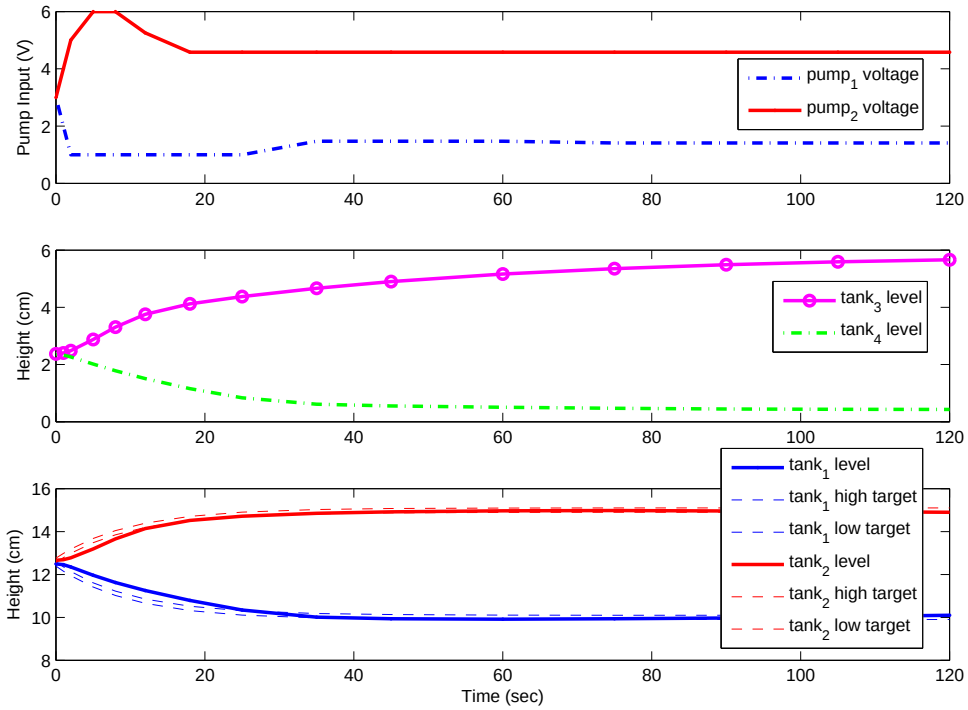

Figure 2.7: Model predictive control solution showing voltage input to the pumps 1 and 2.

will typically be a step to the new solution. For slower CV tuning, the MV ramps to the steady state value. Other MPC ℓ_1-norm formulations have particular drawbacks that either lead to dead-beat or idle control performance [67].

There are many types of CV tuning options that are typical in linear or nonlinear control applications. In this case, an ℓ_1-norm with dead-band is demonstrated for the simulated controller. The speed of the CV response is dictated by an upper and lower first order reference trajectory with time constant τ_c. Only values that are outside this dead-band are penalized in the objective function. The form of this controller objective is desirable for minimizing unnecessary MV movement to achieve a controller objective. In this form, MV movement only occurs if the projected CV response is forecast to deviate from a pre-described range. The bottom subplot of Figure 2.7 displays the CV response along with the upper and lower trajectories that define the control objective.

The quadruple tank process is represented by 14 differential and algebraic equations (DAEs). The following model in Listing 2.1 is expressed in the APMonitor Modeling Language. This file

and others included in the chapter are available at APMonitor.com as a MATLAB toolbox [68] or as a Python package [69].

Listing 2.1: Four Tank Model in APMonitor

```
Model
  Constants
    % gravitational constant (cm/s^2)
    g = 981
    % tank cross-sectional area (cm^2)
    Area[1] = 28
    Area[2] = 32
    Area[3] = 28
    Area[4] = 32
    % relation of level to voltage measurement (V/cm)
    kc = 0.50
  End Constants

  Parameters
    % relation of input voltage to pump flow rate (cm^3/sec / V)
    km = 10.0, >=3.0, <=20.0  % slope
    kb = 0.0, >=-20.0, <=20.0   % intercept
    % correction factors to fit model to real data
    c13 = 0.071, >0.01, <=0.2  % outlet flow corrections
    c24 = 0.057, >0.01, <=0.2  % outlet flow corrections
    % fractional split to tank 1 vs. tank 4
    gamma[1] = 0.43, >=0, <=1
    % fractional split to tank 2 vs. tank 3
    gamma[2] = 0.34, >=0, <=1
    % voltage to pump A
    v1 = 3, >=0, <=10       % Volt
    % voltage to pump B
    v2 = 3, >=0, <=10       % Volt
  End Parameters

  Variables
    % tank height - diameter = 6 cm,  max height = 20 cm
    h[1] = 12.6, >=1e-5
    h[2] = 13.0, >=1e-5
    h[3] = 4.8 , >=1e-5
    h[4] = 4.9 , >=1e-5
  End Variables

  Intermediates
    % correction factors
    c[1] = c13
    c[2] = c24
    c[3] = c13
    c[4] = c24
    % pump flows
    qa = v1 * km + kb
    qb = v2 * km + kb
    % inlet flows from pumps
    q[1] = gamma[1] * qa
    q[2] = gamma[2] * qb
    q[3] = (1-gamma[2]) * qb
    q[4] = (1-gamma[1]) * qa
    % outlet flows
    out[1:4] = c[1:4] * sqrt(2*g*h[1:4])
    % total inlet flows
    in[1] = q[1] + out[3]
    in[2] = q[2] + out[4]
    in[3] = q[3]
    in[4] = q[4]
  End Intermediates

  Equations
    Area[1:4] * $h[1:4] = in[1:4] - out[1:4]  % $ = differential
  End Equations
End Model
```

2.8 Large-Scale Systems

The quadruple tank system is a small-scale system that has been included here and in many other benchmark studies to demonstrate control techniques for multi-variable systems. An additional example is the computational requirements for large-scale systems. A test of the scale-up of the simultaneous approach for optimization is presented here with varying problem sizes with a state space model. In particular, the number of MVs and CVs is varied to reveal computational time required to determine an optimal solution for a single cycle of the controller. The controller has a quadratic objective function and linear constraints as shown in Equation 2.23.

$$\begin{aligned}
&\min_{x\in R^n, y\in R^p, u\in R^m} \Phi = (y-y_t)^T W_t (y-y_t) + y^T c_y + u^T c_u + \Delta u^T c_{\Delta u} \\
&\text{s.t.} \quad \frac{dx}{dt} = Ax + Bu, \quad A = -I_{n\text{x}n}, \quad B = \begin{bmatrix} 1 & \dots & 1 \\ 0 & \dots & 0 \\ \vdots & \ddots & \vdots \\ 0 & \dots & 0 \end{bmatrix}_{n\text{x}m} \\
&\qquad y = Cx + Du, \quad C = I_{p\text{x}n}, \quad D = 0_{p\text{x}m} \\
&\qquad \tau_c \frac{dy_t}{dt} + y_t = sp \\
&\qquad 0 \le u \le 10
\end{aligned} \tag{2.23}$$

The number of MVs (m) and number of CVs (p) are adjusted to vary the problem size. The controller is configured with $W_t = I_{p\text{x}p}$, $c_y = c_u = c_{\Delta u} = 0_{m\text{x}1}$, $\tau_c = 1_{p\text{x}1}$, $sp = 1_{p\text{x}1}$, and initial condition $x_0 = 0_{n\text{x}1}$. Each of the MVs affects each of the CVs, leading to a dense step response mapping. A sparse map would be easier because the optimizer can exploit the sparse relationships. A dense cause and effect relationships between MVs and CVs is more difficult because the optimizer can't exploit sparsity. The cycle time is assumed to be 6 seconds with a prediction horizon of 120 minutes. The discretization times are chosen as 0, 0.1, 0.2, 0.4, 0.8, 1.5, 3, 6, 12, 25, 50, 60, 80, 100, and 120 seconds. The non-uniform time steps allow near-term resolution for control

action and long-term predictions for control target calculations. An active set solver (APOPT) and an interior point solver (IPOPT) are tested for the combination of MVs and CVs quantities as shown in Figure 2.8.

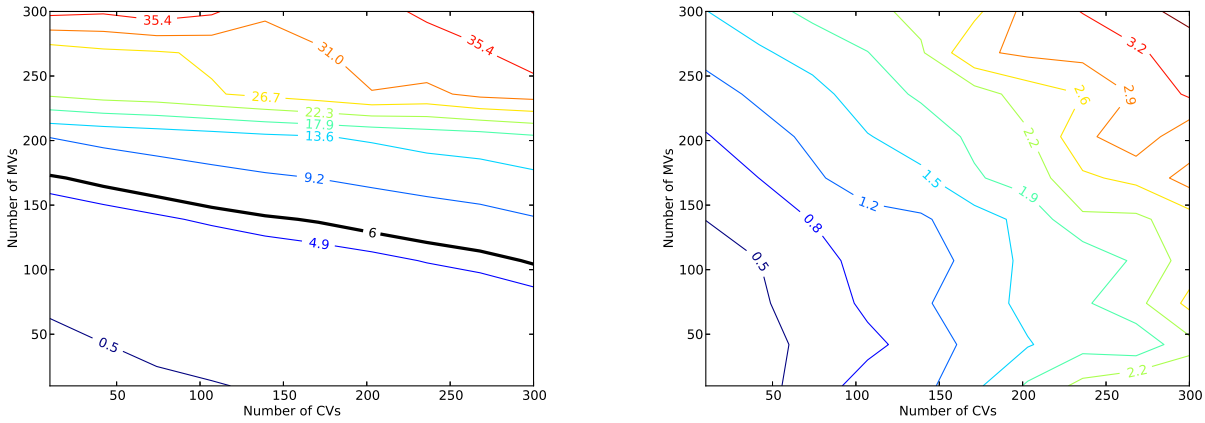

Figure 2.8: Contour plot of CPU times for varying numbers of MVs and CVs for APOPT and IPOPT, respectively.

The APOPT solver has excellent scaling with increased number of CVs but poor computational scaling with increased number of MVs (decision variables). This is expected from an active set solver where the basis selection and active set switching requires intensive matrix operations. Once the correct set of active constraints is determined, the algorithm can rapidly converge to an optimal solution.

The largest case with 300 MVs and 300 CVs translates into an optimization problem with 12,600 variables, 8,400 equations, and 4,200 degrees of freedom (decision variables) because the equations are discretized over the time horizon. Others have also demonstrated large-scale MPC with an ℓ_1-norm objective such a 400 MV/400 CV application to a paper machine cross direction control [70, 71]. The present case is solved in 3.8 sec with the IPOPT solver and in 39.5 sec with APOPT solver. A known advantage of interior point solvers is the excellent scaling with additional degrees of freedom. An advantage of active set solvers is the ability to quickly find a solution from a nearby candidate solution. A suggested approach is to use the interior point solver to initialize a problem and switch to an active set method for cycle-to-cycle cases that can be initialized from a prior solution.

2.9 Conclusion

This chapter gives details on the implementation of nonlinear modeling, data reconciliation, and dynamic optimization. The examples relate the common steps typically deployed in linear MPC applications to a comparable procedure for nonlinear applications. As a foundation for using dynamic models, the process of converting differential equations into a set of algebraic equations is reviewed. This conversion step is necessary to solve the model and objective function simultaneously with NLP solvers. The application in this chapter is the quadruple tank process that is a well-known example of multivariate control. As a first step, certain parameters of the model are adjusted to fit to PRBS data through dynamic data reconciliation. In a next step, the controller is tuned to provide desirable control responses for set point tracking and disturbance rejection. For both estimation and control cases, alternate squared error and ℓ_1-norm error forms are compared. While the ℓ_1-norm error uses additional variables and equations, it adds only linear equality and inequality constraints. While this is not an exhaustive review of all available techniques or software, it provides a platform and case study to advance the use of nonlinear models in control research and practice.

CHAPTER 3. ADVANCED DEEPWATER MONITORING SYSTEM

Much of the content of this chapter is taken from the following references: [72, 73]

- Asgharzadeh Shishivan, R., D. Brower, D., Hedengren, J., and Brower, A., 2014. New advances in post-installed subsea monitoring system for structural and flow assurance evaluation. In Ocean, Offshore Arctic Engineering OMAE, no. 24300.
- Brower, D., Hedengren, J., Shishivan, R. A., and Brower, A., 2013. Advanced deepwater monitoring system. In Ocean, Offshore Arctic Engineering OMAE, no. 10920.

3.1 Introduction

A Tension-leg platform (TLP) is a floating structure used for offshore production of oil or gas. It is vertically moored using tubular steel cables called tendons. The group of tendons at each corner of the structure is referred to as a tension leg. Balancing and automation of a TLP is of high importance because it facilitates managing offshore oil and gas operations and helps prevent environmental damage and catastrophic failure. This section details a new innovation to replace TLP load monitoring systems that use load cells with fiber optic load advanced sensors that are attached to the tendons. A unique aspect of this work is that the sensors are designed to be installed on existing systems such as flow-lines, risers, tendons, and other subsea structures. Designing the hardware part is not the contribution of this research but the monitoring and control system utilizes the sensor results. This research also details the strategy to find critical parameters such as stress, strain, temperature, pressure, and vibration based on the wavelength values from fiber optic sensors. And finally, it details the design of a control system for the TLP load balance automation based on calculated parameters. In the 'Fiber Optic Sensor Description' section (3.2), a brief overview of the fiber optic sensors is given. Next, in the 'Load Balancing System' section (3.3), the contribution of this project to the upstream oil industry and its tasks are discussed in more detail.

The results section, 3.4 discusses tests that compare fiber optic sensors with conventional strain gauges using tension, compression and bending tests and post installation results such as sensor calibration and data acquisition system sensitivity to different events. Finally the data obtained from the control system performance in a simulated environment is presented in section 3.4.3.

3.2 Fiber Optic Sensor Description

Fiber optic systems rely on different types of sensors that can detect reflected wavelengths based on etched grating backscatter, known as fiber Bragg gratings (FBGs), or on light scattering such as Rayleigh, Brillouin, or Raman scattering. The choice of sensor technology depends on the application parameters such as length, spatial distribution, number of point locations, and accuracy requirements. Some of the key advantages of FBG sensors include a high sensitivity to temperature and strain [74]. A FBG contains gratings that are etched on an optical fiber to create periodic changes in the index of refraction. The FBG sensors consist of a single-mode optical fiber with gratings positioned at various locations along its length. The gratings are produced by doping the fiber with germanium and exposing it to an interference pattern of coherent light. Each grating is designed to reflect a certain frequency of light. Multiple such gratings can be placed along a single fiber optic strand. The system is interrogated with a broadband light source, and multiple wavelength sensors within this source are detected [75].

The FBG wavelength is sensitive to dimensional and temperature changes. The instrumentation senses the reflected frequencies and in turn determines the grating location and the dimensional change. Changes in strain or temperature to which the optical fiber is subjected consequently shift this Bragg wavelength, leading to a wavelength-encoded optical measurement. Reflected wavelength value is highly sensitive to strain and temperature changes. By detecting strain-induced wavelength shift, a determination of absolute strain is made. Similarly, temperature-induced shifts are detected resulting in absolute temperature. Temperature compensation is provided by placing an additional FBG in the strain field area so that it is exposed to temperature but isolated from the strain field. The temperature-induced shift is then subtracted from the strain measurement. Fiber optic sensors have several distinct advantages over conventional sensing systems. Some of the major advantages are as follows:

- Low vulnerability to water ingress and shorting.
- No electric current required.
- Immune to electromagnetic interference (EMI).
- Multifunctional-can measure strain, temperature, pressure, and vibration.
- Have high strain sensitivity.

3.3 Load Balancing System

Current designs of TLP platforms have manual ballast operations that use submersed load cell on the four porches of a platform. Measuring tendon load values with data acquisition from fiber optic sensors allows a significantly different TLP design because a porch structure is not required. This design modification has the potential to significantly reduce construction costs (10M dollar) and improve the reliability of the tendon tension monitoring by replacing load cells that tend to fail quickly in practice. The challenge in this work is to design a sensing technology that can be installed on existing subsea systems by divers or remotely operated vehicles (ROVs). Another contribution of this work is automation of platform leveling and load balancing. This will facilitate more aggressive top-side operations like heavy lift events and provide early fault detection of tendon fatigue. This project was completed based on the following tasks:

- Design a data acquisition system based on fiber optic sensor technology to calculate the load and temperature values of tension legs.
- Develop a model for platform dynamics that captures the dynamics and design a control scheme using the data acquisition and TLP load model to automatically balance the TLP.

The aforementioned tasks are detailed in the following sections.

3.3.1 Data Acquisition Software

Data acquisition software was designed which collects the temperature and strain sensor wavelengths from the post-installed load sensors on two pre-tensioned TLPs (Foxtrot and Echo

platforms of the Okume Equatorial Guinea field in West Africa) and converts them to temperature and load values on each one of the tendons. This data acquisition work was performed as part of an internship and although it is project-based work, it builds the foundation for the proposed research activities in designing a novel control system for automating ballast control. The post-installed load sensors are installed on pretensioned systems and are calibrated to current load conditions at steady-state conditions [76]. Web-based control and troubleshooting features were added to the software [19] to facilitate control [13,56,77–79] and monitoring [53,54,80] of the data acquisition system from a corporate network. For example, the calibration feature was one of the capabilities of the software in the web interface and makes it possible for the operators to calibrate the load values after installation. The monitoring system includes interfaces to allow access from a corporate network as well as a distributed control system as shown in Figure 3.1.

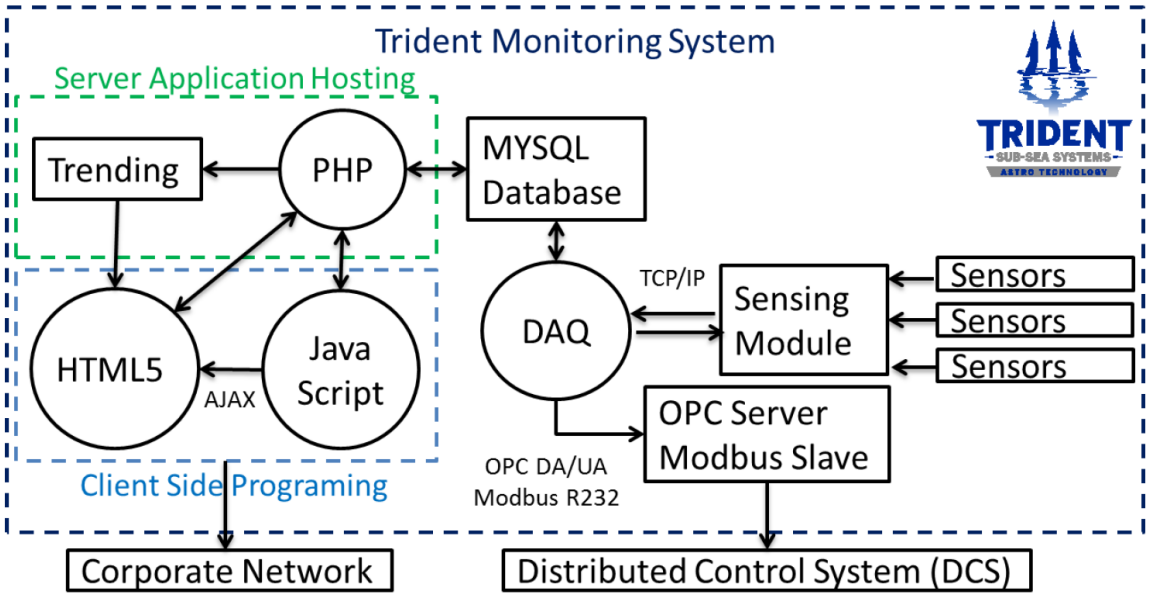

Figure 3.1: Monitoring system.

An innovation from this project is the data processing that converts raw wavelengths into actionable information by ballasting operators or by a computer control system. The flow of information is done with software interfaces that allow computer and human interaction. Figure 3.2 shows the load trend of the four tendons on the Echo platform from the data acquisition web in-

terface. As it is shown, loads calculated using fiber optic sensors are very sensitive to the wave effects.

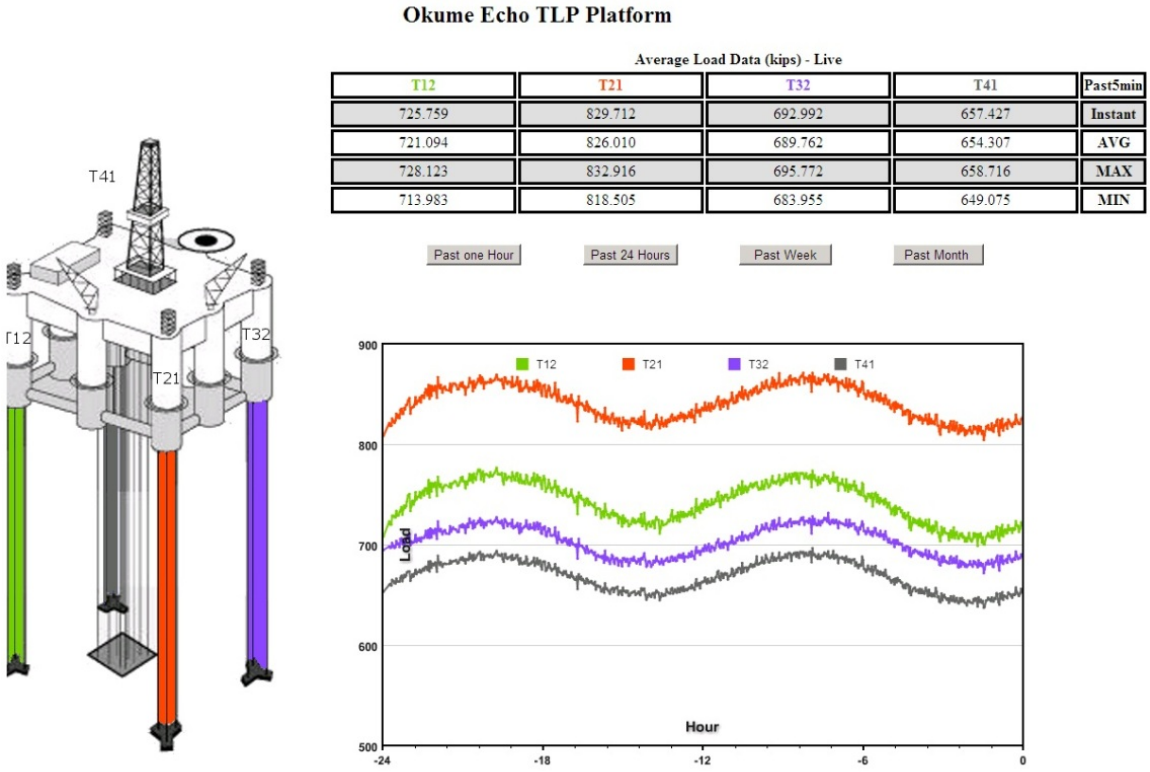

Figure 3.2: Load trends of Echo platform tendons.

Strain Calculations

Changes in strain at the fiber Bragg grating (FBG) and along the fiber optic line cause the frequency of the peak λ_b to shift by $\Delta\lambda = \lambda_b - \lambda_0$ which is used to calculate strain and ultimately the load. The thermal expansion causes a change in micro-strain ($\mu\varepsilon_T$) that is the strain induced by thermal expansion differences between the sensor and the test article and depends on the coefficient of thermal expansion for the strain sensor (CTE_S), the coefficient of thermal expansion for the test article (CTE_T), the shift in wavelength from the nominal value ($\Delta\lambda$), the nominal wavelength (λ_0), and the temperature sensitivity that relates changes in wavelength to changes in micro-strain (S_T). The strain sensors are sensitive to temperature changes and include temperature compensation due to changes in material thermal expansion as

$$\mu\varepsilon_T = (CTE_S - CTE_T)\frac{(\Delta\lambda/\lambda_0)_T}{S_T} \tag{3.1}$$

and thermal sensitivity of the fiber optic cable as

$$\mu\varepsilon = 10^6[\frac{(\Delta\lambda/\lambda_0)_S - (\Delta\lambda/\lambda_0)_T}{F_G}] - \mu\varepsilon_T \tag{3.2}$$

One of the most important advantages of FBG sensors is the direct relation between the Bragg wavelength and the fiber strain, which makes absolute measurements of the strain possible. The shift in the Bragg wavelength ($\Delta\lambda$) is observed and related to strain $\mu\varepsilon$ in Equation 3.2. Equation 3.2 is the basis for the strain and load measurements used in this analysis. The source of temperature compensation $(\Delta\lambda/\lambda_0)_T$ is a series of FBGs on the fiber optic line that is not purposefully attached directly to a surface although bonding to the polyurethane coating may occur. In this disconnected condition, only fluctuations in load affect the probe location because the temperature effects are removed. The deformation due to changes in load produces a strain in the tendon wall. Using Hooke's law and compensating for temperature, a load is calculated from the strain data according to

$$F = \mu\varepsilon\, E\, A \tag{3.3}$$

in which E is the Youngs Modulus and A is the cross-sectional area of the test article. The load F is monitored in units of $kips(= 1000lb_f)$ on the TLP to ensure that the pilings are not pulled out due to over-pull or the connectors are not unlatched due to under-tension. The load monitoring is especially critical during drilling rig loading and movement across the platform where up to a million pounds of additional weight is supported.

3.3.2 Model Development

There are several main sources that dynamically change the stability of an offshore oil platform. Among those, drilling operation, boat docking, tidal action, tropical squalls, ocean waves, and the crane movement can be mentioned. Currently, the balancing of offshore platforms is done manually through ballasting operations. Inability to maintain platform stability in the face of large

disturbances has led to platform damage (e.g. Thunderhorse platform 2005) [81]. Adding a control of upstream platforms can prevent unwanted incidents and ensure personnel safety. For this purpose, a model predictive controller is proposed to maintain the platform stability. It is suspected that this previously was not implemented because of the unreliability of the measurements (i.e. load cells). An enabling part of this research is the use of fiber optic sensors to replace the load cell measurements. The load data collected from the fiber optic sensor measurements validate a model to balance the platform stability. Model forms such as empirical (e.g. artificial neural networks) and first principles (e.g. structural load location information) will be investigated as part of this research. A model for the TLP platform balance is introduced in this section and is used to simulated thee TLP platform. Load on each leg is a combination of TLP Platform weight ($L_{Platform}$), buoyancy effect ($L_{Buoyancy}$), load due to wave action (L_{Wave}), tide action (L_{Tide}) and the load due to the water ballast tanks (L_{Tank}) as

$$L_{Total} = L_{Platform} + L_{Tank} - L_{Buoyancy} - L_{Wave} - L_{Tide} \tag{3.4}$$

L_{Wave} and L_{Tide} are treated as an input disturbances and L_{Tank} is calculated from Equation 3.5:

$$Load_{Tank} = \rho g V \tag{3.5}$$

In which V represents the tank volume filled with water, ρ is the water density, and g is the gravitational constant. The dynamic change in water volume can be related to the water flow rate through the equation

$$\frac{dV}{dt} = q_{in} - Z\,\alpha \tag{3.6}$$

where q_{in} is the seawater flow into the tank, z is the opening percent of the ballast tank discharge valve and α is a factor determining the size of the ballast tank discharge valve.

To calculate the buoyancy effect, the fraction of the platform that is under water needs to be determined. To do this, a force balance is derived based on

$$x_B = (L_{Tank_A} + L_{Platform} - L_{Wave} - L_{Tide} - K * L_{Tendon})/(L_{Platform}), \tag{3.7}$$

Where, x_B represents the fraction of the platform that is under water, $V_{Platform}$ represents the total volume of the platform, K is the stiffness factor of tendons, L_{Tendon} is the length of the tendon, and ρ_{water} is the water density.

The effect of wave and tide actions are modeled as sinusoidal functions. Wave load has a small cycle time (about 1 minute) and load magnitude. The tide effect has much higher cycle time (6 hours) and load magnitude

$$L_{Wave} = A_{Wave} \sin(B_{Wave} * time) \tag{3.8}$$

$$L_{Tide} = A_{Tide} \sin(B_{Tide} * time), \tag{3.9}$$

where A_{Wave} and A_{Tide} determine the magnitude of the wave and tide forces while B_{Wave} and B_{Tide} determine the frequency of the the wave and tide actions.

3.3.3 Control Scheme

Equation 2.4 along with Equations 3.4 through 3.7 are used to design a general nonlinear controller for stabilizing this class of platforms. The manipulated variables are the water flow rate flowing into the ballast tanks along with the discharge valve positions for each ballast tank. Wave and tide actions are treated as disturbance variables. The Model Predictive Controller (MPC) is used for the platform balance automation. When the rig is out of balance or there are anticipated load disturbances, the control system attempts to balance the platform by driving the load values to their required set point. For this purpose the controller decides whether the load change effort should be done through turning on and increasing the pump flow rate or through opening the discharge valves of the ballast tanks as follows:

- If the tide is rising, the controller pumps the water to the ballast tanks and keeps the discharge valve closed until the required load is achieved.
- If the tide is falling, the controller turns off the pumps and decreases the volume of water in the tank by adjusting the discharge valve opening.

The control variables are the four load values obtained from the monitoring system on the four tendon legs. The schematic diagram for the data acquisition and control system is shown in Figure 3.3.

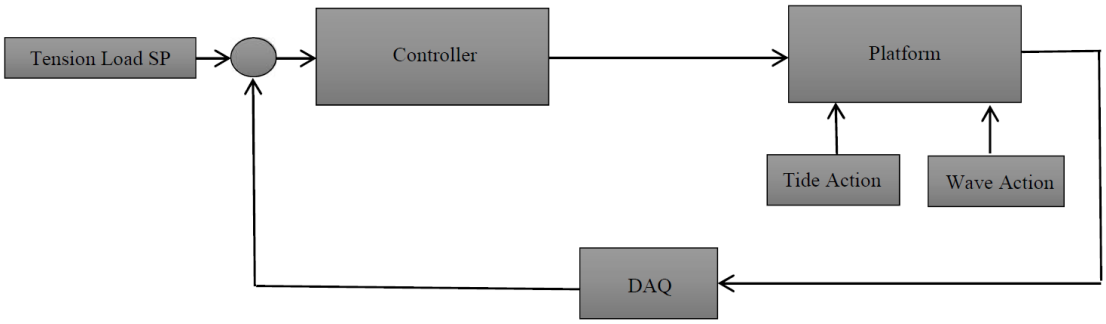

Figure 3.3: Data acquisition and control scheme for the load balance system.

3.4 Results

The first part of this section (3.4.1) presents the results from tests performed on the FBG sensors. Next section (3.4.2) and monitoring system performance results after being installed in the real environment. The last part of this section (3.4.3) includes the results from developed control system for ballast operation automation. The controller is tested in a simulation. All the tests related to monitoring system are experiments conducted at Versabar, Inc. and all the tests related to control system are simulations.

3.4.1 Fiber Optic Sensor Tests

The goal of FBG sensor testing is to qualify the post-installed monitoring system for field service. In addition to the fiber optic sensors, four resistive (conventional) strain gauges were attached directly to the test articles. The strain gauges were oriented to measure uniaxial strain on the two 36 inch specimens. The location of the sensors was in a region near the fiber optic strain gauge section so as to produce nearly equivalent results. The location matched the strain field of that analyzed (by finite element analysis performed by a third party) for the mid pipe section

containing the fiber optic sensors. The strain gauges were placed at 0, 90, 180, and 270 degree azimuth to detect all of the bending modes and stress and compression of the article. The fiber optic sensors included temperature compensation to correct the raw wavelengths in the calculation of strain. To ensure valid test results, a constant temperature environment was attempted during test runs. For any variation in the temperature, a continuous record of the temperature was collected during testing to provide temperature compensation for the sensors and data acquisition variations. Sensors were placed in pairs and positioned to avoid overlap of the peak wavelength values. As the strain increased, the peak wavelength associated with the strain gauge increased and the strain decreased when the strain dropped. The position of the unstrained peaks was chosen to avoid possible overlap of the peak values during normal operating ranges.

Point Bending Test

In the bending test, the sample pipe was pulled from both ends at 280 kips (1 kip = 1000 lbs) and was held for 5 min, resulting in a bending force in the sensor locations. The 4-point bending test was performed on the test article as shown in Figure 3.4. The pipe was placed in the test fixture and tested with pipe at 0 degree azimuth facing up. The test was then repeated with rotated pipe and at 90, 180, and 270 degree azimuth after cycles of that lasted approximately 15 minutes.

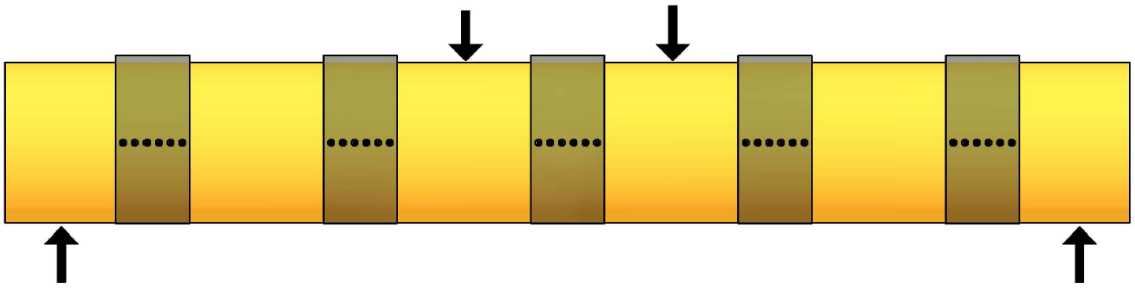

Figure 3.4: Bending test with loads at four points.

A direct comparison between the fiber optic sensors and resistive strain gauges shows excellent agreement, as shown in Figure 3.5. It is noted that an error in the software configuration caused the 270 feet sensor measurement to report bad values during the last of four bend tests on

the fourth subplot. It is also noted that the strain recorded by the FBG sensor was less than that recorded by the resistive strain gauges. This occurs because the clamp serves as an extensometer to transfer strain from the pipe to the FBG sensors and as a result, the FBG sensors do not measure the actual strain directly. In the case of the compression and tension testing, an additional fiber optic sensor was attached directly to the surface of the pipe for verification purposes.

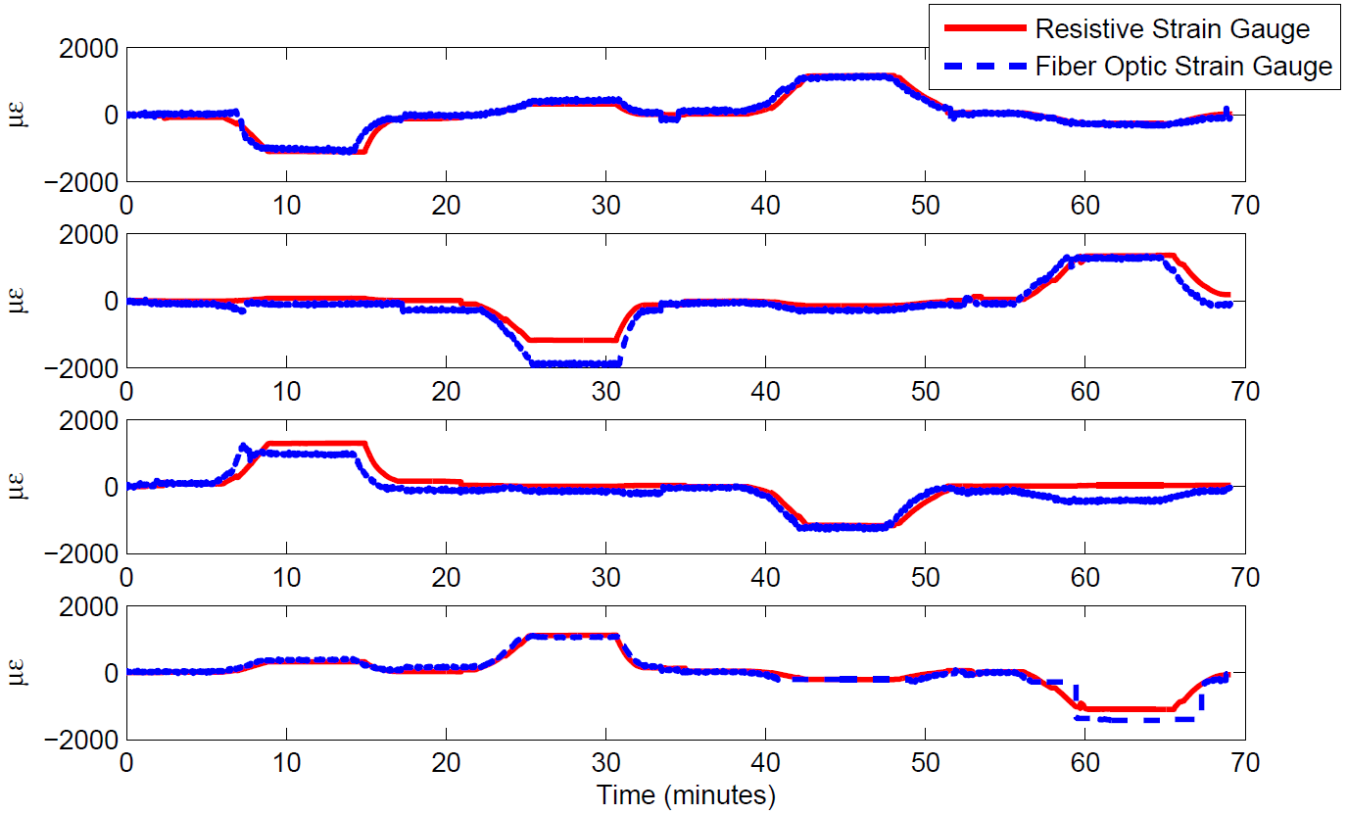

Figure 3.5: Results of the 4-point bending tests with resistive and FBG sensors.

One aspect of the comparison was the time stamping of the data acquisition so direct measurement comparisons could be made between the fiber optic gauges and the resistive gauges. Without the time stamps, the resistive strain gauge data at four points were synchronized for the results provided by each test article by aligning the leading edges of the initial peaks.

Tension Test

Tension loading was achieved by pulling the test article in uniaxial tension to a strain level of 70% of yield stress in tension. The strain levels were recorded and repeated through a number of cycles with equivalent strain level in compression (see Figure 3.6). The tension cycle was repeated for a total of ten cycles for a slow rate of change followed by ten cycles of a fast rate of change. Testing was conducted at a strain rate of one inch per minute and then at the completion of the cycle tests, strain values were recorded. Any relaxation effects were observed by recording the data for one hour following the stress and compression tests. The final values after the stress relaxation were then compared to the data from pre-testing. The entire test sequence was repeated again with a reduced strain rate of 0.1 inch per minute which is referred to as the fast rate of change tests. In both tension and compression tests the load was increased up to 1000 kips and was held up to 5 min. Each experiment was repeated 10 times to ensure data consistency and to validate the sensor robustness for large cycles in the strain. Both tension and compression tests were performed in fast and slow rates. Results for the tension testing are shown in Figure 3.6 All sensors showed some level of inelastic deformation due to the polyurethane coating used in the bonding and coating process.

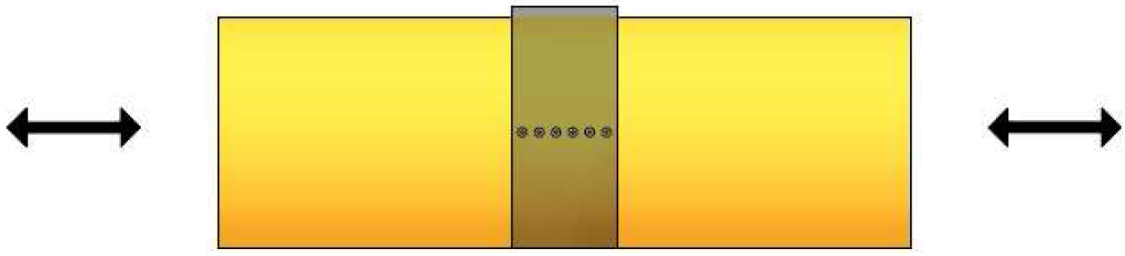

Figure 3.6: Tension testing with slow (1/min) and fast (0.1/min) rates of change.

A comparison with the unbounded sensors in the fourth subplot of Figure 3.7 reveals that there is some hysteresis when compared with the pipe-bonded sensors. For sensors installed with a polyurethane coating, this implies that there is a settling period where the sensors may need to be recalibrated after initial cycles of operation. The recalibration is built into the software design to allow for adjustment of both the absolute load as well as the sensitivity of the load measurement

to changes. To avoid recalibration concerns, a protective lubricant was applied to the sensors to prevent bonding of the sensors to the viscoelastic polyurethane encasement. This modification is expected to show improved performance for the sensor clamps installed on the TLP. The sensors returned to pre-load conditions after the compression load was released demonstrating the ability of the sensors to withstand loads at least up to 70% of failure. The extensometer configuration of the clamps and polyurethane coating caused a slight lag in the strain readings during the load and relaxation periods. Note that the strain values continue to slightly decrease during the plateau period. The load sensitivity and relaxation time is nearly immediate for the resistive and FBG sensors attached directly to the pipe.

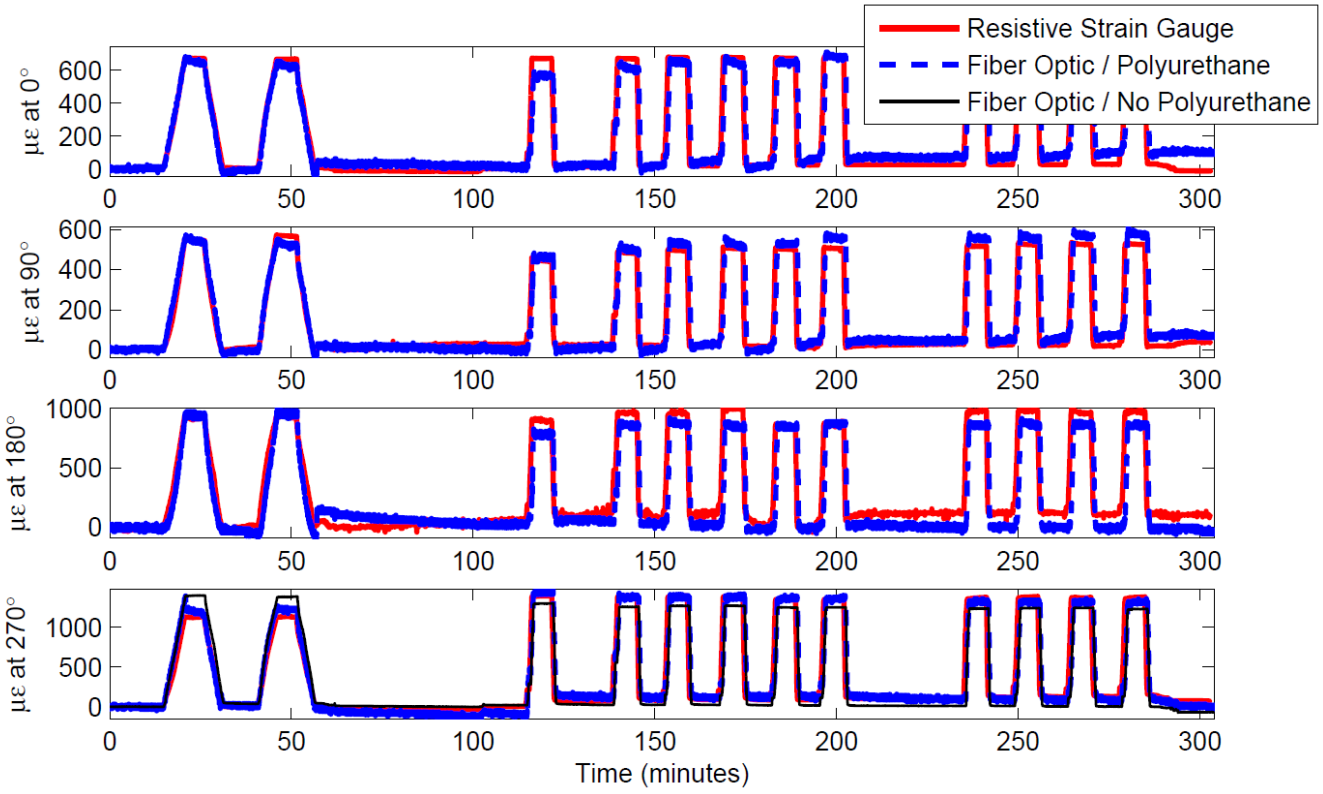

Figure 3.7: Fiber optic and resistive strain gauge under repeated tension load cycles.

Compression Test

Compression loads were achieved by pushing the test article in uniaxial compression to a strain level of 70% of yield stress in compression. The strain levels were recorded and repeated through a number of cycles with equivalent strain levels at the tension tests. The compression cycle was also repeated for a total of ten cycles for first a slow rate of change followed by ten cycles of a fast rate of change. Testing was conducted at a strain rate of one inch per minute and then, at the completion of the cycle tests, strain values were recorded. Any relaxation effects were observed by recording the data for one hour following the stress and compression tests. The final values after the stress relaxation were then compared to the data from pre-testing. The entire test sequence was repeated again with a reduced strain rate of 0.1 inch per minute for the fast rates of change. As expected, the resistive strain gauge reading became negative during the compression testing as well as the FBG compressive readings on each of the four sensor stations as observed in Figure 3.8.

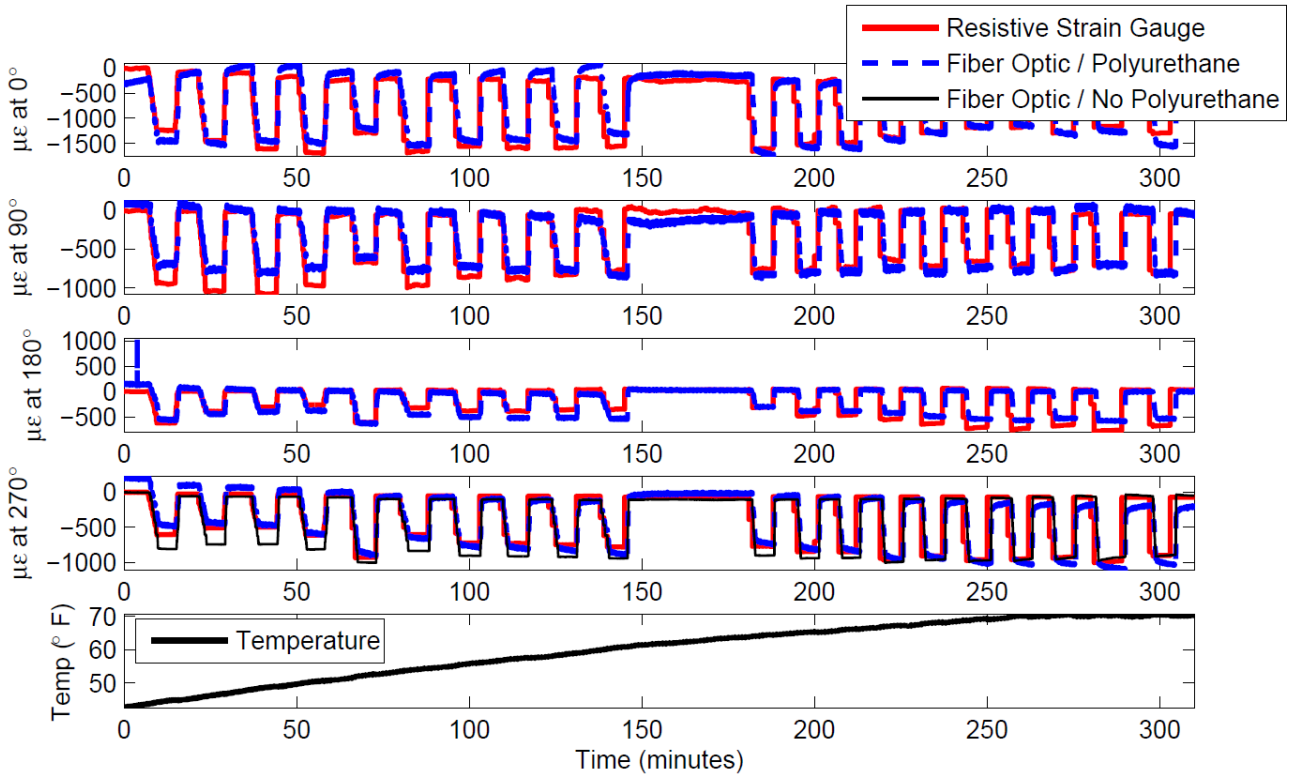

Figure 3.8: Fiber optic and resistive strain gauge under repeated compression load cycles.

The fast and slow rates of compression load had little effect on the outcome of the sensors that were attached directly to the pipe. The fast compression cycles did have a more pronounced effect on the clamp sensors with polyurethane coating as shown in Figure 3.8. These tests reveal that the installed sensors will have varying levels upon initial installation due to their configuration as extensometers of strain. After calibration, the sensors will be adjusted to report the same base-line level of load and have equal sensitivity to load changes. It appears that these calibration values cannot be predicted a priori but likely depend on a number of factors related to construction and installation. Regardless of the rate of strain, it was observed that the sensors responded nearly the same in the two cases. The figures show relaxation to original values after each cycle and the need for calibration when initially installed. The sensors showed good repeatability and relaxation to original values. Load values obtained from the fiber optic sensors were compared with the ones from conventional strain gauge sensors. Good agreement was found between the two data sets with the multiplication factors to account for the polyurethane extrusion effect. To check the polyurethane extrusion effect on the data reading, a sensor set was attached to the pipe body without the protection of external coating material. The results in Figure 3.8 show that the aforementioned sensor set is much more sensitive over external forces than the ones encapsulated in the polyurethane which require a multiplier factor. It was concluded that installation on external clamps and encapsulating the sensors in polyurethane decreases the strain sensor sensitivity over external forces. To overcome this, a multiplication factor was added to the calculations and its optimal value was found from the aforementioned tests. This additional factor compensates for the extensometer nature of the clamp including the polyurethane effect by increasing sensitivity of the load values due to changes in the wavelength values. After the installation of the fiber optic strain sensors, the gauges will be calibrated with historical and current available values from operating load cells before the aging system is replaced.

3.4.2 Monitoring System Results

This section includes results from a monitoring system that was installed on a tension leg platform. The laboratory validations are discussed previously.

Subsea Sensor Calibration

Post-installed sensors require a unique calibration approach based on two issues. The first issue is that installation causes slight variations in the baseline strain values as the clamp is secured to the structure. Because of the strain induced during installation, the sensor baseline or zero-state cannot be calibrated before installation. This leads to an interesting challenge because the baseline value must be obtained from a known state. In most situations, an alternative measurement is either not available or not trusted for calibration of the sensors. A second issue for sensor calibration is in the sensitivity of the sensor because in most instances the sensor is unable to make direct contact with the item of interest. To make the fiber optic sensors robust to subsea installation, the delicate fiber optic sensors are protected in a sensing device designed to withstand the harsh environment and typical equipment handling found on offshore rigs. Therefore, changes in strain observed at the sensor may be less than actual strain changes on the structure. As long as the correct sensitivity is known, the conditioned sensor reading can report the actual changes, not just the changes at the sensor. The fiber optic is therefore calibrated with two parameters α and β as shown in

$$\mu\varepsilon_S = \alpha\mu\varepsilon_F + \beta \tag{3.10}$$

Equation 3.10 relates measured strain, $\mu\varepsilon_F$ to calibrated strain, $\mu\varepsilon_S$. Methods were developed for both accurate baseline and sensitivity calibration based on testing where 3 inch pipe samples were raised to 70% of failure in both compression and tension tests over multiple cycles. The correlation of Equation 3.10 is valid over repeated loading cycles and nearly to the point of inelastic deformation. The results of this calibration were then used to obtain approximate baseline values for the tendon tension monitoring system on the TLPs of West Africa. Once the clamps were installed, the load management system was used to approximate loads based on position and approximate weight of all objects on the platform, including loads of risers and buoyancy induced by tidal fluctuations. The sensitivity of the sensors was calibrated from the high and low peaks of the tidal fluctuations as shown in Figure 3.9 [72]. Time averaged values were used over a 5 minute horizon to eliminate the 4-8 second period for the wave action and natural platform harmonics.

In the absence of known environmental disturbances, a movement of ballast on the platform would have been required to calibrate the range or parameter α. Once the sensitivity value was set,

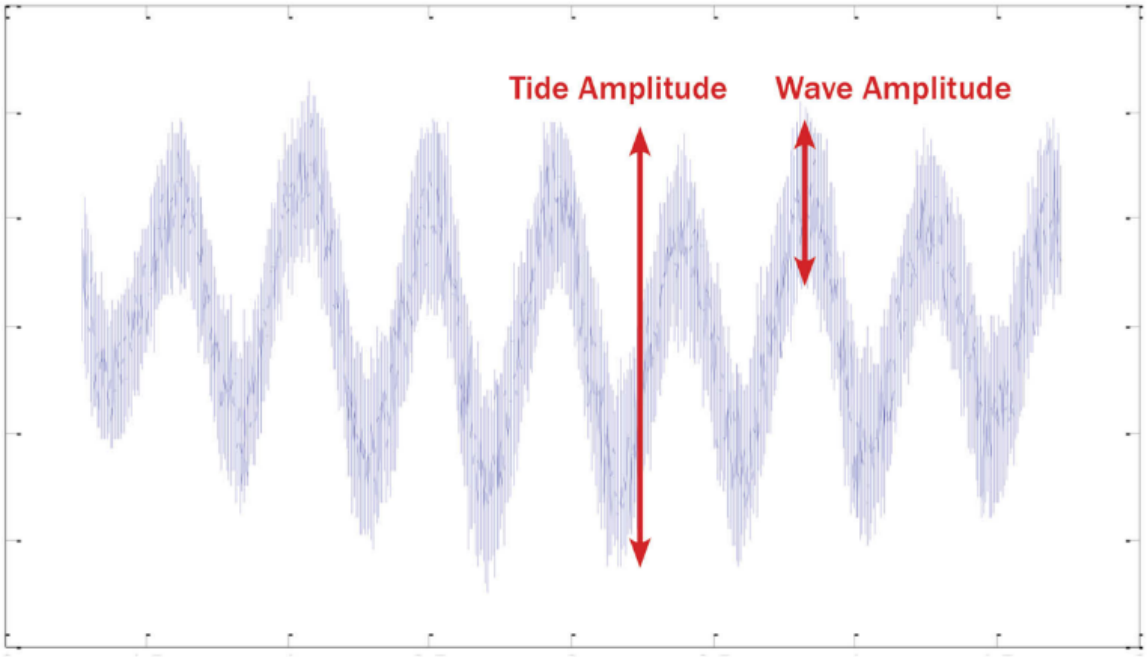

Figure 3.9: Tide action amplitudes for calibration of sensor sensitivities.

an adjustment to was made to remove the installation induced strain and calibrate to a baseline value. This process was repeated over a week to verify load measurement accuracy. Another challenge with this particular installation is that the first sensor station was installed at 60 feet depth at the location of a thermocline. The depth of the thermocline moves above and below the sensor station, sometimes multiple times per day and has an abrupt 4^oC change between the warmer and well-mixed waters above and the cooler deep water below. Without temperature compensation, this would cause a false apparent shift of several hundred kips. This temperature change effect was isolated and eliminated using a compensation technique. Because the temperature compensation sensor and the strain sensor were separated by approximately 3 cm, the strain values were kept largely free of temperature effects, however, there was some observed shift. Future clamps on TLP tendons or risers will be placed away from known thermocline areas if possible.

Post Installation Sensitivity of Data Acquisition System

A few other events observed after the installation of the tendon tension monitoring system were boat docking events, squall effects, crane movement, or other operations on the platform.

Notable ones have a noticeable lift on two of the tendons and a decrease on the load for the tendons on the opposite side of the platform. During the squall event, the tendons were trending up as the tide was increasing. During the boat docking event, the back of the boat was applying a lateral force to the platform as the reverse thrusters kept the boat up against the docking platform. In both cases, the sensitivity of the sensors allowed the operators to observe events that were previously undetectable.

Thermocline Effect

One of the unexpected issues after installation was the presence of a thermocline at the 60 feet sensor locations. This thermocline is the transition layer between surface and deep water levels. This level regularly moves up and down due to changes in the currents, tidal action, and other environmental factors. The change in temperature required the use of temperature compensation of the strain sensors. The changing temperature profiles were measured and analyzed at this moving boundary. A method to isolate temperature effects from structural data was developed and integrated into the software algorithm. In order to do this, the sensors that are subject to thermocline effects were identified and excluded from the temperature and strain calculations.

3.4.3 Automated Load Balancing

A model predictive controller is designed based on Equation 2.5 with a cycle time of five minutes to balance the tension leg platform. Wave and tide action is assumed as disturbance variables while the ballast tank pump flow rates and discharge valve positions are considered the manipulated variables. The model equations for the controller include Equations 3.5 and 3.6 along with a load balance equations which contains a disturbance variable and is updated based on the measurements

$$L_{Total} = L_{Platform} + L_{Tank} - x_B(L_{Platform}) + disturbances \tag{3.11}$$

The initial conditions used for simulation of this case study is shown in Table 3.1.

Figure 3.10 shows the change in load values on a sample tendon without the controller. The effect of tide and wave actions can be seen. The load caused by the tide (+/- 50 kips (1 kip = 1000

Table 3.1: Initial conditions used in the simulation

Parameter	Value
Initial tank volumes, V (gal)	0
Initial discharge valve openings, Z $(\%)$	0
Initial water pump flow rates, q_{in} (gal/hr)	0
Platform weight on each corner , $L_{platform}$ (kips)	10000
Tank discharge valve constant, K (gal/hr)	100

lb_f)) is much larger than the wave effect (+/- 12 kips) and has a cycle time of about 6 hours. Wave loads are small and have a cycle time of about 7 seconds. For the purpose of this simulation wave action cycle time is assumed to be 1 minute.

The Figure 3.10 also shows the change in the load values with the controller turned on. As is seen, the controller is able to cancel out the tide effect by changing the pump flow rates and the valve positions. A high cost value was used in the objective function of the controller to encourage use of either the valve or the pump to control tank volume, but not both.

The change in the manipulated variables (ballast pumps and valves) over time is also shown in Figure 3.10. This figure shows that while the tide is falling (between about 0-2.5, 8-10 and 22.5-25 h), the valves open to decrease the water in the ballast tanks. When the tide is rising (between about 2.5-8, 10-22.5 h), the valves shut and the pumps turn on to fill up the ballast tanks as needed. This automated control scheme is not typical for floating platforms and ballasting operations is performed manually with a ballast control operator. In this case, the automation system replaces the manual operation to achieve continuous and improved control performance for enhanced platform stability. In addition to tide and wave action, equipment movement on the platform is also a major consideration during heavy lift operations or drilling rig movement. The proposed controller is the first application of model predictive control for automatic platform stabilization.

Figure 3.11 shows the change in tank volumes over time. It is this change in the volume of water in the ballast tanks that affects the buoyancy and the platform weight to maintain platform stability.

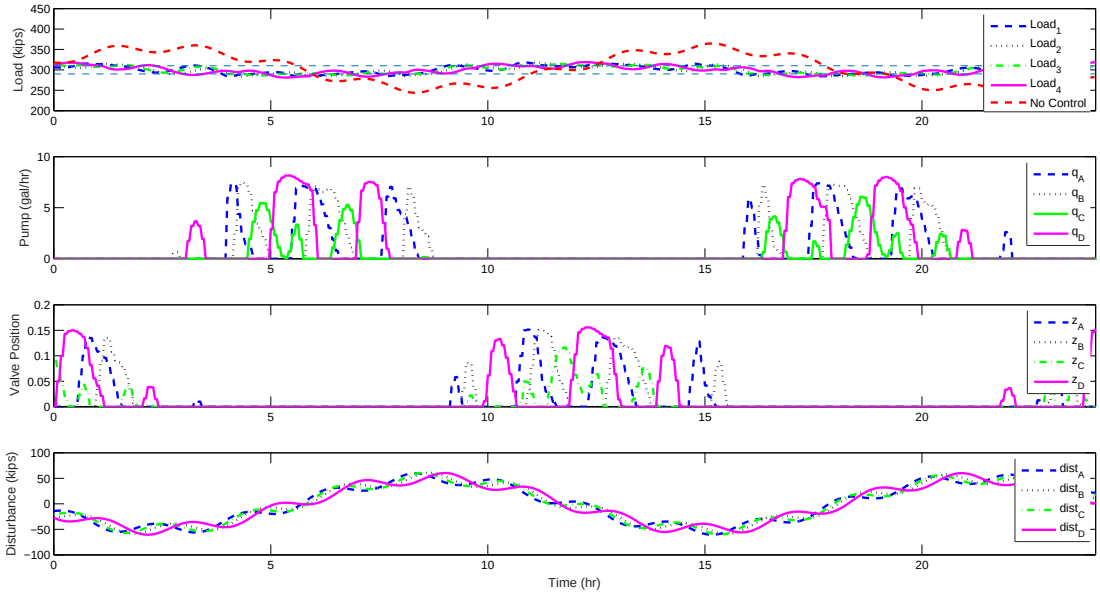

Figure 3.10: The change of loads, pump flow rates, valve positions and disturbance over time.

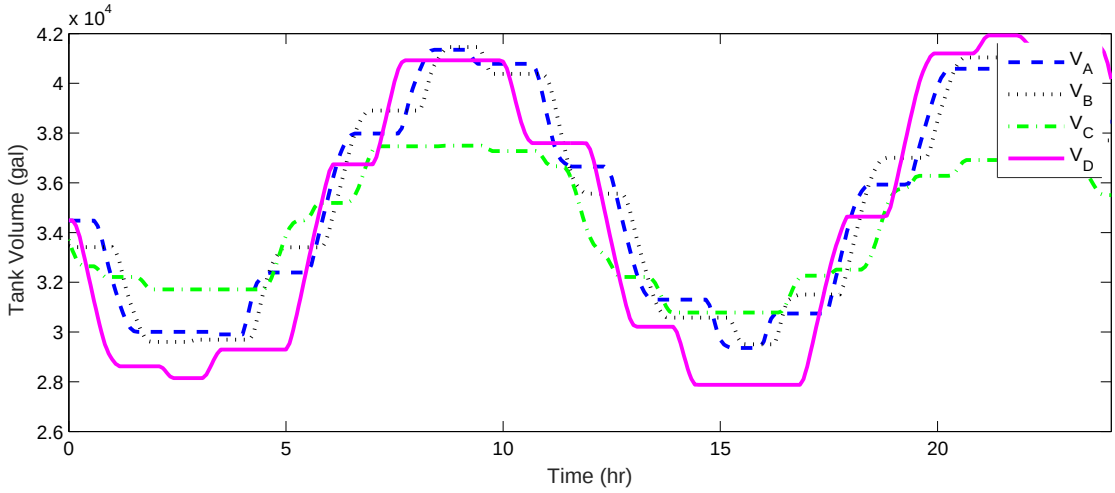

Figure 3.11: The change of ballast tank volumes over time.

As it is seen from Figure 3.10 the model predictive controller is able to successfully balance the platform and compensate for disturbance effects. This is the first time in upstream industry that an MPC application has been developed for TLP load balancing.

3.5 Conclusion

This chapter details current progress on subsea monitoring, and calibration of advanced sensors for post-install applications. These Intelli-field systems are a comprehensive monitoring solution to sense, predict, and respond immediately to anticipate issues before undesirable conditions arise. The objectives of this study are to extend the service life of equipment, gain new understanding of flow properties and dynamics, prevent unplanned downtime, and detect problems earlier and more accurately. These objectives are becoming increasingly important as operations move to deepwater and arctic regions. A control system was designed using the monitoring system which regulates each of the load values by manipulating the ballast water tank levels. The simulation results show that the controller and monitoring system are able to successfully control the loads and balance the platform.

CHAPTER 4. COMPREHENSIVE PRESSURE AND ROP CONTROLLER

Much of the content of this chapter are taken from the following reference [82, 83]:

- Asgharzadeh Shishsavan, R., Pixton, D., Eaton, A N., Park, J., Perez, H D. and Hedengren, J.D. and Craig, A., 2015. Addressing UBO and MPD challenges with wired drillpipe and model predictive control. Submitted to SPE Journal.
- Asgharzadeh Shishavan, R., Hubbell, C., Perez, H., Hedengren, J., and Pixton, D. S., 2014. Combined rate of penetration and pressure regulation for drilling optimization using high speed telemetry. Drilling and Completions Journal, Accepted for publication.

4.1 Introduction

Maintaining downhole pressure is a critical and difficult element of deepwater drilling. While conventional (overbalanced) drilling operations are suitable for some wells, effective conventional drilling can be more difficult in various deepwater drilling environments. This is particularly the case when tight windows of safe pressure levels are encountered. As such, managed pressure drilling (MPD) has become a successful technique for staying within the tight pressure margins necessary for increased safety and efficiency of deepwater applications. In light of increasing regulation, MPD allows for a more controlled environment without compromising economic payoff. This chapter proposes alternative methods of data transfer and modeling that would improve MPD methods and further increase the benefits they provide.

MPD for deepwater drilling has become more attractive with the development of advanced telemetry technologies. Previous MPD systems have relied on surface measurements and limited downhole information, which limits the response time of the system. However, wired drill pipe (WDP) telemetry is capable of high bandwidth communication that stands independent of fluid flow and rock formations [84]. By wiring each tubular in the drill string, sensors in the bottom-hole

assembly (BHA) and at other points along the string can return quality information quickly without degradation. This means that the controller is capable of receiving high-resolution information as soon as downhole conditions begin to fluctuate, resulting in faster kick attenuation and precise pressure management.

These new developments open the door for more sophisticated and accurate modeling schemes that allow for more rapid and intelligent automation. This automation can be achieved by an ideal controller that maintains both the rate of penetration (ROP) and annular pressure throughout drilling, even during kick events. Currently, ROP is treated as dependent on weight-on-bit (WOB) and revolutions per minute (RPM), while pressure is controlled only with choke valve opening and mud pump flow rate. These are typically implemented as independent controllers. However, in these models, the influences that RPM has on annular pressure as well as the influences that the mud pump flow rate and choke valve opening have on the ROP are modeled with disturbance variables, meaning these effects are essentially ignored. It is, therefore, proposed that a multivariate controller that uses WOB, RPM, choke valve opening, and mud pump flow rate as manipulated variables would be capable of simultaneously regulating ROP and annular pressure even faster than if approached separately. This simultaneous control scheme would not only improve the response time for kick attenuation, but would also avoid compromising ROP.

The purpose of the present study is to design a controller that relies on direct pressure measurements from wired pipe telemetry technology for both kick detection and attenuation. This novel controller is a continuation of previous work [5, 84, 85]) and it is capable of optimizing ROP while maintaining the bore hole pressure (BHP) at the desired level. This technique provides significant advantages to deepwater drilling by overcoming the challenges resulting from the significant delays in the surface flow rate measurements used to represent downhole conditions.

4.2 Literature Review

This section provides background information and prior work in the area of automation for upstream drilling. The main goal of this research is to integrate the borehole pressure, drill string pressure, and rate of penetration controllers together. The background section is divided into three

parts: 1) borehole pressure control, 2) kick detection and attenuation and 3) rate of penetration control.

4.2.1 Borehole Pressure Control

Pressure is an important factor in determining the success of a drilling process into a formation. The development of a model-based solution consists of three components: 1) the model, 2) the controller, and 3) the observer or estimator. Process control research publications typically make contributions in one or more of the before mentioned components. Therefore, the review of prior work in borehole pressure control details the different approaches used by researchers in developing models, controllers and observers.

Modeling

To design controllers and observers for drilling, a model of the system is needed. Different approaches have been used for deriving and using the drilling models. They are generally categorized as detailed models, lower order models, or empirical models. Detailed models consist of multi-component, multi-phase equations derived using momentum and mass balance principles which come in the form of partial differential equations [86, 87]. Detailed models are typically computationally expensive to solve, making them more difficult to use for control purposes. However, some researchers have used the detailed models to validate the performance of their controllers due to the lack of experimental data [86, 88, 89].

Lower order models capture the main dynamics of the drilling wells. They are developed based on the assumption that the well consists of two compartments with different dynamics; the drill string and the annulus. The interaction between these two compartments is modeled using mass balance and pressure balances [86, 87, 90]. In addition to mass and pressure balances, closure relations between masses, flow rates, and pressures are further developed. Two types of lower order models have been utilized in the literature. These are the one phase flow model, which only assumes one phase, and the two phase model, which assumes gas and liquid phase throughout the drilling well. The two phase flow model was developed by Nygaard et al. and has been used in various studies [86, 90–93]. Controllers and observers derived using this model can regulate the

downhole pressure and estimate the measured states closely to the real data or the data derived from the detailed models [86, 93]. A one phase flow model was originally developed by Kaasa et. al [94] and Stamnes et. at al [95]. Although the single phase flow model has some simplifying assumptions, it captures the system dynamics relatively well. The single phase flow model is the most widely used model in the drilling control studies because of robustness [96–112]. It has been shown that controllers and observers designed based on this model are capable of capturing the main dynamics of the system with sufficient accuracy compared with real systems on a full scale drilling test rig [96]. Other than lower order models, some researchers used the same approach in modeling fluid flow through pipe segments and approximated the system with a first order model. The results showed that the empirical models are able to accurately describe the dynamics to fit the real or simulated data [87, 113, 114].

Controller

The goal in designing the control scheme for the drilling process is to maintain the downhole pressure in a normal drilling operation range. Different types of controllers have been used in the literature. Most of the pressure control research has taken advantage of linear controllers. Among those, PI [107, 112, 114], internal model controller [114, 115], fuzzy logic controller, backstepping controller [100], feedback controller [96–99, 101, 104, 109, 111], and linear model predictive controller (MPC) [114] can be mentioned. While able to control the borehole pressure, the efficiency of linear controllers can be further improved using nonlinear controllers. Nonlinear model predictive controller [86, 113], adaptive nonlinear controller [102, 106–108, 110], and Nonlinear Output Regulation Controller [115] have been developed by some researchers for pressure control in oil well drilling. A nonlinear model predictive controller is proposed in the current research.

Observer Design

This section gives a brief overview of the existing estimation/observer designs for borehole pressure control found in the literature. Table 4.1 gives a brief overview of the observer types and estimated variables used in the literature to indirectly infer the bottom hole pressure.

Table 4.1: Overview of Observer Type and Estimated Variables Used in the Literature

Author	Observer Type	Estimated Variables	Purpose
Zhou et al. [100]	nonlinear adaptive observer	drill bit flow rate - annulus friction factor annulus density borehole pressure	MPD Control
Hauge et al. [98]	adaptive observer	pump and choke valve pressures drill bit flow rate choke valve flow rate - magnitude and position of the kick	MPD control and kick mitigation
Zhou et al. [111]	adaptive observer	drill bit flow rate annulus flow rate reservoir influx flow rate - reservoir pore pressure	MPD control and kick management
Zhou et al. [101]	adaptive observer	drill bit flow rate annulus friction factor annulus flow rate bottom hole pressure reservoir influx	DGD control and kick management
Nygaard et al. [113]	unscented Kalman filter	drill string friction factor annulus friction factor choke line well head friction factor mud compression	MPD control
Zhou et al. [112]	adaptive observer	bottom hole pressure drill bit flow rate	MPD control
Breyholtz et al. [110]	adaptive observer	drill string and annulus friction factor drill string and annulus density bottom hole pressure	MPD control
Nygaard et al. [91]	Kalman filter, ensemble Kalman filter, unscented Kalman-filter	reservoir production index	Underbalanced Drilling
Siahaan et al. [87]	custom built nonlinear observer	bottom hole pressure	Conventional Drilling
Zhou et al. [104]	adaptive observer	drill bit flow rate reservoir influx reservoir pore pressure	MPD control and kick management

Nazari et al. [93]	unscented Kalman filter	drill string bottom pressure annulus bottom pressure mixture velocity of drill string and annulus	MPD Underbalanced drilling control
Imsland et al. -2012 [116]	adaptive observer	drill bit flow rate- Drill string and annulus friction factors bottom hole pressure	MPD control
Stamnes et al. 2011 [105]	adaptive observer	drill bit flow rate drill string and annulus friction factors	MPD control
Stamnes et al. [103]	adaptive observer	annulus friction factor and density drill bit flow rate	MPD control
Zhou et al. [106]	nonlinear adaptive observer	drill bit flow rate annulus friction factor reservoir influx	MPD control
Stamnes et al. [117]	adaptive observer	drill bit flow rate annulus friction factor	MPD control
Li et al. [107, 108]	adaptive observer	drill bit flow rate bottom hole pressure	MPD control
Zhou et al. [102]	nonlinear adaptive observer	drill bit flow rate - annulus friction factor	MPD control
Zhou et al. [109]	adaptive observer	bottom hole pressure reservoir influx drill bit flow rate reservoir pore pressure	MPD control and kick management

Distributed Pressure Control

Researchers have designed controllers assuming that downhole pressure measurements, located in a wellbore (a hole that is drilled) than at the Earth's surface are not available for control [86, 90, 99, 115, 118]. Conventionally, the downhole pressure signal is streamed through the mud pulse, which limits the bandwidth significantly [110]. Because of lack of high speed data com-

munication network, most researchers have considered pump and choke pressures as the control variables and attempted to control the downhole pressure indirectly through estimating the downhole pressure value [97, 100–103, 105–108, 110, 112]. So far, the indirectly controlling downhole pressure through estimating its value has been considered more realistic among researchers due to the unavailability of the sensors to be used for control purposes. Recently a new sensing system, namely wired pipe technology, has been introduced for drilling that uses high speed bi-directional telemetry (operating at 57,600 bits/sec) [119]. This technology makes it possible to measure the pressure both at the borehole and along the annulus and utilize it for control purposes. There are very few academic articles published based on this novel technology. Vajargah et al. [120] developed a simulator which relies on identifying and modeling the flow regions in the annulus using conservation of mass and momentum equations. They used a numerical scheme and a transient gas simulator for solving the model and detecting kicks. They claim that the proposed simulator can contribute to well control practices but it is not a controller itself. Gravdal et al. [121, 122] have developed a methodology to maintain pressure within desired bounds during kick events, capitalizing on the wired drill pipe technology. The proposed methodology estimates the formation pore pressure value using pressure build-up curves to find the kick size [121] distribution and depth of influx [122]. However they did not use an observer and utilized a PI controller which is a conventional controller and is not based on the process model. MPC, proposed in this work, has advantages for multivariable problems and is chosen to extend the prior studies.

4.2.2 Kick Detection and Attenuation

Research on kick management can be divided into studies on kick detection methods and studies on kick attenuation methods. Regarding kick detection studies, Hargreaves et al., developed a detector system that uses Bayesian probabilistic framework on the surface for kick detection [123]. Techniques like Micro-Flux Control (MFC) [124], adaptive observer [100,111] and dynamic neural network of surface data [125] have also been used in the literature. An early kick detection method based on ultrasonic with Doppler Effect was proposed by Zhou et al [126]. Hauge et al. used a PDE model of the hydraulic system and the method of backstepping to design an observer that detects and quantifies any in- or outflux [97]. Gravdal et al. have developed a technique that uses distributed pressure measurements from wired pipe telemetry system (other than flow

measurements) as a kick detection methodology [127]. Regarding kick attenuation techniques, Zhou et al. designed a switched controller that is based on estimated downhole pressure and bit flow rate values for kick attenuation for dual gradient drilling [101] and managed pressure drilling [104, 109, 112]. The objective of this controller is to regulate the pressure and flow rate during normal drilling conditions, but switch to pure flow controller when a kick happens. A pure flow controller that relies on estimated bit and influx flow rates was used by Hauge et al. [98]. This controller is also able to locate the gas influx location. Carlsen et al. have developed three different controller types: PID, internal model controller (IMC), and a linear model predictive controller. They have evaluated the performance of these controllers in three main well control steps, which include shut-in, pump start-up and circulation during unwanted gas influx occurrence [114].

4.2.3 Rate of Penetration

The main goal of this research is to design a comprehensive controller to maintain borehole pressure, drill string pressure, and ROP simultaneously in a comprehensive controller. To the author's knowledge, no academic paper has been published on this type of comprehensive controller. One study demonstrates control of borehole pressure and hook position while manipulating mud pump, subsea pump flow rates and drill string velocity [118]. However, this study does not attempt to combine ROP maximization. The literature on borehole pressure control has already been reviewed in the previous section. This section will give a brief background on ROP and the factors that affect it.

The relationships between drilling parameters are complex, but finding the optimum value of the parameters that have significant effect on the drilling rate can effectively contribute to minimizing the cost of drilling by increasing the rate of penetration. It is a hard task to find and model the major variables' effect on the rate of penetration [128]. For this reason, accurate mathematical models capturing all of the possible effects on rate of penetration have not been suggested yet, but researchers have tried to include the known relationships in their proposed models. These suggested models usually try to find the optimum value of the weight on the bit (WOB) and rotary speed of the bit with the goal of achieving the minimum drilling cost.

Among the factors having an effect on rate of penetration, reservoir properties are considered to be uncontrollable, while hydraulics, weight on the bit, and rotary speed are considered controllable.

Although drilling fluid properties and bit type have an effect on the rate of penetration, they are considered to be almost constant in every bit run; therefore, they are not considered as manipulated variables [129].

The empirical drilling rate equations based on the accumulated and statistically processed data are more desirable in the drilling optimization than the implicit relations [130]. It has been shown that using a simple rate of penetration model can reduce the cost of drilling by at least 10% [131].

Many rate of penetration models have been suggested in literature over the past years. Among them, the Bourgoyne and Young [95] model is the most common method in the industry because it is based on the statistical synthesis of past drilling data [130]. This model has been used in previous studies to find the best value of WOB and rotation speed for ROP real time optimization [99, 132, 133]. This empirical modeling approach will be reviewed and improved in this research.

4.3 Modeling

In this section, the equations that are used to model the different dynamics for the comprehensive controller are discussed. The combination of all these models forms a comprehensive drilling model, which includes the interacting effects of pressure, ROP, RPM, and WOB.

4.3.1 Pressure Hydraulics

A lower order model, introduced by Stamnes et al. [103], was used to model the pressure dynamics of the drill string. This model was derived based on mass and momentum balances. It has had extensive usage among researchers and has also been tested on actual drilling rigs [96]. The Stamnes et al. model includes four state variables: Pump Pressure (P_p), Choke Valve Pressure

(P_c), Drill Bit Flow Rate (q_{bit}) and Drilling Height (h_{bit}). The dynamic equations of these state variables are shown in

$$\dot{p}_p = \frac{\beta_d}{V_d}(q_{pump} - q_{bit}) \tag{4.1a}$$

$$\dot{p}_c = \frac{\beta_a}{V_a}(q_{bit} + q_{back} - q_{choke} + q_{res} - ROP\, A_a) \tag{4.1b}$$

$$\dot{q}_{bit} = \frac{1}{M}(P_p - F_d|q_{bit}|q_{bit} + \rho_d g h_{bit} - P_{bit}) \tag{4.1c}$$

$$\dot{h} = ROP \tag{4.1d}$$

where q_{back}, q_{choke} and q_{res} represent back pressure pump, choke valve and reservoir gas influx flow rates respectively. V is the volume, A is the cross sectional area, β is the bulk modulus, ρ is the fluid density and F is the friction factor. M represents the lumped density per length, which is determined by Equations 4.1e through 4.1g. The subscripts "a" and "d" refer to annulus and drill string properties, respectively:

$$M_a = \rho_a \int_0^{l_w} \frac{1}{A_a(x)}\, dx \tag{4.1e}$$

$$M_d = \rho_d \int_0^{L_d N} \frac{1}{A_d(x)}\, dx \tag{4.1f}$$

$$M = M_a + M_d \tag{4.1g}$$

Equation 4.1a describes the pump pressure time derivative based on a mass balance about the drill string. Equation 4.1b determines the choke pressure time derivative from a mass balance about the annulus section of the well. Equation 4.1c models the rate of change of the drill bit flow rate from a momentum balance about the entire well, balancing the pressures on the drill string side with those on the annulus side. The second term on the right hand side of this equation describes the pressure drop effect due to fluid flow in the drill string and annulus.

The downhole pressure is determined from the following equation, which sums up all the pressure terms that contribute to the downhole pressure (static and dynamic)

$$P_{bit} = P_c + \rho_{ai} F_{ai} |q_{bit} + q_{res}|(q_{bit} + q_{res})h + \rho_a g h_{bit} \tag{4.1h}$$

The choke valve flow rate, q_{choke}, is related to the choke valve percentage opening, z_{choke} as

$$q_{choke} = K_c z_{choke} \sqrt{\rho_a (P_c - P_0)} \tag{4.1i}$$

Where K_c is the valve coefficient and is determined based on valve characteristics and p_0 is the pressure downstream of the choke valve.

4.3.2 ROP Equation

The Bourgoyne & Young model is the most common method used in the industry to model the *ROP*. This empirical model is valuable because it is based on the statistical synthesis of past drilling data [129]. The Bourgoyne & Young model is

$$\frac{dF}{dt} = f_1 . f_2 . f_3 . f_4 . f_5 . f_6 . f_7 . f_8 \tag{4.2a}$$

$$f_1 = exp(a_1) \tag{4.2b}$$

$$f_2 = exp(a_2(8000 - D)) \tag{4.2c}$$

$$f_3 = exp(a_3 D^{0.69}(g_p - 9)) \tag{4.2d}$$

$$f_4 = exp(a_4 D(g_p - \rho_c)) \tag{4.2e}$$

$$f_5 = exp\left(a_5 ln\left(\frac{\frac{W}{d_b} - (W/db)_t}{4 - (W/db)_t}\right)\right) \tag{4.2f}$$

$$f_6 = exp\left(a_6 ln\left(\frac{N}{100}\right)\right) \tag{4.2g}$$

$$f_7 = exp(-a_7 h) \tag{4.2h}$$

$$f_8 = exp\left(a_8 \frac{F_j}{1000}\right) \tag{4.2i}$$

Equation 4.2 shows the rate of penetration as a function of controllable and uncontrollable variables for roller-cone bit types. The parameters for these equations are defined in Table 4.2. Table 4.3 defines each of the 8 sub-functions (Equations 4.2b through 4.2i) in the Bourgoyne & Young model.

Table 4.2: Parameters used in Bourgoyne & Young model [128]

D	true vertical depth of drilling, ft
g_p	pore pressure gradient, lbm/gal
ρ_c	equivalent circulating density, lb/gal
$(W/db)_t$	threshold bit weight per inch of bit diameter at which the bit begins to drill, $1{,}000lbf/in$
(W/db)	bit weight per inch of bit diameter, $1{,}000lbf/in$
h	fractional tooth dullness
F_j	hydraulic impact force beneath the bit, lbf
a_1 to a_8	constants that must be chosen based on local drilling conditions

Table 4.3: Model parameters

Parameter	Effect of Parameter
f_1	Formation Strength
f_2	Compaction
f_3	Compaction
f_4	Pressure Differential
f_5	Bit Diameter and Weight Function
f_6	Rotary Speed Function
f_7	Tooth Wear Function
f_8	Hydraulics

4.3.3 Effect of Rotational Speed on the Friction Factor

Changing the rotation speed of the drill string (RPM) has an effect on the friction factor. This is a result of the two types of motion that the drilling fluid and cuttings have in the annulus. These two motions are 1) movement along the annulus (axial movement) and 2) rotational movement. As reported in the literature, the rotational movement of the fluid has a substantial effect on

the friction factor [134–139]. This effect of the drill string rotation on the friction factor has been modeled previously. Among those reported in the literature, the model proposed by Ozbayoglu et al. was selected for this research because it is based on empirical data and is simple to implement in the controller model [139]. The Ozbayoglu et al. model is an empirical model that uses the fluid Reynolds numbers to determine the friction factor (Equation 4.3a). The parameters a and b can be determined based on the empirical drilling data as

$$f_a = a\, {Nu_{Re_a}}^b + c\, Nu_{Re_\omega} \tag{4.3a}$$

where Nu_{Re_a} and Nu_{Re_ω} are Reynolds numbers in the axial and rotational direction, respectively, given by

$$Nu_{Re_a} = \frac{757\rho v_a(D_o - D_i)}{\mu_{e_a}} \tag{4.3b}$$

$$Nu_{Re_\omega} = \frac{2.025\rho N(D_o - D_i)D_i}{\mu_{e_\omega}} \tag{4.3c}$$

where v_a is the velocity in axial direction, D_i and D_o are wellbore and pipe outer diameters, respectively, and μ_{e_a} and $\mu_{e_\omega}$are the effective viscosity in axial and rotational directions.

4.3.4 Drill String Dynamics

As mentioned earlier, the rotation speed of the drill string applied on the surface is different from that at the downhole because it changes as it is transferred along the drill string. The drill string rotation effect was modeled as multiple mass-spring-damper pendulums connected to each other in series [140] as

$$\begin{aligned} J_1\ddot{\theta}_1 &= T_1 - T_2 - \mu\dot{\theta}_1 \\ J_i\ddot{\theta}_i &= T_i - T_{i+1} - \mu\dot{\theta}_i \\ &\cdots \\ J_n\ddot{\theta}_n &= T_n - (\mu + \mu_b)\dot{\theta}_n \end{aligned} \tag{4.4}$$

$$
\begin{aligned}
T_1 &= d_1(\dot{\theta}_{td} - \dot{\theta}_1) + k_1(\dot{\theta}_{td} - \dot{\theta}_1) \\
T_i &= d_i(\dot{\theta}_{i-1} - \dot{\theta}_i) + k_i(\dot{\theta}_{i-1} - \dot{\theta}_i) \\
&\cdots \\
T_n &= d_n(\dot{\theta}_{n-1} - \dot{\theta}_n) + k_n(\dot{\theta}_{n-1} - \dot{\theta}_n)
\end{aligned}
\tag{4.5}
$$

Each of the parameters used in this model (Equation 4.4 and 4.5) are defined in Table 4.4

Table 4.4: Parameters used in Equation 4.4 and 4.5

θ_{td}	angle of the top drive i
θ_i	angle of joint i
k_i	stiffness coefficient for string section i
d_i	internal damping coefficient for string section i
μ_b	friction coefficient for the bit i
μ	wall friction coefficient for the string sections
T_i	torque from string section i to $i+1$
j_i	inertia for string section i

4.3.5 WOB Dynamics

When some of the weight of the drill string is applied to the drilling bit, a reduction in deadline tension is observed. In the drilling industry, this reduction is considered to be the surface weight on the bit, which is usually not equal to the downhole weight on the bit. For estimating the downhole weight on the bit, the real time hook load data should be transferred into the system for further treatment [141].

The surface weight on the bit can be a true value if the well is vertical and the axial friction force between drill string and the wellbore is negligible. When the well deviates from a vertical straight line, the surface and downhole weight on the bit cannot be the same due to the axial friction force between the drill string and the wellbore [141]. WOB dynamics were modeled using an empirical first order plus dead time model

$$\tau_p \frac{d(BWOB(t))}{dt} + (BWOB(t)) = K_p SWOB(t - \theta_p) \tag{4.6}$$

empirical first order plus dead time model is the most well-known model used in industry to capture simple dynamics. In Equation , $BWOB(t)$ is the downhole WOB and is considered the controlled variable. $SWOB(t-\theta_p)$ is the controller output and is the surface WOB with a time delay of θ_p. K_p is the process gain and τ_p is the process time constant for the first order model. The values of K_p, τ_p, θ_p change with different rig capabilities and drill string configurations and effectively capture the dynamics between a commanded change in the surface WOB and the actual downhole WOB.

4.3.6 Estimator

The controller designed in this study can only utilize a drilling process model as far as measurements are accessible. However, variables such as annulus friction factor, density, and gas influx flow rates can be accurately approximated because data for these values are not readily available. In this controller, a nonlinear Moving Horizon Estimator (MHE) is used to estimate the annulus friction factor and density and an extended Kalman filter is designed for gas influx flow rate estimation. Choke valve pressure, downhole and pump pressures are considered as measured variables and are used as the estimation criteria. The MHE uses a squared error objective function as detailed in Sun, et al [142]. Its formulation is

$$\begin{aligned} \min_{d} \quad & \phi = (y_x - y_m)^T W_m (y_x - y_m) + (\Delta d)^T c_{\Delta d} + (y_m - \hat{y}_m)^T W_p (y_x - \hat{y}_m) \\ s.t. \quad & 0 = f(\dot{x}, x, u, p, d) \\ & 0 = g(y_x, x, u, d) \\ & a \geq h(x, u, d) \geq b \end{aligned} \tag{4.7}$$

Table 4.5 defines each of the terms used in the MHE formulation.

The Extended Kalman Filter (EKF) formulation used in this study is

1. Initialize: $\hat{x} = 0$.

Table 4.5: Summary of parameters used in the objective function (Equation 4.7)

Parameter	Description
ϕ	objective function
y_x	measurements $(y_{s,0},...,y_{s,n})^T$
y_m	model values $(y_{m,0},...,y_{m,n})^T$
$\hat{y}_m$	prior model values $(\hat{y}_{m,0},...,\hat{y}_{m,n})^T$
W_m	penalty outside measurement dead-band
W_p	penalty from the prior solution
Δd	change in parameters
$c_{\Delta d}$	penalty from the prior disturbance values
F	equation residuals
X	states
U	inputs
D	parameters or unmeasured disturbances
G	output function
H	inequality constraints

2. Perform step (3) at each sample time T_{out} (output sample rate is less than the sample rates of the sensors):

3. for $i = 1$ to N do (Prediction Step)

   (a) $\hat{x} = \hat{x} + \left(\frac{T_{out}}{N}\right) f(\hat{x}, u)$

   (b) $A = \frac{\partial f}{\partial x}(\hat{x}, u)$

   (c) $P = P + \left(\frac{T_{out}}{N}\right)(AP + PA^T + Q)$

   If a measurement has been received from sensor i then proceed with measurement update below

   (d) $C_i = \frac{\partial h_i}{\partial x}(\hat{x}, u[n])$

   (e) $L_i = PC_i^T(R_i + C_i PC_i^T)^{-1}$

   (f) $P = (I - L_i C_i)P$

   (g) $\hat{x} = \hat{x} + L_i(y_i[n] - h(\hat{x}, u[n]))$

Where $\hat{x}$ is the estimate of the state, and Q, R and P are the symmetric covariance associated with the process disturbance, sensor noise and estimation error respectively.

4.3.7 Controller

Nonlinear model predictive controllers (NMPC) are designed to regulate the downhole pressure, ROP, WOB and RPM during drilling. Figure 4.1 shows the schematic of the control system. During normal drilling conditions, the controller determines the optimum downhole pressure, weight on the bit and drill string rotation speed values that would lead to the ROP value determined by the operator. The controller then uses the values found from optimization as set points for the WOB and RPM NMPCs. The topside WOB and RPM are adjusted to regulate the downhole WOB and RPM at the specified set points. At the same time, the NMPC manipulates z_{choke} and q_p to regulate the downhole pressure. Figure 4.2 shows the control method during normal operation.

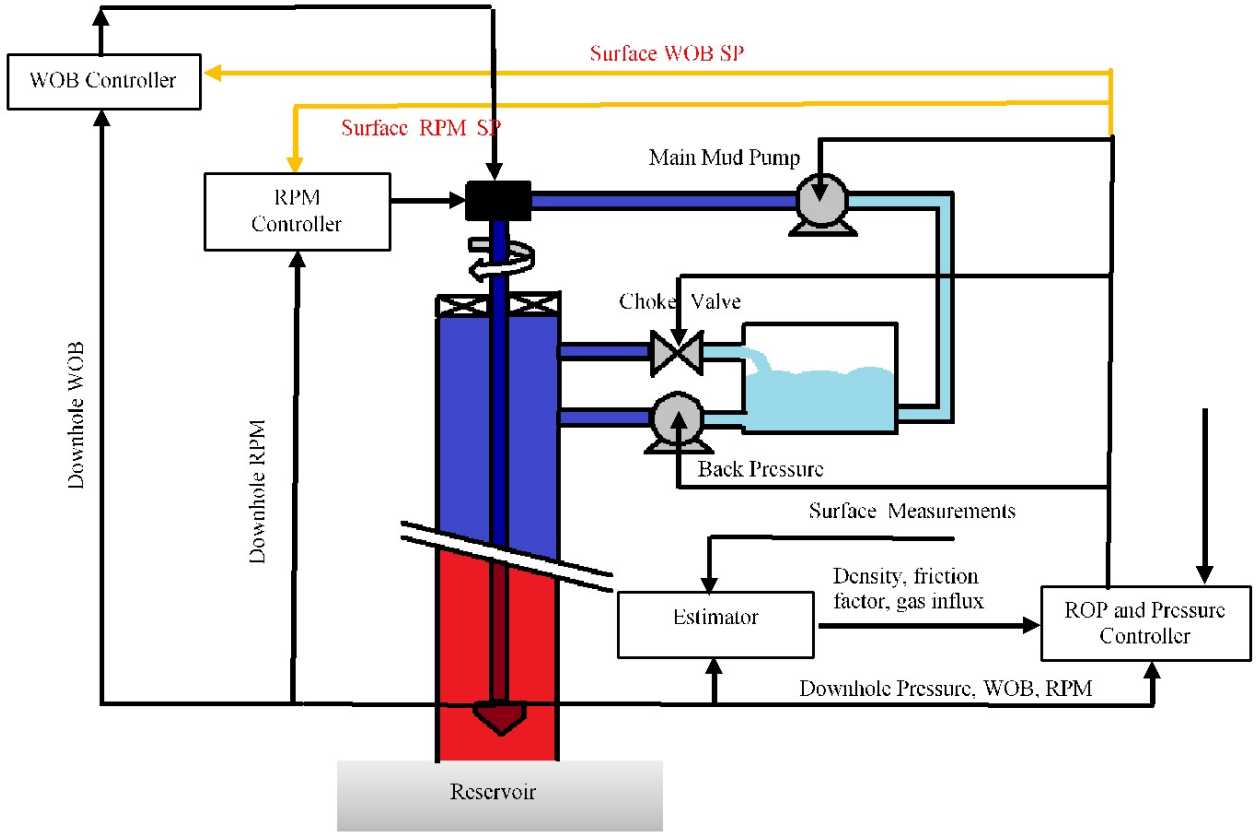

Figure 4.1: Schematic of the control system.

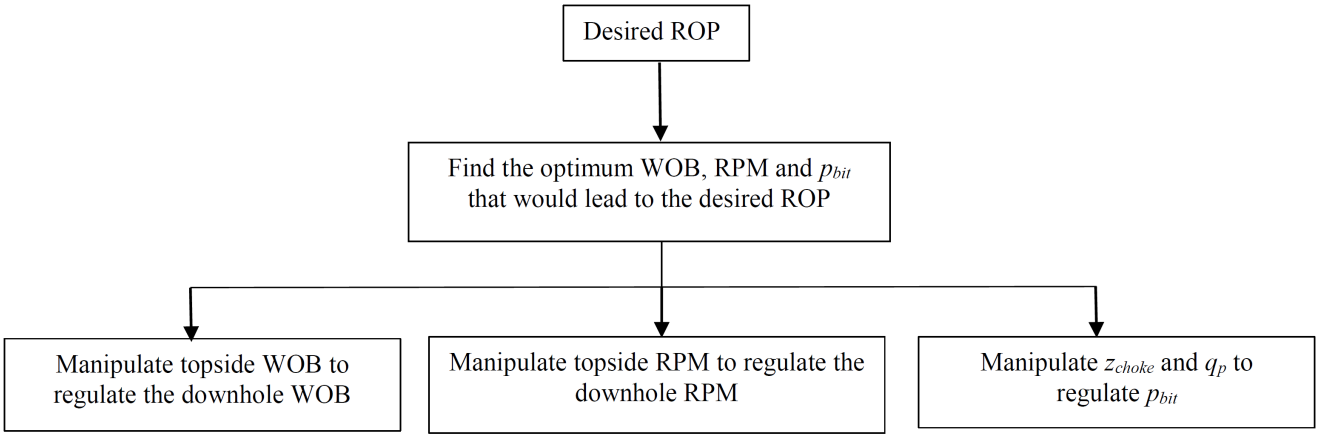

Figure 4.2: Schematic of the control system during normal operation.

When a kick happens, the controller first detects the kick situation through a rise in the measured downhole pressure or estimated gas influx flow rate. Second, it switches the controlled variable from downhole pressure into choke valve pressure and sets the new set point as

$$p_C^{SP} = p_C^{before\,kick} + k_1(p_{bit}^{current} - p_{bit}^{sp}) \tag{4.8}$$

This increases the choke pressure set point by some amount proportional to the increase in downhole pressure. Third, the NMPC manipulates the choke valve opening, mud pump flow rate and topside RPM until influx gas flow rate begins to decrease. At the same time, the new reservoir pore pressure is estimated. Finally, it switches the controlled variable back from choke valve pressure to downhole pressure and defines the new set point as

$$P_{bit}^{SP} = P_{res} + k_2(P_{res} - P_{res}^{before}) \tag{4.9}$$

where $P_{res} - P_{res}^{before}$ is the change of pore pressure value at the last time instant. This new set point stabilizes the downhole pressure to the final reservoir pressure.

While attenuating the kick, the controller also changes the WOB to compensate for the RPM change to hold the ROP constant. Figure 4.3 shows the structure of the control system during kick condition.

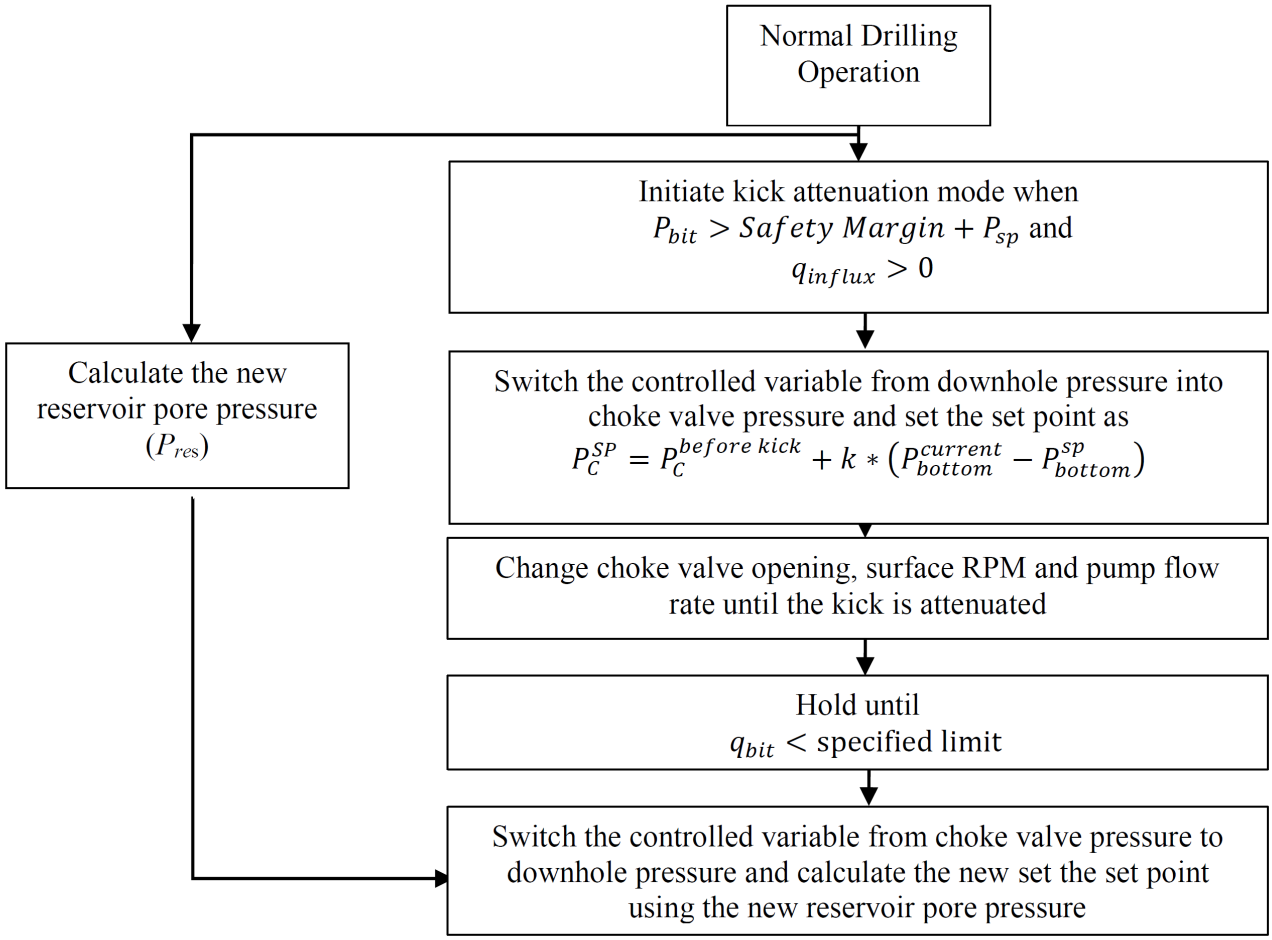

Figure 4.3: Summary of the control method for kick attenuation.

The NMPC formulation used in this study is shown in Equation 4.10. The objective function in the NMPC formulation is an ℓ_1-norm that forms a dead band of no controller movement as long as the process variable is close to a desired set point as discussed in Chapter 2. The advantage of ℓ_1-norm versus conventional squared error norm can be seen in noise, data outlier and drift rejection [5, 142]. The formulation of ℓ_1-norm is

$$
\begin{aligned}
\min_{d} \quad & \phi = w_{hi}^{T}(e_{hi}) + w_{lo}^{T}(e_{lo}) + (y_m)^T c_y + (u)^T c_u + (\Delta u)^T c_{\Delta u} \\
s.t. \quad & 0 = f(\dot{x}, x, u, d) \\
& 0 = g(y_x, x, u, d) \\
& a \geq h(x, u, d) \geq b \\
& \tau_c \frac{\delta y_{t,hi}}{\delta t} + y_{t,hi} = sp_{hi} \\
& \tau_c \frac{\delta y_{t,lo}}{\delta t} + y_{t,lo} = sp_{lo} \\
& e_{hi} \geq (y_m - y_{t,hi}) \\
& e_{lo} \geq (y_{t,lo} - y_m)
\end{aligned}
\tag{4.10}
$$

Table 4.6 summarizes all the variables used in Equation 4.10.

Table 4.6: Summary of parameters used in ℓ_1 objective norm (Equation 4.10)

Parameter	**Description**
ϕ	objective function
y_m	model values $(y_{m,0}, ..., y_{m,n})^T$
$y_{t,hi}$, $y_{t,lo}$	desired trajectory dead-band
w_{hi}, w_{lo}	penalty outside trajectory dead-band
c_y, c_u, $c_{\Delta u}$	cost of y, u and Δu, respectively
f	equation residuals
x	States
u	Inputs
d	parameters or unmeasured disturbances
g	output function
h	inequality constraints
a	lower limits
b	upper limits
τ	time constant of desired controlled variable response
e_{lo}	slack variable below the trajectory dead-band
e_{hi}	slack variable above the trajectory dead-band

4.4 Results and Discussion

Developing the controller for the drilling process is performed in three steps. First, a single pressure controller (Section 4.4.1) is developed that only uses a hydraulics model in maintaining the pressure during different scenarios, normal operation, connection procedure and unwanted gas influx. Second, a comprehensive controller (Section 4.4.1) is developed that regulates both pressure and ROP at the same time using a hydraulic and drillstring model. This controller is tested in normal operation and during unwanted gas influx scenarios. Third, a multivariate controller (Chapter 5) is designed to be the same as a comprehensive controller but uses multiple pressure sensors along the annulus. The results improve unwanted gas influx and cuttings build up detection.

4.4.1 Pressure controller

The controller structure used is different for different drilling scenarios in terms of which variables should be considered as manipulated or controlled. In this section a brief explanation of the controller in each of the drilling scenarios is given.

Normal Operation

Choke valve opening and mud pump flow rates were selected as manipulated variables (MVs) for maintaining the downhole pressure at a desired value during normal operation. Having multiple MVs improves the controller performance and increases complexity. A respective cost value associated with each MV determines which one of the MVs the controller is able to change more than the other.

Connection Procedure

During pipe connection procedure, the main drilling mud pump flow rate ramps down to zero and stays there until the new drilling pipe is connected and then it ramps back up to the normal value. In this procedure, pump pressure head will no longer be available in the drill bit section which can increase the possibility of unwanted gas influx. To compensate for this, the

controller uses the choke valve opening and back pressure pump flow rate as manipulated variables to maintain the drill bit pressure at the target value.

Kick Attenuation

Unlike previous studies where the change in the estimated influx flow rate, friction factor, or density is used to detect and attenuate the kick, this study uses direct downhole pressure measurements offered by high frequency wired pipe telemetry network for kick detection purpose. Relying on direct downhole measurement other than estimation techniques which use topside measurements makes it possible to detect and attenuate the kick faster and more effectively than conventional methods. The kick detection and attenuation procedure used in this study is novel and is described as follows: when the pressure measured in the drill bit section changes beyond a specific limit, the controller detects that a kick is happening. When this occurs, the controller changes its control variable from downhole pressure (P_{bit}) to choke valve pressure (P_c) and adjusts the choke valve pressure set point value to the current P_c value plus the most recent change in P_{bit}. This rise in P_c prevents any unwanted gas influx from coming upwards through the annulus. The controller achieves this goal through manipulating the main pump flow rate and choke valve opening only as will be illustrated in control case 3 section (4.4.1). Table 4.7 summarizes the manipulated and controlled variables (CVs) in different scenarios.

Table 4.7: Different configurations for manipulated and controlled variables used in the controller scheme for each scenario

AA	Normal operation	Connection procedure	Unwanted gas influx
MVs	Choke valve opening Main pump flow rate	Choke valve opening Back pressure pump flow rate	Choke valve opening Main pump flow rate
CVs	Drill bit pressure	Drill bit pressure	Choke Valve pressure with the new set point

Case Study

A simulated test case consisting of normal operation, a pipe connection procedure, and kick attenuation is presented in this section. The initial conditions for this well model simulation case are given in Table 4.8. The simulated well is equipped with a main mud pump, choke valve, and back pressure pump as was shown in Figure 4.1. The controller and wired pipe telemetry technology performance was evaluated and compared as a function of data bandwidth in different simulation cases.

Table 4.8: Initial well conditions used for simulations

Variable	Value (SI units)	Value (US units)
Distance between two successive pressure sensors h_a	150 m	492.1 ft
ROP	0.01 m/s	0.033 ft/s
Fluid density in the drill string - ρ_d	$0.012 \times 10^5\ kg/m^3$	$74.9\ lb/ft^3$
Fluid density in the annulus - ρ_a	$0.014 \times 10^5\ kg/m^3$	$87.4\ lb/ft^3$
Bulk modulus in the annulus β_d	14000 bar	$2.03\ 10^5 psi$
Bulk modulus in the annulus β_d	14000 bar	$2.03\ 10^5 psi$
Annulus cross sectional area	$0.021\ m^2$	$0.226\ ft^2$
Friction factor in the drill string F_d	$10000\ barm^{-6}s^2$	$116.3\ psift^{-6}s^2$
Friction factor in the annulus F_a	$1250m^{-5}$	$3.29ft^{-5}$
Lumped density per length parameter for the drill string - Md	$5700\ 10^{-5}kg/m^4$	$108.5 \times 10^{-5}lb/ft^4$
Lumped density per length parameter for the annulus Ma	$800 \times 10^{-5}kg/m^4$	$15.22\ 10^{-5}lb/ft^4$
Well depth (h_bit)	2000 m	6562 ft

Parameter estimation

Figure 4.4 and Figure 4.5 show the change in the estimated annulus friction factor and density over time. The nonlinear estimator gets the pressure values at points along the annulus as well as topside measurements of choke valve pressure, choke valve flow rate and also main pump flow rate and solves an optimization problem by looking back in time at the data over a horizon. Based on this the estimator is able to find the correct values of density and the friction factor in about 30 seconds. This is a big improvement in the estimation time in comparsion with

previous studies which require a time in the order of minutes to find the unknowns [95]. The optimum annulus friction factor and density are sent to the controller. The controller uses these values online to feed all the required information into the process model that it uses.

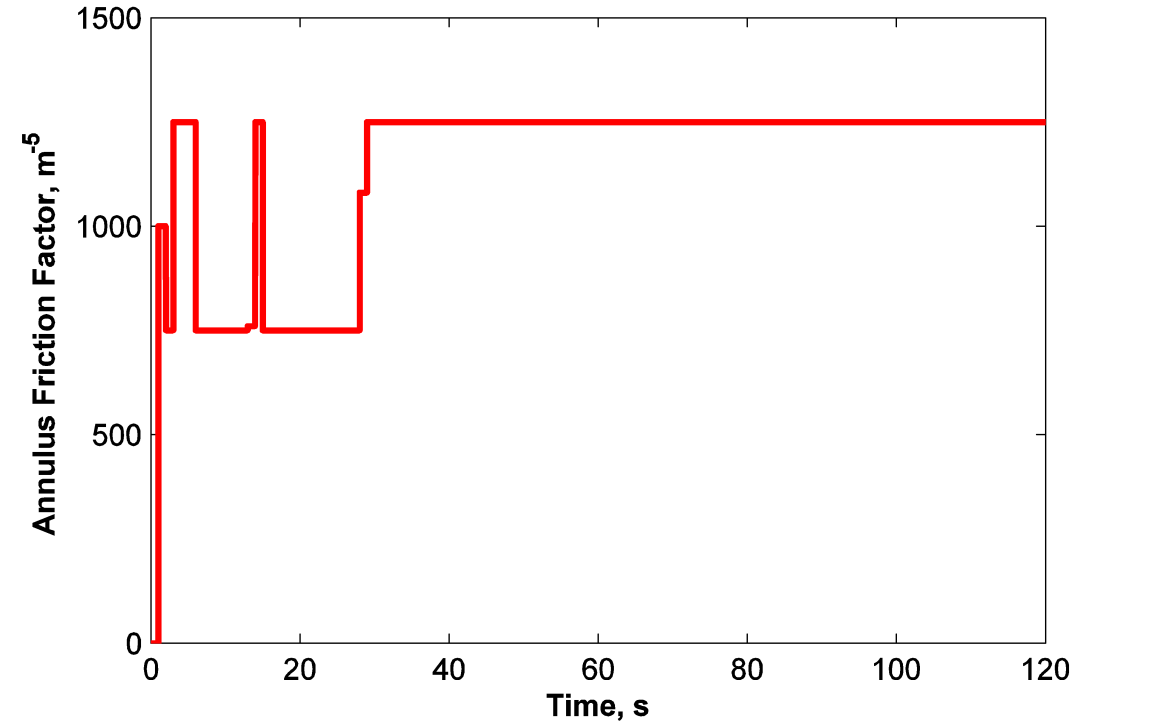

Figure 4.4: Annulus friction factor estimation performed by the estimator online.

Control Case 1: Normal Operation

Figure 4.6, Figure 4.7, and Figure 4.8 show the change in the controlled and manipulated variables during start up from the initial condition reported in Table 5. The controller is easily able to regulate the pressure at the target value of 348 bar within 100 seconds. For this purpose, it increases the drill bit pressure by adjusting the choke valve opening to 33% and main pump flow rate at 1244 L/min. The controller works with the estimator online, which provides the friction factor and density values to be used in the NMPC model.

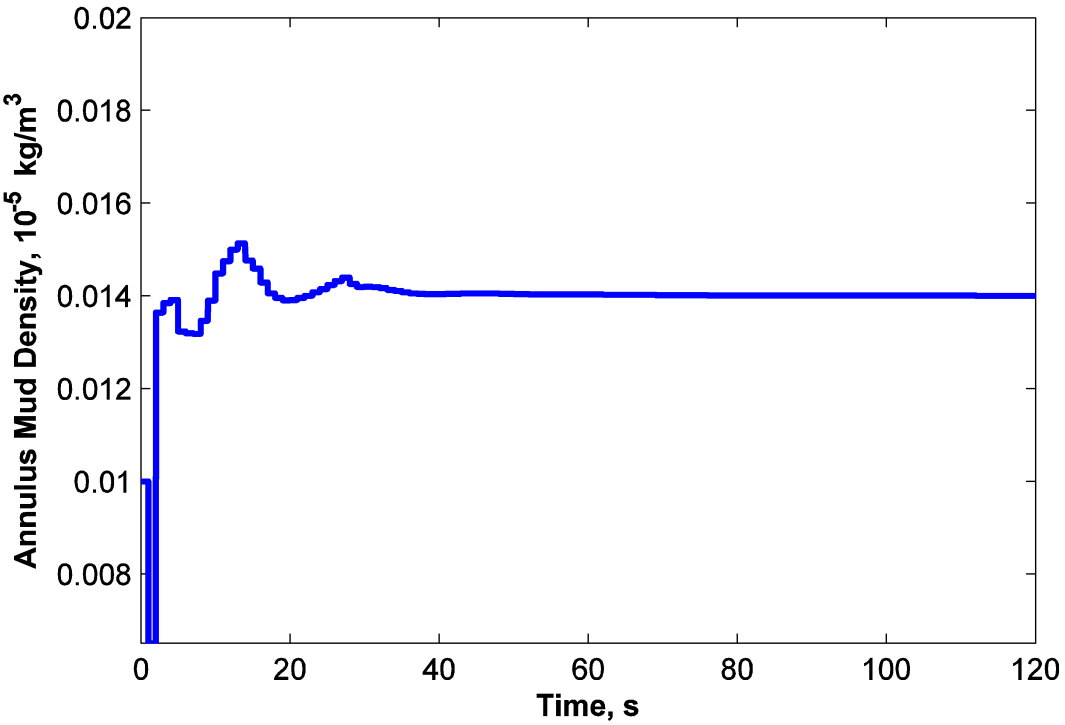

Figure 4.5: Annulus mud density estimation performed by the estimator online.

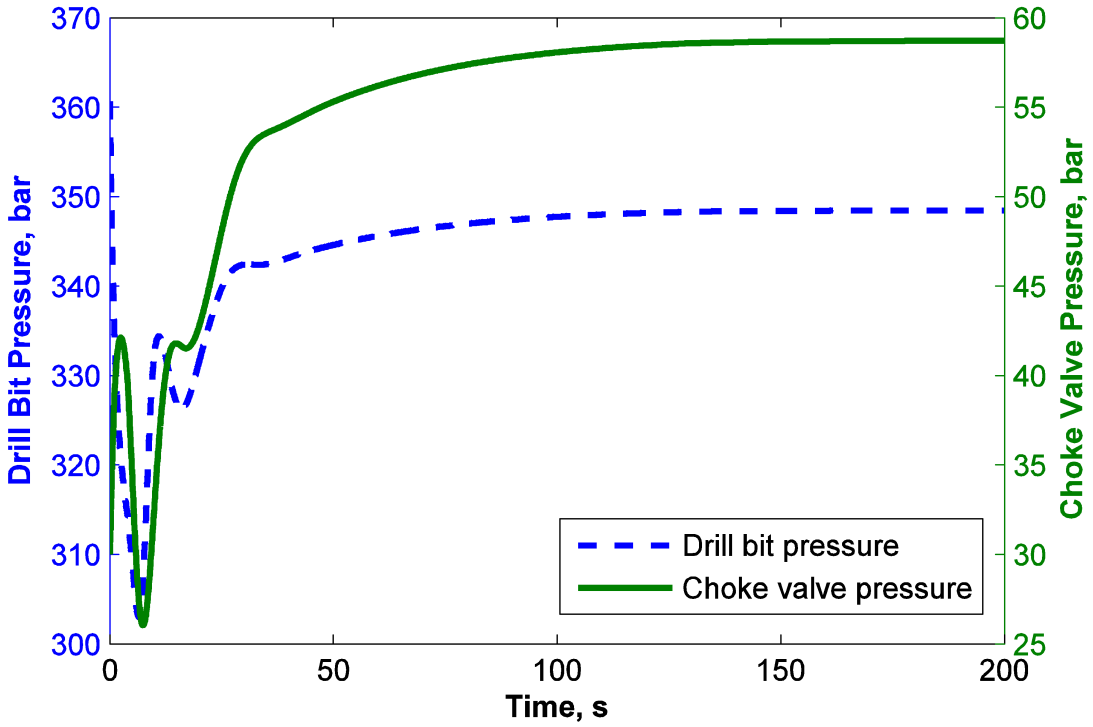

Figure 4.6: Drill bit and choke valve pressures during normal operation.

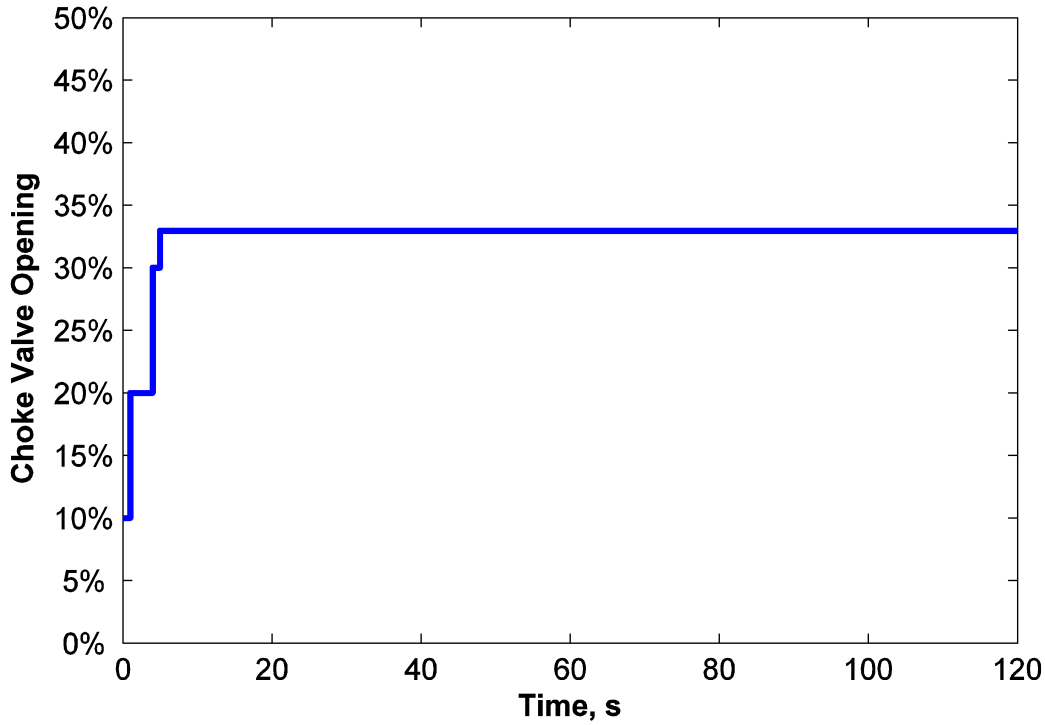

Figure 4.7: Choke valve percentage opening (MV) during normal operation.

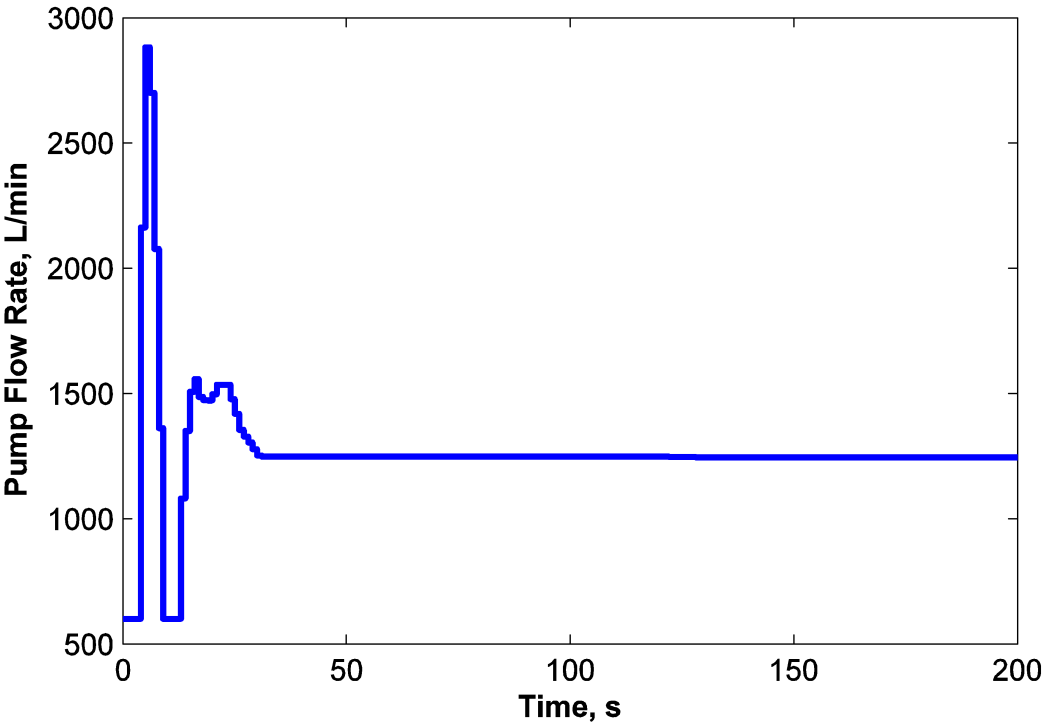

Figure 4.8: Main pump flow rate (MV) during normal operation.

Control Case 2: Pipe Connection Procedure

The simulation results during a connection procedure are shown in Figure 4.9 through Figure 4.11 . The NMPC controller is highly accurate and is able to maintain the drill bit pressure at the target value within less than 1% error margin. When the main mud pump flow rate starts ramping down, the controller compensates for that by decreasing the choke valve opening from 38% open to 15% open and increasing the back pressure pump flow rate to 280 L/min. This process takes about 70 seconds. When the main pump flow rate gets to zero, it is disconnected and the new pipe stand is added to the drill string. This part of the connection procedure takes 50 seconds. The use of NMPC may allow for a significantly faster connection procedure, relative to conventional manual processes, by automation of the pump and choke control process. This is important as it limits the additional drilling time required to implement MPD and can improve the cost effectiveness of deploying this technique. Since the controller has two manipulated variables, it can decide which one to favor based on the cost and change cost values associated with each one. These cost and change cost values can be tuned for the controller depending on the well conditions.

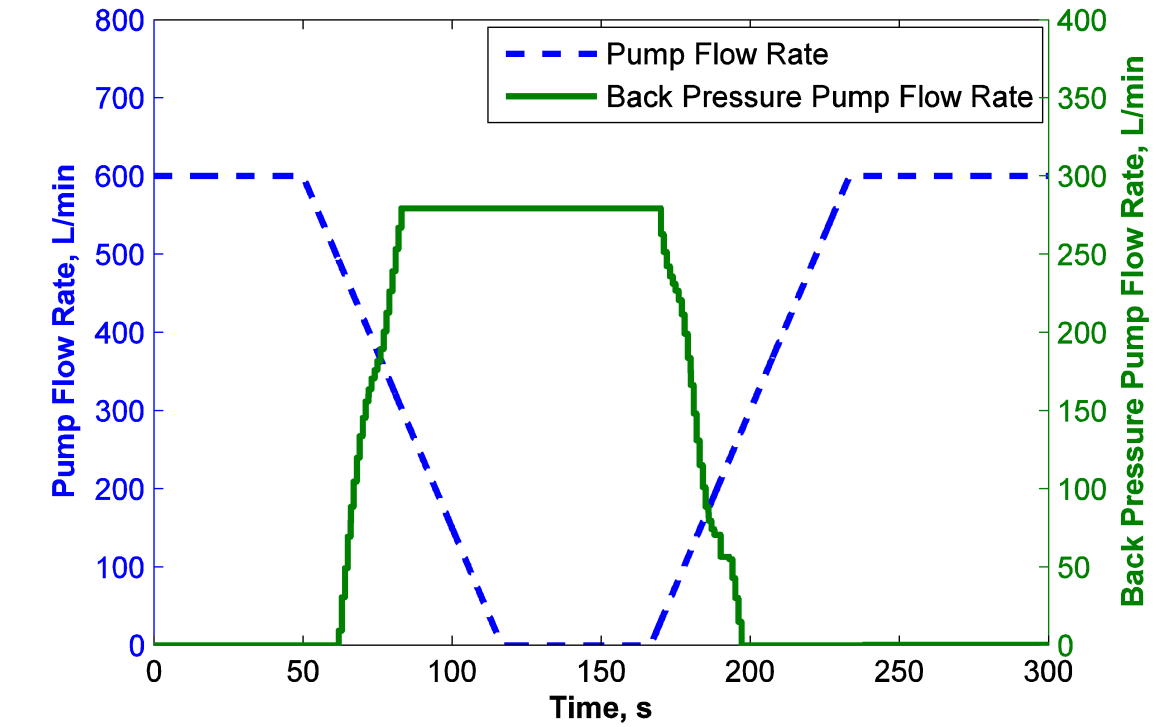

Figure 4.9: Main pump and back pressure pump flow rate during connection procedure.

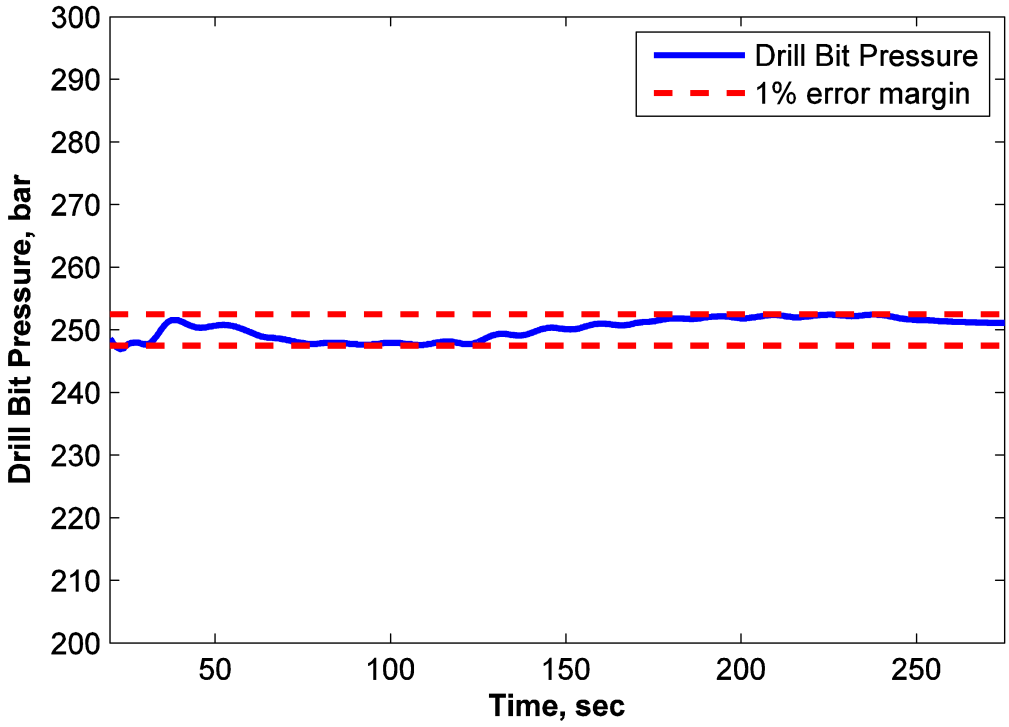

Figure 4.10: Drill bit pressure during connection procedure.

Control Case 3: Unwanted Gas Influx

Figure 4.12 through 4.15 Figure illustrate the behavior of the controller during a simulated unwanted gas influx. Originally the pressure at the drill bit is adjusted to 345 bar. At 50 s, the unwanted gas influx occurs which causes a rise in the drill bit pressure. When the change in drill bit pressure is above a certain specified limit, the controller switches the controlled variable from drill bit pressure into choke valve upstream pressure and the new set point in PC is defined as

$$\mathrm{P}_C^{SP} = K\,(\mathrm{P}_b^{current}it - \mathrm{P}_{bit}^{SP}) + \mathrm{P}_C^{current} \tag{4.11}$$

The increase in P_C increases the pressure over the drilling annulus starting at the choke valve. This balances the pressure and impedes further gas influx to rise towards topside devices. During this event, the controller uses both the main pump flow rate and the choke valve opening as the manipulated variables. The NMPC holds q_{pump} at 600 L/min and decreases the z_{choke} from 40%

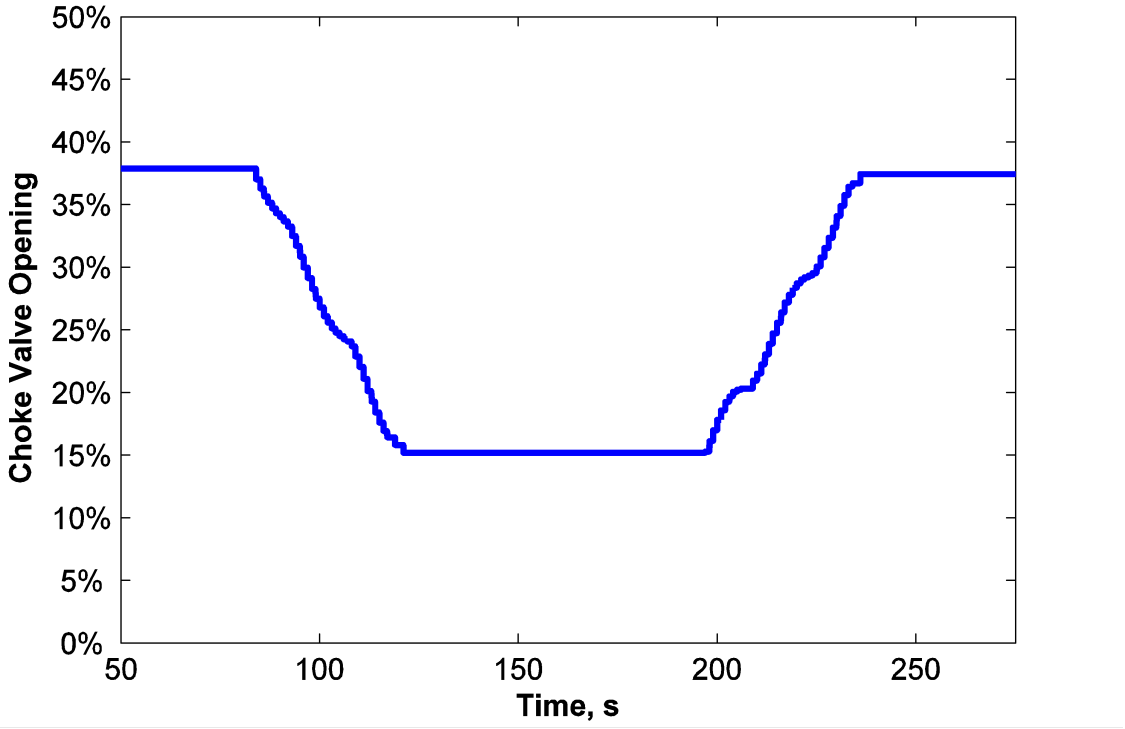

Figure 4.11: Percentage choke valve opening during connection procedure.

to 10% open. Interestingly, in the present scenario, the controller preferentially manipulates the choke valve opening, as changes in this variable can be done more quickly than changes q_p. The controller makes this choice based on the change cost that is given to its configuration. Obviously, the higher the severity of the kick, the bigger the change the NMPC will have to make to the manipulated variables. When the PC stabilizes at the new set point, the controller switches the controlled variable back to the drill bit pressure and establishes the new set point at its current value. The results demonstrate that the designed NMPC controller is able to detect and attenuate the kick quickly and effectively. Figure 4.12 shows the impact of controller cycling time on the ability of the controller to attenuate the unwanted gas influx. For the present well design conditions (see Table 4.7), it can be seen that the controller performance decreases with the cycle time, which is a proxy for data bandwidth. The controller is able to attenuate kicks at cycling times of 1, 2, and 4 s, but is incapable of attenuating them at 8 seconds. For the latter case, the process would need to be switched to manual operation and more intrusive well control efforts would be required. This graph shows the advantage of high speed data communication made available through WDP

telemetry for advanced NMPC. This novel kick attenuation method is a remarkable improvement to the efforts taken so far in industry for ensuring safe drilling operations, based on the rapid response attained.

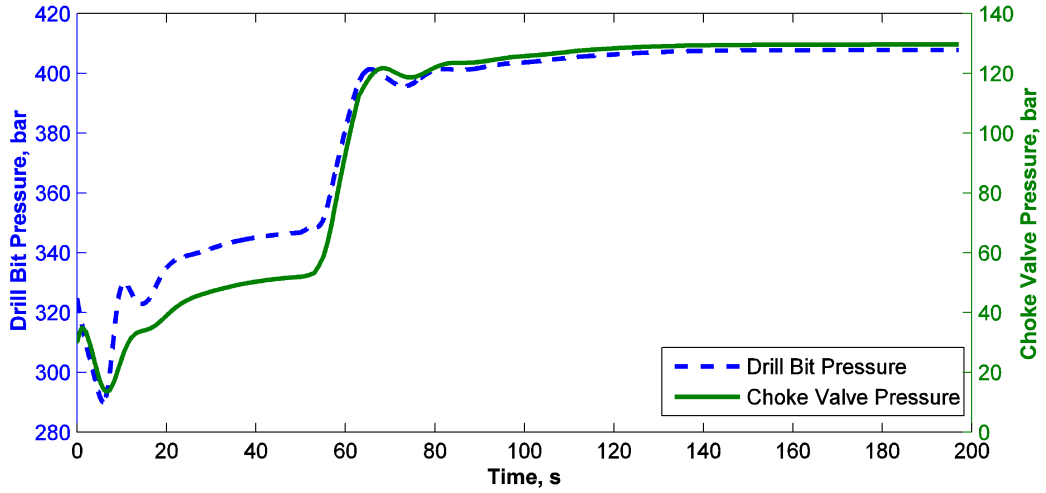

Figure 4.12: Drill bit pressure during unwanted gas influx.

This case study demonstrates an effective future application for WDP telemetry and the specific benefits associated with distributed sensing along a drill string with a high-speed data communication network. In particular, one simulation shows the pressure regulation during a connection procedure where a new pipe stand is added to the drill string. Using an automated choke valve and backpressure pump with the high speed sensing, the pressure is maintained at the drill bit throughout the connection procedure. This improved pressure control is enabled by the direct measurement of downhole pressure even when drilling mud is not flowing or is aerated. This improves pressure regulation drastically during transient drilling operations. The high data availability also enables a nonlinear model predictive controller that detects and responds to unexpected gas influx. In prior work, this response time has been on the order of minutes while with this new approach, the response is decreased to the order of seconds. This is due to direct measurement of pressure as opposed to inferential sensing and advanced algorithms that best utilize this information. An additional novel feature of this approach is that when a kick is detected, the downhole pressure control switches flawlessly to choke valve pressure control, and then back to downhole control.

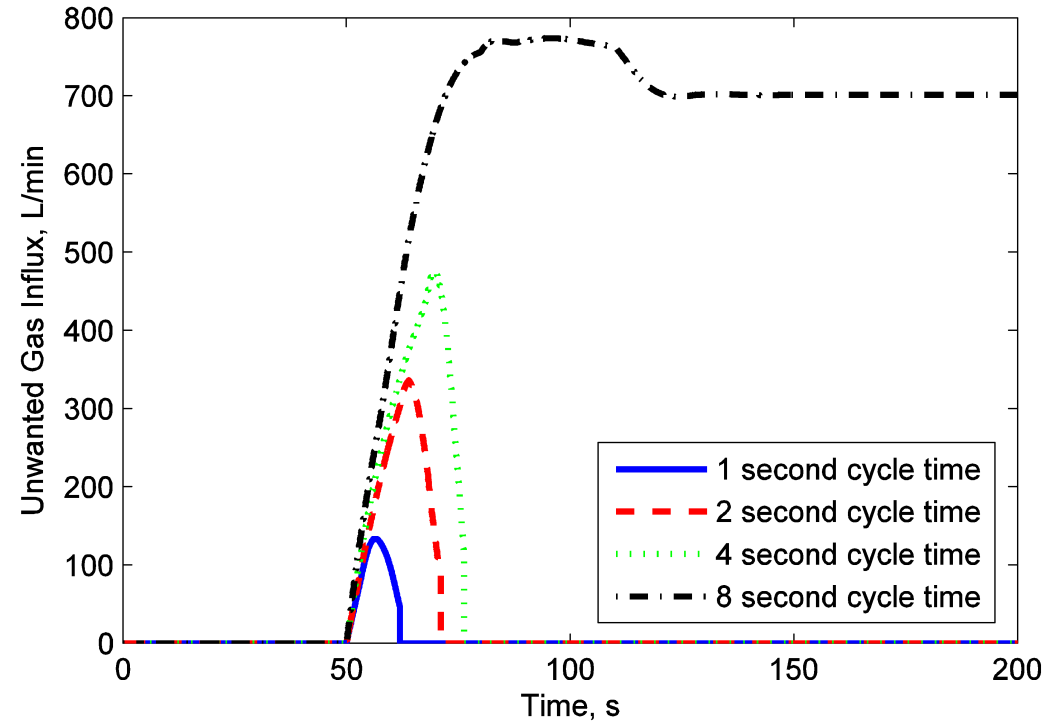

Figure 4.13: Unwanted gas influx at different controller cycle times.

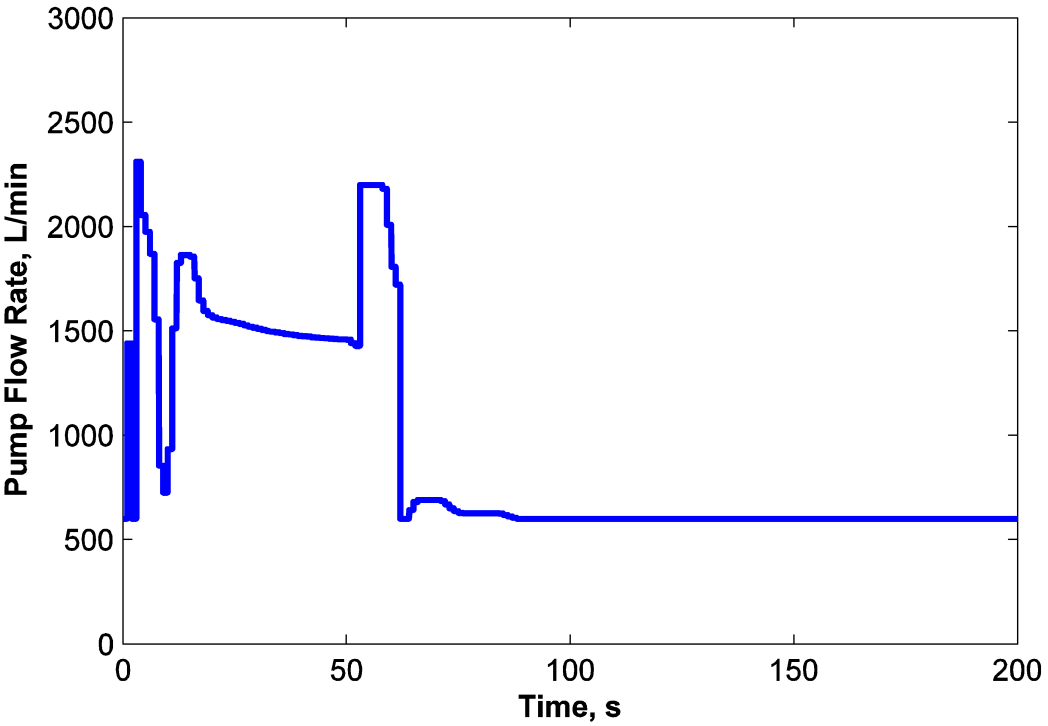

Figure 4.14: Main pump flow rate during unwanted gas influx.

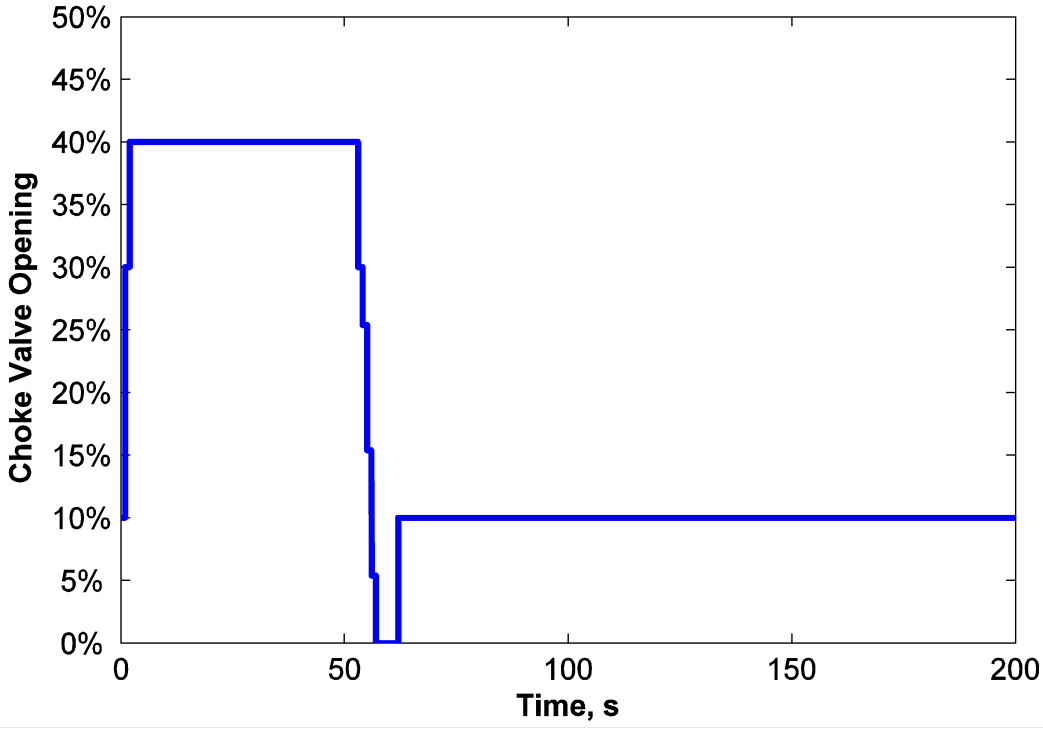

Figure 4.15: Choke valve percentage opening during unwanted gas influx.

4.4.2 Comparing the Results for the Two Variable Versus Three Variable Case

The results of kick attenuation and comprehensive controller performance are shown in this section. These results are compared with a controller with separate pressure and rate of penetration control. Both control scenarios (comprehensive and independent controllers) rely on data from high speed telemetry and demonstrate a superior performance compared with the case in which manual control is used for kick attenuation. In manual operation, it takes 1 to 5 minutes for an operator to respond to a kick. For the purpose of this simulation, an 80 second response time of the operator was assumed following which the operator closes the choke valve to initiate kick attenuation (see Figure 4.16 for manual kick control). In general, superior performance of the automated controllers with respect to manual control case is because of two main features: (1) Downhole sensors and high speed telemetry system, which enable the changes in downhole conditions to be seen at the surface very fast, enabling the controller to react quickly, (2) the predictive feature of the controller, which enables it to predict the system's dynamic behavior using the system model and past data analysis in a prediction horizon and therefore react accordingly and in

advance, and (3) Optimization feature of the controller with MPC determines the optimum combination of the manipulated variables' values (main mud pump opening, and choke valve opening and RPM) to regulate the kick. This enables the controller to change the manipulated variables a minimal amount and avoid potentially causing mud loss to the reservoir or additional gas influx. Figure 4.16 also compares the unwanted gas influx attenuation results with the same characteristics from both controller simulations: (1) comprehensive controller and (2) single pressure controller. The single pressure controller uses a wired pipe telemetry system and is detailed in [85]. It changes two variables, choke valve opening area and mud pump flow rate for this purpose. The comprehensive controller attenuates the kick more effectively and quickly than the pressure controller alone. This is because it has an additional manipulated variable (surface rotation speed) that can change the downhole pressure. Increased surface RPM leads to an increase in the downhole RPM, as dictated by the drill string dynamics. This increase in rotation speed increases the friction factor, leading to an increased resistance to mud flow and therefore higher pressure along the annulus. This increase in pressure provides more effective kick attenuation.

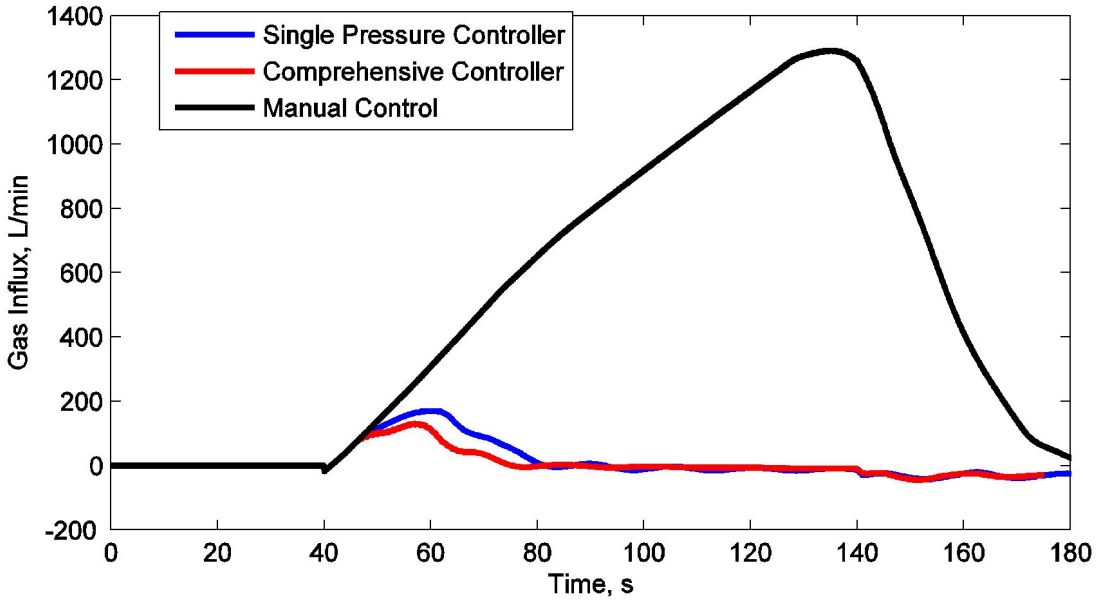

Figure 4.16: An unexpected gas influx that starts at 40 seconds of simulation time.

Figure 4.17 shows the downhole and choke pressure changes over time during a kick event for the comprehensive controller. During normal drilling operations, the downhole pressure set

point or target value is 300 bar. When the kick occurs at 60 seconds of simulation time, the NMPC switches the controlled variable from downhole pressure to choke valve pressure (the grey area). This switch is enacted because the dynamics at the downhole area change once the gas influx enters the annulus. Therefore it is better to control the choke valve pressure that has not been affected by the gas influx. This enables the controller to react more effectively during the initial kick event. The increase in the choke valve pressure leads to an increase in the pressure along the annulus. This continues until the gas influx trend changes from ascending to descending (at the time of 72 seconds). Then the controller switches the target pressure control to downhole pressure and calculates the new set point based on the new estimated pore pressure. Because the kick is attenuated quickly, reservoir pressure may continue to increase slowly even after the kick is attenuated, leading to multiple kicks. To overcome this problem, as the reservoir pressure rises, the downhole pressure set point increases to stop the reservoir gas from entering the annulus. In general, if gas influx enters the annulus and is detected, the controller switches to maintain the choke valve pressure. Otherwise the controller continues to maintain the downhole pressure even if the reservoir pressure increases.

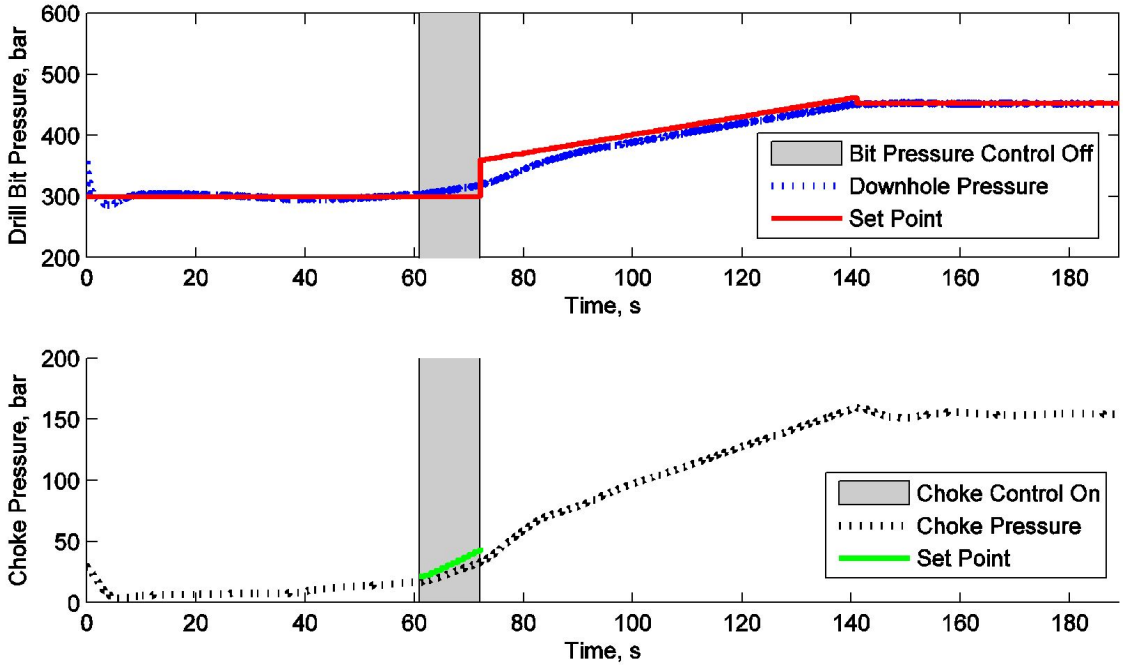

Figure 4.17: Switched control between bit pressure and choke pressure during the kick event.

As is shown in Figure 4.18 and 4.19, the controller responds to the unexpected gas influx by reducing the choke valve opening and increasing the RPM and main pump flow rate. This set of coordinated actions is shown in Figure 4.18 and Figure 4.19. The controller tends to change choke valve opening (z_{choke}) and RPM more than mud pump flow rate because changing RPM and z_{choke} have a faster effect on annulus pressure than the pump flow rate. Also, when gas influx enters the annulus it tends to decrease the density in the annulus which reduces the hydrostatic head. Therefore, increasing pump flow rate in this situation is not as effective as during normal drilling operations. The NMPC considers the changing relationships in the multivariate controller and favors choke valve and rotational speed movement more than adjustment to the pump flow rate.

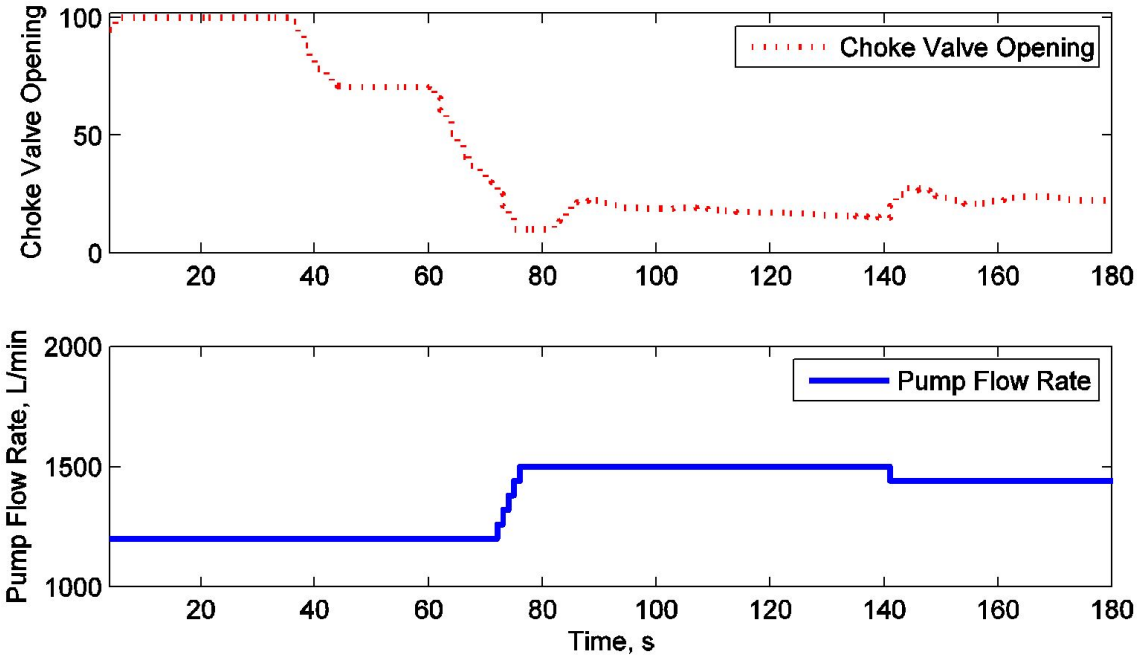

Figure 4.18: NMPC favors movement of the choke valve opening over pump flow rate.

Figure 4.19 shows the change in rotational speed of the drill string at the surface, downhole RPM, and the desired set point. When a kick happens at a simulated time of 40 sec, the downhole set point increases with action by the master controller after 20 seconds when the kick is detected and automatically increases from 80 to 180 RPM. The increase in RPM has the effect of increasing the annulus pressure by increasing the friction factor associated with the rotating drill string.

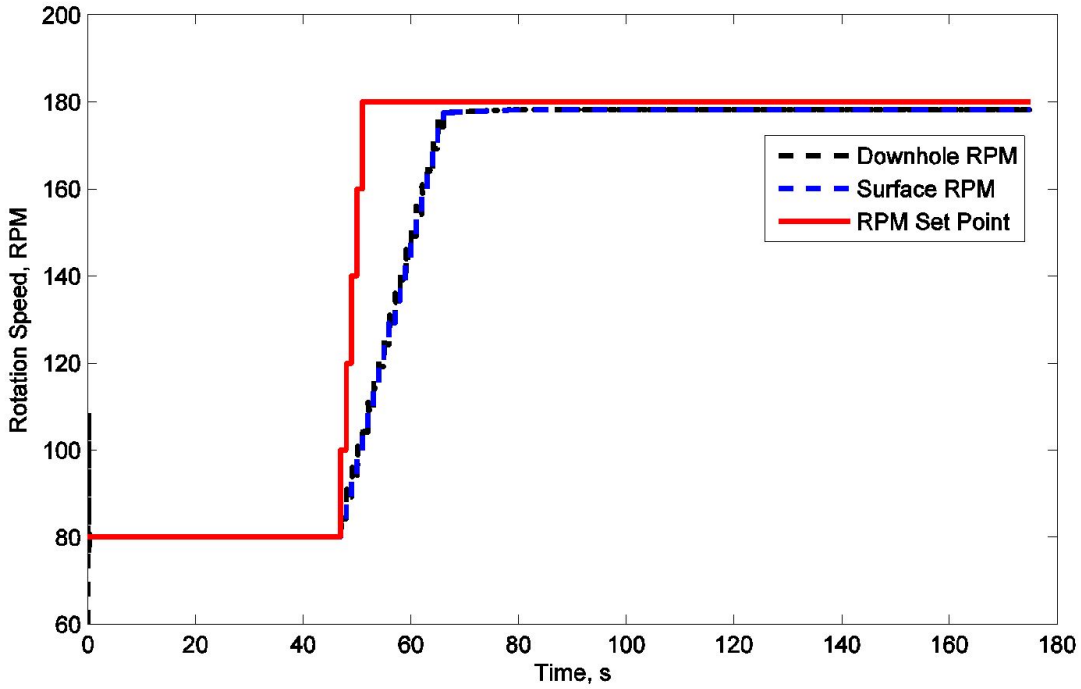

Figure 4.19: RPM adjustments are constrained by a rate of change limit towards the desired target for this particular simulation.

A benefit of the comprehensive controller is that, during a kick event, the operator does not need to stop drilling and the drilling continues with a consistent value of ROP. As RPM is increased for kick attenuation purpose, the comprehensive controller decreases the WOB to compensate for the effect. This is determined by the master controller using the Bourgoyne & Young model. A consistent value of ROP not only helps to achieve drilling depth targets, but also avoids cutting loading issues associated with fluctuations in ROP. As the ROP fluctuates, the drilling mud must transport a variable amount of cuttings away from the bit. Localized sections of high cutting loading may lead to pack-off or other undesirable consequences related to mud flow. Figure 4.20 shows the trends of the surface, downhole and set point weight on the bit. As is shown, the slave controllers are able to adjust the downhole values to the specified set points determined by the master controller within 15-20 seconds. The WOB value at the downhole location is lower than surface WOB due to the axial friction force between drill string and the wellbore. The WOB slave controller uses direct measurements and does control calculations using an empirical model to adjust the surface WOB so that the downhole WOB value can be regulated at the required set point

determined by the master controller. This ability to quickly compensate for RPM changes leads to the more consistent ROP.

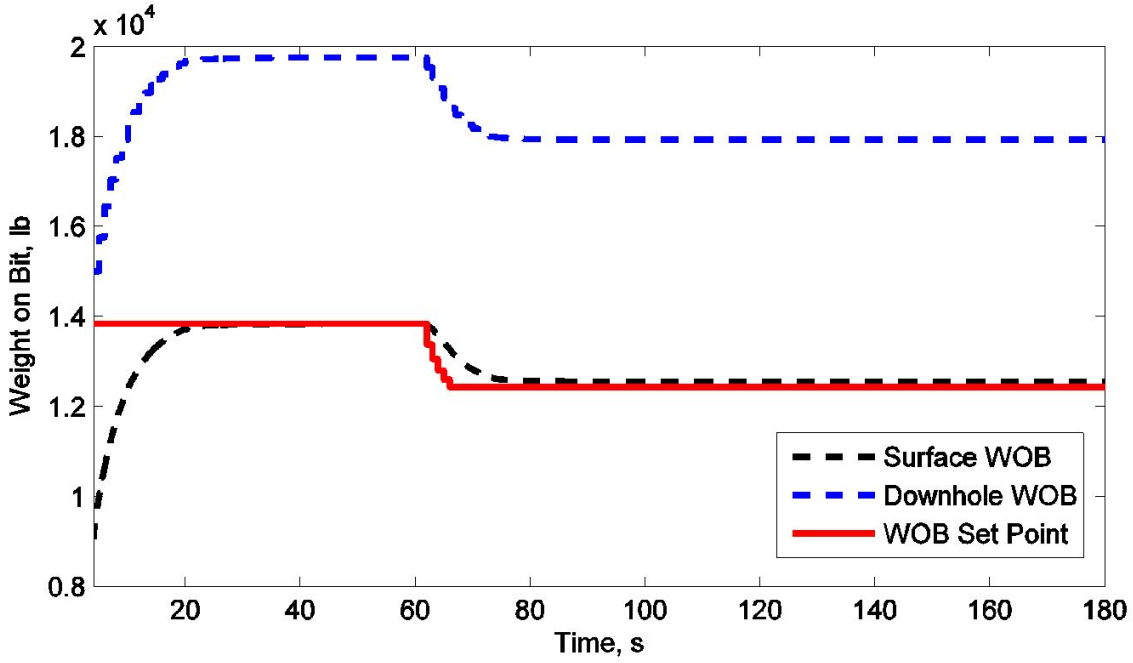

Figure 4.20: Weight on bit adjustments compensate for RPM adjustments to maintain a consistent ROP.

4.4.3 Steady State Drilling Operations

An important aspect of any controller design is not only to investigate the controller response during upset conditions, but also during all phases of operation. It is shown that the proposed multivariate controller is effective at attenuating unexpected gas influx, but this is expected to occur only a small fraction of the total time drilling. During steady state operations without unexpected gas influx, the controller determines the optimum downhole rotation speed, weight on bit, and pressure that lead to the desired ROP. The controller then sends the required set points to the respective RPM and WOB slave controllers and uses choke valve opening and mud pump flow rate to adjust the downhole pressure at the required value. One difference between steady state operation and kick attenuation cases is that in the kick attenuation, the desired value of RPM is

determined based on the hydraulic changes and with the goal of gas influx attenuation using the hydraulic and rotational friction factor models. While in the steady state operation, the desired value of RPM is determined to achieve the required ROP and the Bourgoyne & Young model is used for this purpose. In the comprehensive controller case, a higher ROP is achieved compared with the case with only real-time ROP optimization. This is because, in the case of a comprehensive controller, it is able to adjust to the minimum possible downhole pressure that leads to the highest ROP value. The decreased downhole pressure leads to higher ROP as demonstrated in Figure 4.21. As can be seen in the case of a comprehensive controller, ROP is approximately 20 percent higher than the separate ROP and pressure controller case (126 vs 105 ft/hr).

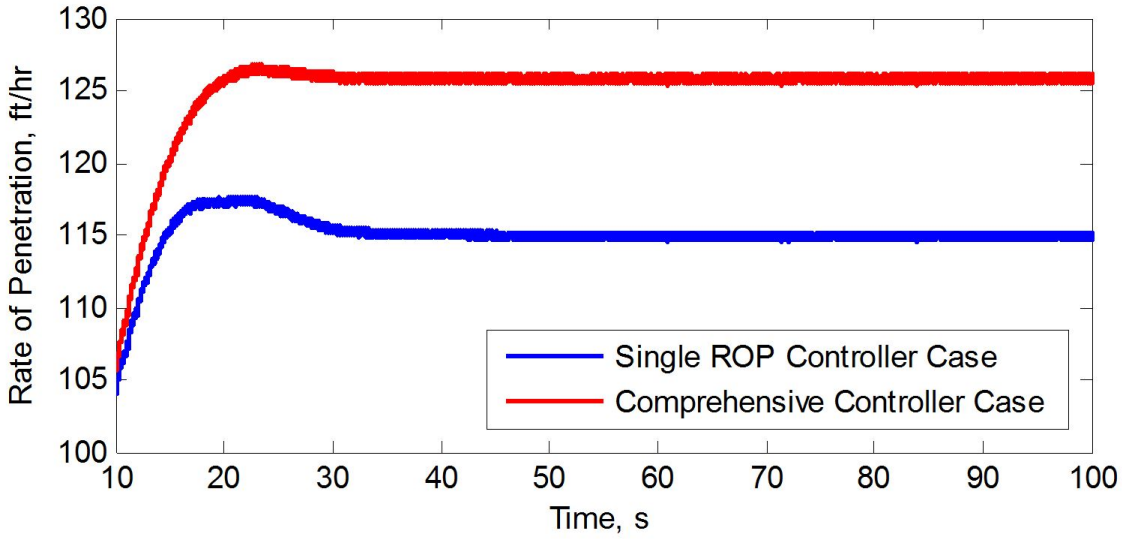

Figure 4.21: Rate of penetration is increased while maintaining pressure control.

4.5 Conclusion

A comprehensive multivariate controller for ROP and pressure is superior compared to the case where separate controllers are employed. The combined controllers are able to synchronize changes in drill string rotation speed (RPM), weight on bit (WOB), pump flow, and choke valve opening to best achieve targets of pressure and rate of penetration (ROP). With controllers that are split between ROP and pressure control objectives, the actions are not coordinated and lead to a feedback response, instead of an anticipatory response with the multivariate case. With the

comprehensive controller, a more consistent and higher ROP is achieved and any unexpected gas influx is attenuated more effectively. Wired pipe technology, or other high speed telemetry, is critical for this control scheme because it enables high frequency data to both update the underlying models and implement control actions. Using an advanced NMPC and estimators (both EKF and MHE), the different drilling situations are optimized to achieve operational targets. This work is the second phase of a project that builds upon prior results. The prior results demonstrated the value of speed of response for kick attenuation. In future work, the value of distributed drill string sensing and gas kick location detection will be determined across sensors that are positioned along the drill string, not only at surface and bottomhole locations.

CHAPTER 5. COMPREHENSIVE PRESSURE AND ROP CONTROLLER IN CASE OF MULTIPLE SENSOR LOCATIONS

Much of the content of this chapter is taken from the following reference: [143]

- Asgharzadeh Shishavan, R., Hubbell, C., Perez, H., Hedengren, J., Pixton, D. S., Pink, A. P., Multivariate control for managed pressure drilling systems using high speed telemetry. Submitted to SPE Journal.

5.1 Introduction

The safety and profitability of a drilling project depends on efficient control of the drilling process. Providing such control is no trivial task - the nature of subterranean environments and the drilling process itself create dynamic conditions that must be detected and addressed by the drilling control system in a timely manner. Such conditions include changes in formation characteristics encountered while drilling ahead, unexpected fluid influx or losses, and transient conditions (mechanical and hydraulic) that result from common drilling operations such as adding a section of drillpipe to the drillstring or tripping the string in and out of the well. Additional challenges are encountered that are specific to many of the aggressive drilling environments commonly found in today's drilling programs. Technologies such as managed pressure drilling (MPD) have become more popular in areas where an increased level of control of borehole pressures is required to enable drilling in regions with tight pressure margins.

Manual control methods involve some level of human decision-making and often depend on surface level observations or limited downhole information. Unfortunately, with these types of data sources, dynamic conditions may not be detected and understood until well after these new conditions have developed downhole. As such, even the best methods of manual control are limited by relatively slow reaction time and potentially inconsistent results.

Wired drill pipe (WDP) technology [84, 126, 144] offers a step improvement in the timeliness and quality of downhole data so that the dynamic subterranean environment is more fully understood. Most notably, this data delivery method is independent of fluid flow or formation characteristics, enabling continued flow of information during a large percentage of the well construction process; for example, even when mud pumps are offline. Further, WDP enables placing sensors along the entire length of the wired drill string, providing quality information about multiple points of interest in the well that can be transferred to the surface in real-time [145]. Information delivered real-time by WDP has already been found to be of great benefit in improving drilling efficiency [146]. However, in order to more fully leverage the value of these new sources of data and the high-speed feedback provided, and to enable further improvements in the ability to control the drilling process, the marriage of this technology with automated control methods is extremely desirable. In particular, when a model predictive controller has access to this high-resolution data, it quickly processes the data into information regarding changing well conditions and begins control adjustments as soon as conditions fluctuate, yielding more precise management of dynamic events such as pressure fluctuations and fluid influx (kick attenuation). This chapter discusses more complete utilization of the unparalleled data transfer speed and bandwidth that WDP provides and proposes models that improve MPD methods and further increase the benefits they provide.

Developments in high-speed telemetry allow for more precise modeling that, in turn, provides for rapid automation. Previous studies on kick management have focused on either kick detection methods or kick attenuation methods. Hargreaves et al., used Bayesian probabilistic framework to create a detecting system based on surface measurements [123]. In response to a variety of drilling environments, techniques like automated control of flow out to match flow in [124], adaptive observer [101, 111] and a dynamic neural network of surface [125] have been suggested. Some early kick detection methods utilizing the Doppler Effect were proposed by Zhou et al [126]. A partial differential equation model of the hydraulic system and the method of backstepping was used by Hauge et al. to design an observer that quantifies and detects in- or outflux from the annulus [98]. Similarly, Gravdal et al. developed a kick detection methodology that uses a wired pipe telemetry system to collect distributed pressure measurements other than flow measurements [122]. Zhou et al. designed a switched controller that is based on estimated downhole pressure and bit

flow rate values for kick attenuation for managed pressure drilling [109,111,114] and dual gradient drilling [101]. This controller regulates pressure and flow rate during normal drilling conditions. However, when a kick is detected it switches into a flow controller to reduce the effect of the sudden gas influx and circulate out the kick. Hauge et al. [147] additionally proposed a pure flow controller that relies on both influx and estimated bit flow rates and also estimate, the gas influx location. Carlsen et al. utilized three separate controllers including proportional-integral-derivative (PID), an internal model controller (IMC), and a linear model predictive controller. Each of these controllers were evaluated in three main well control scenarios including pump start-up, shut-in, and in circulating out kicks [103]. Each of these methods involves a simplification of a nonlinear system to fit within a modeling or control framework. The purpose of this work is to extend previous studies by quantifying the improved performance of a semi-empirical nonlinear dynamic model directly in a real-time estimation and control framework. Many types of controllers have been proposed in the past but the combination of nonlinear estimation, wired drillpipe, and nonlinear model predictive control is a unique contribution.

The goal of the developed controller is to maintain the annular pressure and the rate of penetration (ROP) during the course of drilling, even during kick events. The models utilized in this controller are capable of both faster kick detection and attenuation than previous schemes. This controller is presently applied to pressure control equipment typically installed in MPD operations. In other controllers, pressure is a function of the choke valve opening and mud pump flow rate, while ROP is a function of the revolutions per minute (RPM) and weight on bit (WOB). These are then monitored with separate controllers. However, in the models outlined below, the influences of each variable on the other controlled variable are also considered, meaning RPM and WOB are variables of annular pressure and the mud pump flow rate and choke valve opening are variables of ROP. This implies that, combined with the high rate of data transfer possible through WDP, a multivariate controller that uses WOB, choke valve opening, RPM, and mud pump flow rate as manipulated variables performs the roles of both separate controllers simultaneously and faster than before. Common practices in MPD recommend stopping drilling while dealing with an influx in the annulus because the main influx indicator (mass balance, i.e. flow out vs. flow in) is lost due to influx expansion in the annular. Because of the fast response time and quick access to additional measurements, this controller improves borehole pressure regulation while still optimizing ROP,

even during complex influxes. This not only decreases response time for attenuating kick events, but also minimizes the impact that these adjustments have on ROP. The significant advantages of this method over previous techniques are greater cost effectiveness and safety of drilling programs. Future work with high fidelity simulators and on test rigs will be used to validate this potential that is indicated with lower-order models.

Previous work by Godhavn et. al has demonstrated the value of this approach [96]. The present study represents a continuation of this work and further refines the overall model predictive control system in several significant ways. In particular, work is presented that explores variable locations of an influx event with respect to the sensor location, and the utility of multiple sensors arrayed along the drillstring. Previously, an assumption was made that the location of an influx event generally coincided with the sensor that detected the event; in this study, however, the effects of the distance between event and sensor, or the speed of event detection, are considered. Other enhancements to the system include the addition of real-world equipment characteristics, including their associated time constants and delays, and the refining of the downhole model by information obtained from distributed measurements. In this latter consideration, provision is made for fluid characteristics that vary along the length of the wellbore, which enables more realistic modeling and opens the door in the future for more sensitive controls based on localized cuttings loading. Finally, consideration is given to the possibility of dynamic events occurring during periods of disconnection of the data sources (such as during tripping or making a connection) and the effect on controller function during these modes of operation is explored.

5.2 Modeling

A brief review of the model is given here to explain the source of the equations that are used for the simulation and control studies. A simple, but industry-tested, model is used for the present work; however, the process described may be applied to more complex models that may become available in the future, if such models offer improved utility. In this case, the simulation model is applied directly in the nonlinear controller to both simulate the future time evolution of certain critical control variables, but also look backwards from the current time to reconcile unmeasured or uncertain parameters and states within the model to available controlled variable measurements. This process of updating the model when new measurements arrive is important to avoid offline

tuning of the controller. In this case, a semi-empirical model of the drilling process is described by a series of differential and algebraic equations with adjustable parameters. This set of equations constitutes a virtual drilling process that an optimizer can adjust to maintain pressure, ROP, rotation rate, WOB, cuttings loading, and other key values that are of concern during all phases of operation. One of the innovations of this work is a simplified, lower-order, comprehensive model from literature sources. A more rigorous expression of drillstring dynamics, wellbore hydraulics, rate of penetration, multi-phase flow, and topside equipment dynamic response is possible, but not attempted in this work. Lower-order models are selected to enable real-time estimation and control. In future work, lower-order models will be updated from high fidelity simulators that run in parallel to the drilling process.

5.2.1 Pressure Response to Control Action

This first section of the model description is a review of the dynamic relationship between pump pressure (p_p), choke valve pressure (p_c), drill bit flow rate (q_{bit}), and drilling height (h_{bit}). Stamnes et al. [148] introduced a lower order model that describes the pressure dynamics of a drill string and is derived from mass and momentum balances. Although it is a simplified model, it has a wide adoption in case studies that utilize lower-order models and has been implemented in the field with satisfactory agreement to actual drilling operations [130]. This model includes ordinary differential equations that were originally proposed in semi-explicit form (such as $\dot{x} = f(x)$) that describe the dynamics of four corresponding variables. The equations are modified into open-equation form (such as $0 = f(\dot{x}, x)$) where the differential term does not necessarily need to be isolated on the left side of the equation. The model is also expressed in open-equation form in the modeling and simulation platform used in this study [133]. Equation 5.1 describes the dynamics of the pump pressure that depends on the difference between the pump volumetric flow rate (q_{pump}) and the volumetric flow through the bit (q_{bit})

$$\frac{V_d}{\beta_d}\frac{dp_p}{dt} = q_{pump} - q_{bit} \tag{5.1}$$

where the time constant of $\frac{V_d}{\beta_d}$ is related to the volume (V_d) and compressibility (β_d) of the drilling fluid inside the drilling pipe between the pump and the drilling bit. The time constant of a

first order differential equation such as this is the amount of time for a change in one of the inputs to affect the output. This time constant is the amount of time to reach 63.2% (or $1-e^{-1}$) of the change towards the final steady state value. A similar time constant is also found in Equation 5.2 as follows:

$$\frac{V_a}{\beta_a}\frac{dp_c}{dt} = q_{bit} + q_{back} - q_{choke} + q_{res} - ROP\ \ A_a \tag{5.2}$$

But this time constant depends on the annulus values for volume (V_a) and compressibility (β_a). The equation is derived from a mass balance where volumetric flows into the annulus (such as mud through the bit (q_{bit}), back pressure flow (q_{back}), and reservoir influx (q_{res})) are positive, and flow out of the annulus through the choke valve (q_{choke}) has a negative sign.

The rate of increase in the volume of the annulus is represented by the product of ROP and the cross-sectional area of the annulus (A_a). The choke valve volumetric flow rate (q_{choke}) is related to the percentage opening of the choke valve (z_{choke}) based on Equation 5.3

$$\dot{m}_{choke} = q_{choke}\rho_a = K_c z_{choke}\sqrt{\rho_a(p_c - p_0)} \tag{5.3}$$

This is a modified form of the volumetric flow correlation for flow through a valve as $q_{choke} = K_c z_{choke}\sqrt{\frac{p_c - p_0}{\rho_a}}$. K_c is the valve coefficient and is determined based on characterization of the valve gain, ρ_a is the fluid density in the annulus, and p_0 is the pressure downstream of the choke valve. The relationship between *ROP* and the height of the drill string (h) is shown in

$$\frac{dh}{dt} = ROP\cos(\theta) \tag{5.4}$$

It is important to reconcile estimation of *ROP* with measured height, including vertical and horizontal distances. For this study, the angle of hole deviation (θ) from vertical is assumed to be zero, although deviated wells are permitted in this framework.

The final expression in this simplified pressure dynamic model is:

$$M\dot{q}_{bit} = p_p - F_d|q_{bit}|q_{bit} + \rho_d g h_{bit} - p_{bit} \tag{5.5}$$

It relates the pump pressure (p_p), frictional pressure loss ($F_d|q_{bit}|q_{bit}$), hydrostatic pressure ($\rho_d g h_{bit}$), and bit pressure (p_{bit}) to the flow through the bit ($\dot{q}_{bit}$).

In this case, F is the friction factor and M represents the lumped density per length. The value of M is determined as follows:

$$M_a = \rho_a \int_0^{l_w} \frac{1}{A_a(x)}\,\mathrm{d}x \tag{5.6a}$$

$$M_d = \rho_d \int_0^{L_{dN}} \frac{1}{A_d(x)}\,\mathrm{d}x \tag{5.6b}$$

$$M = M_a + M_d \tag{5.6c}$$

where l_w represents annulus and L_{dN} represents drillstring lengths. Eqs. 5.6a through 5.6c integrate the reciprocal area of the cross-section of the annulus and inner drill string. Subscript a refers to annulus properties while subscript d refers to drill string properties.

The downhole bit pressure (p_{bit}) can be calculated by including the effects of changes in choke pressure (p_c), frictional losses ($\rho_a F_a|q_{bit}+q_{res}|(q_{bit}+q_{res})h$), and the static head of the vertical height (h_{bit}) of the column of annulus fluid ($\rho_a g h_{bit}$):

$$p_{bit} = p_c + \rho_a F_a|q_{bit}+q_{res}|(q_{bit}+q_{res})h + \rho_a g h_{bit} \tag{5.7}$$

This expression for pressure does not include the dynamics of the pressure wave propagation that becomes significant for extended reach wells. The addition of pressure wave propagation creates a distributed parameter model form that is included in many high fidelity models, but ignored in lower-order models.

This model is further augmented to include pressure sensors at multiple locations along the drill string as follows:

$$p_i - p_{i+1} = \rho_{a,i} F_{a,i}|q_{bit}+q_{res}|(q_{bit}+q_{res})(h_i - h_{i-1}) + \rho_{a,i} g (h_{v,i} - h_{v,i-1}) \tag{5.8}$$

The segments are numbered with the lowest index closest to the BHA. Friction factors ($F_{a,i}$) are estimated for each segment between measurement stations, as well as densities ($\rho_{a,i}$). Changes in density for a segment can indicate either gas influx (lower density) or buildup of solids within a particular zone (higher density).

The preceding equations are important for the controller design because they dynamically relate the influence of choke value and pump flow on the pressure and flow rate at various points along the drill string. Simulation studies have been performed previously to understand the relationships between these design variables in downhole pressure control schemes [85].

5.2.2 Empirical ROP

An empirical model for ROP is commonly applied in industrial practice to describe the response of the penetration rate to adjustable and measureable parameters . Parameters from the empirical model are updated based on geologic properties, bit geometry, and a number of other controlling factors. Statistical analysis of past drilling data determines which effects are significant [129]. One such equation is presented as:

$$\frac{dF}{dt} = f_1 \cdot f_2 \cdot f_3 \cdot f_4 \cdot f_5 \cdot f_6 \cdot f_7 \cdot f_8 \tag{5.9a}$$

$$f_1 = \exp(a_1) \tag{5.9b}$$

$$f_2 = \exp(a_2(8000 - D)) \tag{5.9c}$$

$$f_3 = \exp\left(a_3 D^{0.69}(g_p - 9)\right) \tag{5.9d}$$

$$f_4 = \exp(a_4 D(g_p - \rho_c)) \tag{5.9e}$$

$$f_5 = \exp\left(a_5 \ln\left(\frac{\frac{W}{db} - (\frac{W}{db})_t}{4 - (\frac{W}{db})_t}\right)\right) \tag{5.9f}$$

$$f_6 = \exp\left(a_6 \ln\left(\frac{RPM}{100}\right)\right) \tag{5.9g}$$

$$f_7 = \exp(-a_7 \varepsilon) \tag{5.9h}$$

$$f_8 = \exp\left(a_8 \frac{F_j}{1000}\right) \tag{5.9i}$$

Equation 5.9 predicts the ROP for roller-cone bit types as determined by values that can either be changed during operation, directly measured, or estimated from other available measurements.

The eight constants a_1 to a_8 are chosen to fit specific drilling conditions for a particular well. The predicted ROP is the product of each of the contributing factors, f_1 to f_8, that correspond to the eight empirically determined constants. Each factor contributes an exponentially dependent term computed from measured or estimated values. Factor f_1 is a multiplicative bias that scales the final predicted value up or down to best agree with measured values and relates to the formation strength. Factor f_2 is formation compaction depending on the true vertical well depth (D in ft). The effect is centered at 8000 ft, where f_2 is unity. The pore pressure gradient (g_p in lb_m/gal) affects both factor f_3 (also formation compaction) and f_4 (pressure differential) and accounts for the change in pore pressure on penetration rate. Factor f_4 is different in the sense that it also depends on the equivalent circulating density (ρ_c in lb/gal). Factor f_5 is a fractional ratio that compares the bit weight per inch of bit diameter $\left(\frac{W}{db}\right)$ to the threshold bit weight per inch of bit diameter at which the bit begins to drill $\left(\frac{W}{db}\right)_t$ with both in units of 1,000 lb_f/in. Factor f_6 is the dependence on rotary speed (RPM) and factor f_7 considers the fractional tooth wear with parameter ε. The final factor f_8 is the effect of the hydraulic impact force (F_j in lb_f) beneath the bit.

5.2.3 Exploiting Rotational Speed Effect on Friction Factor

One of the innovations of this work is the coupling of penetration rate and pressure control. It is well known that changing the rotation speed of the drill string increases the effective friction factor for the mud flowing through the annulus. This effect is due to the increased difference in velocity that the drilling mud and cuttings have with the drillpipe and annulus wall. When flowing, but not rotating, the drill string, the annulus fluid has principally an axial direction in the annulus. As the drill string begins to spin, the rotational movement causes an additional frictional flow loss because the mud slurry is in a confined space that has boundary conditions with higher relative velocity between the annulus wall and drillpipe. This rotational movement of the fluid can have a very significant effect on the friction factor, as reported in the literature [132, 134–138]. The effect of rotational speed on the friction factor has been researched and modeled previously. A simple empirical model that is based on the fluid Reynolds number is used for the simulation results in

this study. The model form was originally proposed by Ozbayoglu et al. [138] with parameters a, b, and c that are determined empirically from drilling data as

$$f_a = a \;\; Re_a^b + c \;\; Re_\omega \tag{5.10a}$$

The value of the axial modified Reynolds number is given by Re_a, and the value in the rotational direction is given by Re_ω as

$$\left(Re_a = \frac{757\rho \;\; v_a(D_0 - D_1)}{\mu_a} \right) \tag{5.10b}$$

$$\left(Re_\omega = \frac{2.025\rho \;\; RPM(D_0 - D_i)D_i}{\mu_\omega} \right) \tag{5.10c}$$

In this case, ρ is the density of the fluid, RPM is the rotational rate, v_a is the velocity in axial direction, D_i and D_o are outer pipe and wellbore diameters, respectively, and μ_a and μ_ω are the effective viscosities in axial and rotational directions.

5.2.4 Rotational Dynamics

The rotational dynamics of the drill string can be approximated as a damped torsional spring system. As torque is applied with the top drive, the top sections of the drill string begin to rotate., the drill string transfers the rotational energy to successively lower segments of the drill pipe by torsional strain. The drill bit begins to rotate and eventually the bit rotational rate approximately equals the top drive rotational rate. In the event of stick-slip conditions, the bit stops rotating even though the top drive continues to rotate the top of the drill string. Whether by shear off or the bit breaking free, the drill string releases the stored potential energy and the BHA rotates much faster for a brief period of time. To approximate the drill string rotation dynamics, the drill string is modeled as a series of damped torsional springs [139] as

$$
\begin{aligned}
J_1\ddot{\theta}_1 &= T_1 - T_2 - \mu\dot{\theta}_1 \\
J_i\ddot{\theta}_i &= T_i - T_{i+1} - \mu\dot{\theta}_i \\
&\cdots \\
J_n\ddot{\theta}_n &= T_n - (\mu + \mu_b)\dot{\theta}_n
\end{aligned}
\tag{5.11a}
$$

$$
\begin{aligned}
T_1 &= d_1(\dot{\theta}_{td} - \dot{\theta}_1) + k_1(\dot{\theta}_{td} - \dot{\theta}_1) \\
T_i &= d_i(\dot{\theta}_{i-1} - \dot{\theta}_i) + k_i(\dot{\theta}_{i-1} - \dot{\theta}_i) \\
&\cdots \\
T_n &= d_n(\dot{\theta}_{n-1} - \dot{\theta}_n) + k_n(\dot{\theta}_{n-1} - \dot{\theta}_n)
\end{aligned}
\tag{5.11b}
$$

where θ_i is the angle of the segment of the corresponding segment of pipe i. The rotational rate of the top drive ($\dot{\theta}_{td}$) can be changed to achieve desired penetration rate, solids suspension, and pressure control by changes to the friction factor. Inertia (J_i) is transferred to successive drill string segments and lost proportional to the friction coefficient of the wall (μ) and the bit (μ_b). The internal damping coefficients (d_i) and stiffness coefficient (k_i) for each string section are also important parameters in the transfer of torque (T_i). Figure 5.1 demonstrates the simulated response of a 100 segment drill string to a step change in the top drive rotational rate. The top drive immediately increases at 0.5 seconds to the new rotational rate. The resulting oscillation has a period of approximately 4 *sec* and exhibits a damped response with a settling time within 5% of steady state step change of 19 *sec*.

The discretization of these pipe segments is different than the spatial discretization of pressure sensors. The pressure sensors correspond to physical locations that contain a signal repeater and pressure transducers. It is desireable to have a sufficiently accurate drill string dynamic representation while minimizing the number of segments (n) to improve the computational efficiency of the simulation.

5.2.5 WOB Dynamics

In addition to the transfer of rotational energy, an important adjustable value to maintain penetration rate is the WOB. The dynamics of the transfer of force from the top drive suspension to

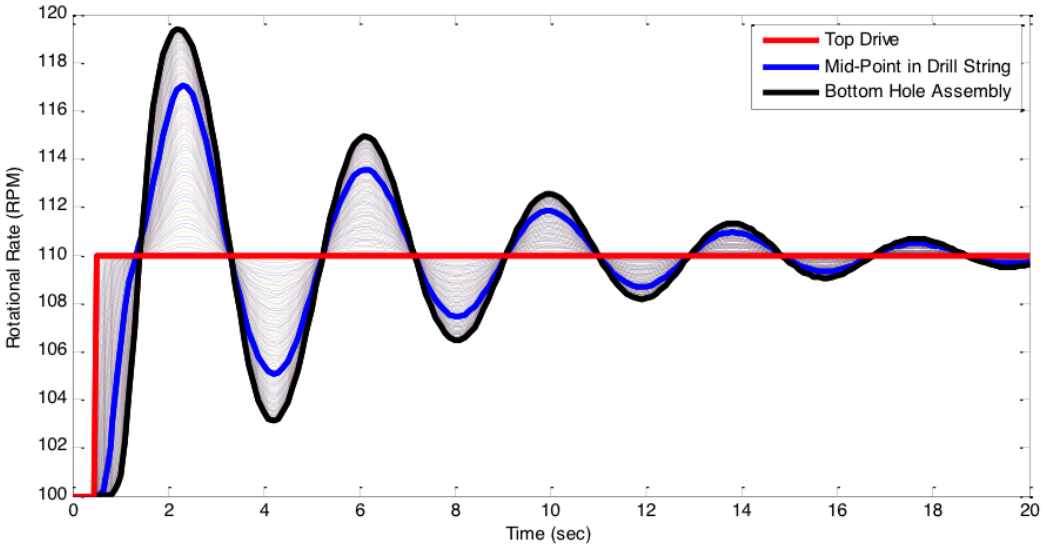

Figure 5.1: Dynamic step response of the drill string model to a change in the top drive rotational rate from 100 to 110 RPM.

the bottom hole are fast. However, the hydraulic or electrical motors used to implement changes in the WOB are not as fast and may have significant lag times that are important for the design of the control system. Without empirically determining the response characteristics of an actual drilling operation, the transfer of weight from the surface (WOB_s) to the bottom hole (WOB_b) is modeled dynamically as a first order linear model with a gain (K_p), a time constant (τ_p), and a time delay (θ_p) as

$$\tau_p \frac{d(WOB_b)}{dt} + WOB_b = K_p WOB_s(t - \theta_p) \tag{5.12}$$

In reality, the relationship between surface and bottom hole WOB is a complex interaction of frictional, rotational, buoyant, and deviated drillstring effects. This relationship influences the transfer of hook load weight to compressive force of the bit on formation, both dynamically and statically. Future work with high fidelity models will use a more rigorous approach for transfer of weight.

To approximate the dynamics between a commanded change in WOB_s and the actual downhole WOB_b, the values of K_p, τ_p, θ_p change with different drill string specifications and rig capabilities.

5.3 Estimating Unmeasured Parameters

Estimation of unknown or uncertain parameters is important in order to align the response characteristics of the model to individual drilling rig configurations. In estimation, the values of certain parameters can be determined from available measurements as long as the parameters are observable. Observability refers to the relationship between the parameter and the measured state value through the equations of the model. If there is no relationship or low sensitivity, then the parameter is said to be unobservable or weakly observable. A sensitivity analysis is also used in many cases to determine the relative relationship between parameters and available measurements or control objectives. Although a parameter may be observable, it may be insignificant for the controller design because of low sensitivity to the control objective.

One of the objectives of this study is to detect certain events, such as unexpected gas influx or buildup of cuttings, within particular sections of the annulus. With along-string measurements, the location and magnitude of these disturbances is more observable by knowing more precisely the specific location of certain changes. A combination of extended Kalman filter (EKF) and Moving Horizon Estimation (MHE) is used to determine the parameters for the model such as density and gas influx flow rate. EKF is used to estimate the gas influx flow rate and MHE is used to estimate the annulus density values. Both estimators communicate with each other and exchange the estimated parameter values in different scenarios. Certain variables such as choke valve pressure, along-string pressures, and pump pressure are directly measured and are used with EKF and MHE for the estimation criteria. The formulation used for EKF is as follows [149]

1. Initialize x_o
2. Select T_{sim}
3. At each T_{sim} {Prediction Step}

$$\hat{x} = \hat{x} + T_{sim} f(\hat{x}, u) \tag{5.13a}$$

$$A = \frac{\partial f}{\partial x}(\hat{x}, u) \tag{5.13b}$$

$$P = P + T_{sim}\left(AP + PA^T + Q\right) \tag{5.13c}$$

Table 5.1: Summary of parameters used in the EKF formulation (Equation 5.13)

Parameter	Description
T_{sim}	Simulation time step (determined by the computational power of server)
A	State Matrix
C_i	Measurement Matrix
P	Covariance of States
Q	Covariance of Measurements
n	Sample number
y	Measurement
F	State functions
h	Measurement functions
X	State variable
U	Inputs

4. If new measurement, Update

$$C_i = \frac{\partial h_i}{\partial x}(\hat{x}, u[n]) \tag{5.13d}$$

$$L_i = PC_i^T \left(R_i + C_i P C_i^T\right)^{-1} \tag{5.13e}$$

$$P = (I - L_i C_i) P \tag{5.13f}$$

$$\hat{x} = \hat{x} + L_i (y_i[n] - h(\hat{x}, u[n])) \tag{5.13g}$$

The parameters used in Equation 5.13 are shown in Table 5.1.

The MHE uses a squared error objective function [140] to penalize deviation of the model values from available measurement, as

$$min_d \phi = (y_x - y_m)^T W_m (y_x - y_m) + (y_m - \hat{y}_m)^T W_p (y_x - \hat{y}_m) + (\Delta d)^T c_{\Delta d} \tag{5.14a}$$

$$s.t.\ \ 0 = f(\dot{x}, x, u, d) \tag{5.14b}$$

$$0 = g(y_x, x, u, d) \tag{5.14c}$$

$$0 \geq h(x, u, d) \tag{5.14d}$$

The parameters used in Equation 5.14 are summarized in Table 5.2.

Table 5.2: Summary of parameters used in the objective function (Equation 5.14)

Parameter	Description
τ	objective function
y_x	measurements $(y_{s,0},\ldots,y_{s,n})^T$
y_m	model values $(y_{m,0},\ldots,y_{m,n})^T$
$\hat{y}_m$	prior model values $(\hat{y}_{m,0},\ldots,\hat{y}_{m,n})^T$
W_m	penalty outside measurement dead-band
W_p	penalty from the prior solution
d	unmeasured or unknown parameters
Δd	change in parameters
$c_{\Delta d}$	penalty from the prior disturbance values
f	differential equality constraints
x	differential of algebraic states
u	inputs or manipulated variables
g	measurement algebraic expressions
h	inequality algebraic constraints

5.4 Controller

One of the innovations of the multivariate controller presented in this chapter is the addition of along-string measurements in the design. Prior studies have focused on combining model predictive control with high speed data telemetry [96]. With wired drillpipe, sensors can be embedded into the communication pathway. These are often places at the location of signal boosters that read a transmission from a nearby transmitter, clean up the signal, and send it along the coaxial cable that is embedded in the drill pipe. The wired connection is inductively coupled between pipe segments to form a continuous communication pathway from the BHA to the surface equipment. In addition to reading measurements from down hole, comminucation signals can also be transmitted down to actuation devices such as pumps, valves, directional drill steering, or infrequent sampling devices. For this study, pressure sensors are assumed at equally spaced locations of 150 m, although it is possible to either increase or decrease the frequency of the sensors. The pressure sensors and other topside transmitters feed data into the estimator that updates and refines the underlying mathematical model in real-time. The parameter and state values are fed into the nonlinear controller, resulting in suggested control adjustments to rotational rate, suspension force for WOB, pump flows, or choke valve position as shown in Figure 5.2.

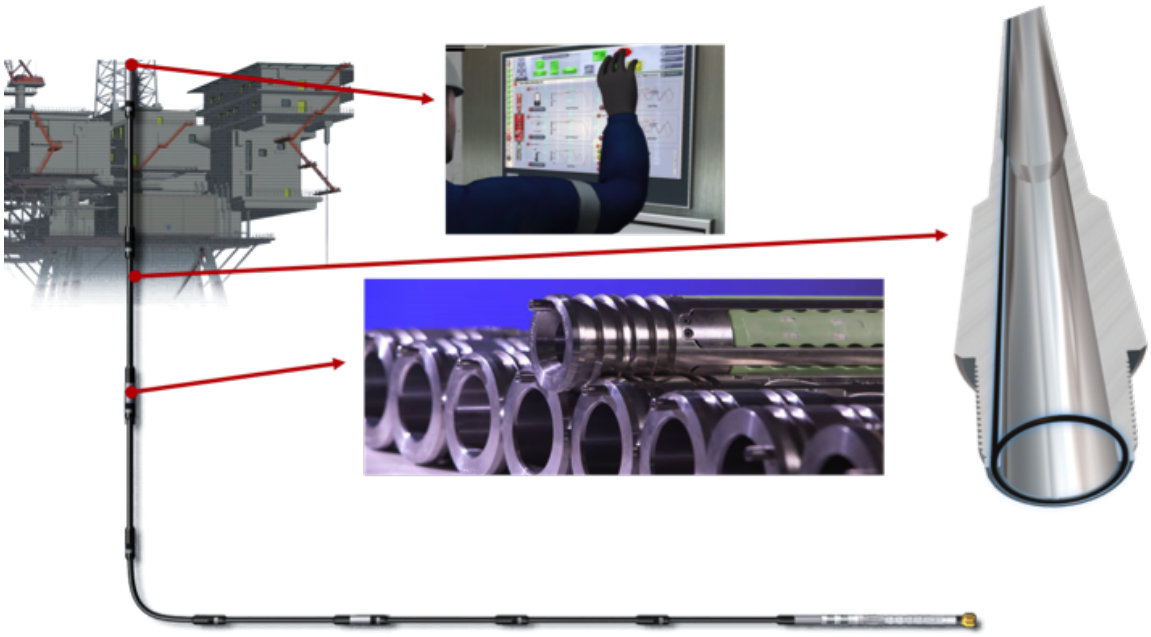

Figure 5.2: Schematic of the control system with multiple along-string pressure measurements.

Table 5.3: Summary of multivariate drilling controller

Manipulated Variables	Controlled Variables	Estimated Values
Rig Pump Flow Rate	Bottom Hole Pressure	Annulus Drill Fluid Density
Choke Valve Opening	Annular Pressures	Annulus Friction Factor
Back Pressure Pump Flow	Choke Valve Pressure	Reservoir Pore Pressure
Weight on Bit	Rate of Penetration	Reservoir Gas Influx
Drillstring Rotational Rate		

The updated multivariate controller design is presented in Table 5.3 with a list of manipulated variables, controlled variables, and estimated values.

The manipulated variables are actively changed by the controller to achieve the best outcome, as described by an objective function. The controlled variables are those values that should either be driven to a target value, such as pressure, or driven to a limit (such as the maximization of penetration rate). Finally, the estimated values are those determined by the estimators and transferred as inputs to the controller.

Figure 5.3 is the step response of the model from input changes at a simulation time of 10 *sec*. Each of the curves corresponds to a separate simulation where either the choke valve opening (nominally 0.3 +1% step), mud pump flowrate (nominally 1440 L/min +1% step), surface WOB

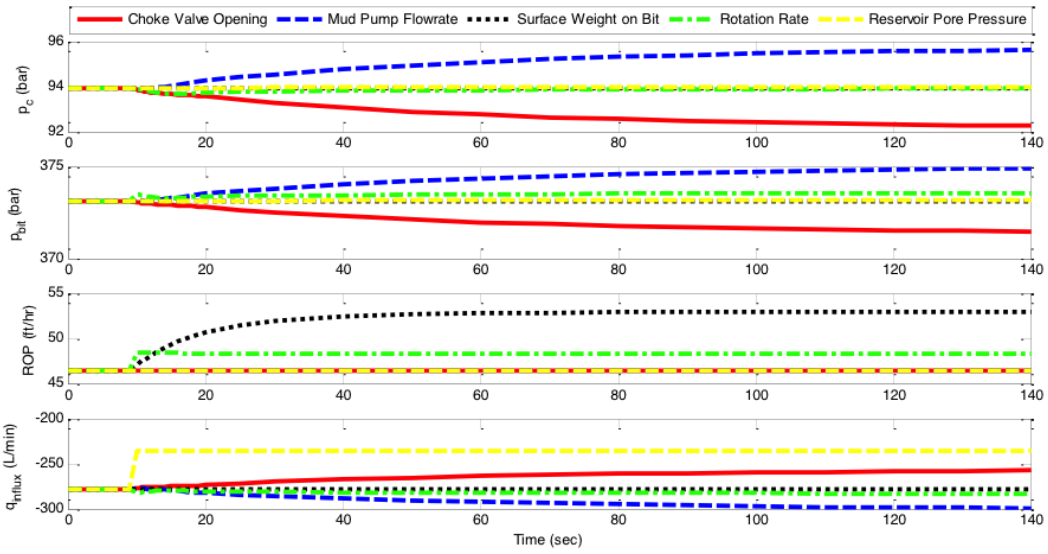

Figure 5.3: Dynamic step response of the model to disturbances or manipulated variables.

(nominally 40,000 *lbs* +10% step), rotation rate (nominally 100 *rpm* +10% step), or reservoir pore pressure (nominally 350 *bar* + 1% step) is changed. Each of the steps occurs in separate simulations at a simulation time of 10 *sec* and affect the dynamic response of four important values to control. The four responses are choke valve pressure (p_c), bit pressure (p_{bit}), penetration rate (ROP), and estimated gas influx into the annulus (q_{influx}).

One of the observations from these plots are that fractional changes in certain variables have a much larger effect on particular responses than others. In the case of choke valve pressure and bit pressure, choke valve opening and mud pump flowrate have nearly equal and opposite responses for a +1% change. In the case of ROP, the top drive rotation rate has a nearly immediate effect on the cutting rate, while adjustments to the surface WOB take longer to affect the ROP because of longer equipment actuation limitations. For gas influx, a change of +1% in the reservoir pore pressure has more effect than a corresponding +1% change in either choke valve opening or pump flow rate. The controller formulation is

Table 5.4: Summary of parameters used in ℓ_1 objective norm (Equation 5.15)

Parameter	Description
ϕ	objective function
y_m	model values $(y_{m,0},\ldots,y_{m,n})^T$
$y_{t,hi}$, $y_{t,lo}$	desired trajectory dead-band
w_{hi}, w_{lo}	penalty outside trajectory dead-band
c_y, c_u, $c_{\Delta u}$	cost of y, u and δu, respectively
f	equation residuals
x	States
u	Inputs
d	parameters or unmeasured disturbances
g	output function
h	inequality constraints
a	lower limits
b	upper limits
τ	time constant of desired controlled variable response
e_{lo}	slack variable below the trajectory dead-band
e_{hi}	slack variable above the trajectory dead-band

$$
\begin{aligned}
&\min_{d}\phi = w_{hi}^T(e_{hi}) + w_{lo}^T(e_{lo}) + (y_m)^T c_y + (u)^T c_u + (\Delta u)^T c_{\Delta u} \\
&s.t.\ \ 0 = f(\dot{x},x,u,d) \\
&0 = g(y_x,x,u,d) \\
&a \geq h(x,u,d) \geq b \\
&\tau_c \tfrac{\delta y_{t,hi}}{\delta t} + y_{t,hi} = sp_{hi} \\
&\tau_c \tfrac{\delta y_{t,lo}}{\delta t} + y_{t,lo} = sp_{lo} \\
&e_{hi} \geq (y_m - y_{t,hi}) \\
&e_{lo} \geq (y_{t,lo} - y_m)
\end{aligned}
\tag{5.15}
$$

The objective function is an ℓ1-norm that forms a region where the controller does not adjust the manipulated variables as long as the controlled variables are within this band. One advantage of an ℓ1-norm versus a squared error objective is in improved noise, data outlier and drift rejection, as shown in Hedengren et al. [133].

Table 5.4 summarizes all the variables used in Equation 5.15.

5.5 Results and Discussion

5.5.1 Test Case

The simulated well has a depth of 2000 m with a drill pipe inner diameter (ID) of 3 $^1/_2$ inches and annulus ID of 4 $^1/_2$ inches. Water-based drilling mud with a density of 12.4 ppg (lb/gal) is used. The well is equipped with 10 wired pipe pressure sensors at 492 ft (150 m) intervals in the openhole area. Temperature effects on the dynamics of hydraulics have been neglected. Initially the well is at a steady state condition and the downhole pressure is kept just above the formation pressure of 300 bar.

5.5.2 Loss of Communication with Surge / Swab Induced Kick

Events such as tripping in or out, or connecting a new pipe stand have traditionally led to loss of communication, with downhole measurements. When there is a loss of communication the estimator and controller receive updates only from the surface instruments. The surface measurements, such as choke valve pressure and back pressure pump action, may be inadequate to detect and respond to an unexpected gas influx. A plausible scenario is one where there is a loss of communication and the surge and swab effects have induced a kick in the annulus. In this specific simulation, the potential loss of communication is shown in Figure 5.4 at the initial time of zero. Ten seconds into the simulation, a kick is induced and the reservoir pressure increases from 300 bar to 450 bar over the next 100 seconds. In reality, the reservoir pressure does not change, but this ramp was induced to simulate a large and changing influx profile, including the effect of reduced hydrostatic head due to gas displacement of the drilling mud. A detectable influx with pit level change is about 10 barrels and is less than 5 barrels with a Coriolis flow meter on the annulus return. The magnitude of this simulated kick is rapid (4 $barrels/min$ immediate change) and large (peak at 9 $barrels/min$) in order to simulate a detectable and nearly worst-case scenario for influx. When there is an interruption in communication, the controller receives no feedback from the downhole measurements until the interruption period has expired and communication is resumed. No topside flow or level measurements are available throughout the simulation. The purpose of this section is to provide guidance on the benefit of restoring communication during connection procedures to better avoid formation damage and kicks induced during tripping in or

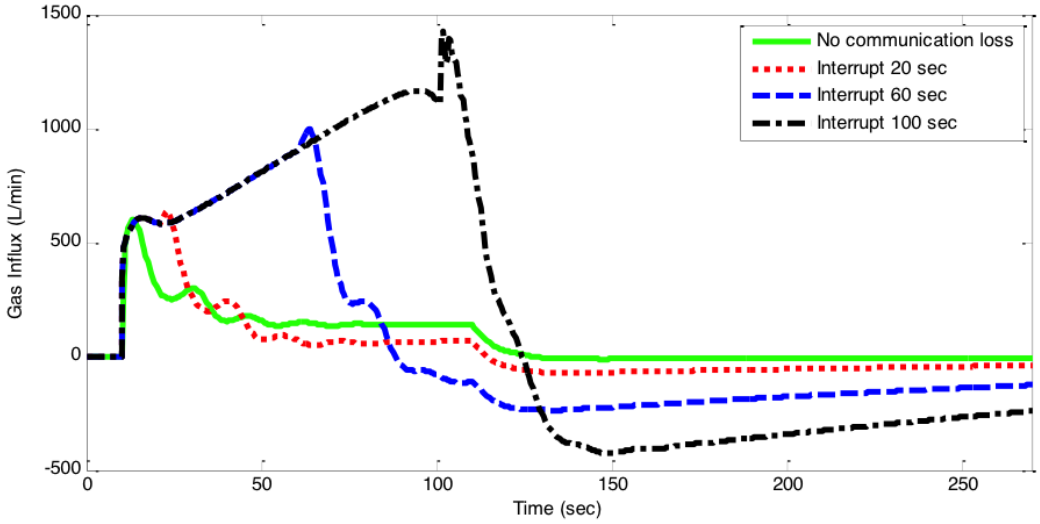

Figure 5.4: Effect of communication loss with an unexpected gas influx at 10 sec simulation time.

tripping out sequences. More realistic simulations will be performed in future work with high fidelity simulators and mass flow measurements.

The size of the kick is expressed in a gas flowrate from the reservoir into the annulus in units of L/min (0.377 $barrels/hr$). The magnitude of this kick is large and the response time is faster for cases that have less time with interrupted communication. In the case of no interruption, the controller is able to respond to the kick immediately and limits the peak influx to less than 600 L/min (226 $barrels/hr$). A communication interruption of 20 seconds also has a peak influx of about 600 L/min but the duration is roughly twice as long. For both 60 and 100 seconds of interrupted communication, there are well control issues as the gas influx begins to ramp up. The immediate controller action causes a slight increase in the gas influx, followed by a rapid decrease as the choke valve closes and the pump increases to add additional pressure to find a balance with the increased reservoir pressure. An inflection in the influx with connection delays of 20 *sec* or larger is due to the initialization of the controller after a period of inactivity and as the estimator correctly detects the influx. Care is taken to not exceed the fracture pressure to avoid damaging the reservoir. In this example, there is a slight overshoot in the annulus pressure over the reservoir pore pressure but this overshoot is well below the fracture pressure.

Another aspect of this controller is that the influx becomes negative as it reintroduces some of the gas influx back into the formation after the controller is restarted. Another method to deal

with gas influx is to increase the density of the mud through the addition of more dense mud components such as barite. This automatic controller does not currently consider the addition of barite as something that is automatically adjusted, but mud mixture density control can be added in future studies.

There is a clear benefit to reducing the time that communication is lost with downhole pressure measurements. The results of this simulation demonstrate that with an automatic model-based controller, the choke valve and back pressure pump or main mud pump are able to reject significant events of unexpected gas influx. An advantage of wired drillpipe is that communication is maintained even when mud is not flowing. One additional opportunity is to create a communication pathway during procedures that require a disconnection to downhole instrumentation.

5.5.3 Cuttings Buildup Detection and Distributed Pressure Control

One of the limiting constraints for ROP is the rate at which cuttings can be removed from the bit and annulus. The cuttings are typically denser than the drilling fluid, leading to potential for settling and aggregation. Buildup happens when significant amounts of cuttings aggregate in a particular zone, especially in deviated well geometries where the drill string transitions from a vertical to horizontal direction such as the kickoff point. Buildup can also occur during extended periods of shutdown when the cutting particles have an opportunity to settle, or in wide areas of the annulus where mud velocity is lower. An accumulation of cuttings may require hole cleaning measures to remove the excess cuttings such as increasing the circulation of mud, increasing the drill string rotation rate, or slugs of alternating mud viscosity to entrain solid particles. Early detection of cuttings buildup can improve the operational strategy for cuttings removal so that less severe measures can be taken to avoid packoff or other buildup issues [144].

This particular simulation introduces a simulated buildup of cuttings along the annulus. With along-string pressure measurements, the buildup is detected through the use of the dynamic model and estimation techniques. The simulated increase in cuttings loading is shown in Figure 5.5 during a startup phase. The estimator begins at the initial time and all of the densities except one converge to a correct value of 1400 kg/m^3. The density estimate from location 5 (middle point in the axial direction of the annulus) converges instead to a value of 1600 kg/m^3. The higher density at this location is an indication of cuttings buildup.

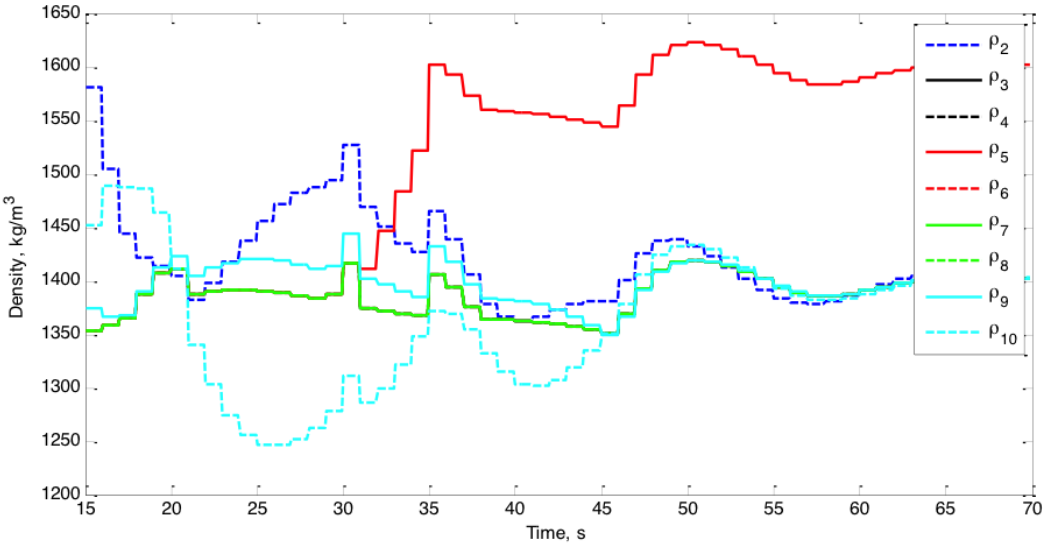

Figure 5.5: Estimation of density values along the annulus.

Figure 5.6 shows the change in ECD and annulus pressure drop during cuttings buildup and control action to maintain downhole pressure. Average estimated density along the annulus was used in the ECD calculation. At a time of 30 sec, cuttings buildup at location 5 leads to an increase in the density at that location and causes an increase in the average density and therefore ECD value. Cuttings buildup doesn't have significant effect on pressure drop; however, it causes a slight initial decrease and then an increase in value. This is because cuttings buildup increases the downhole pressure and the controller opens the choke valve to compensate for this effect. The subsequent oscillations in pressure drop are due to the dynamic action of the controller. If cuttings buildup would have happened in a drilling rig without the controller, it would have increased the pressure drop due to a constant choke valve opening.

The distributed pressure sensor readings are shown in Figure 5.7 during an approximate 50 bar increase in pressure due to the control target of P_1 to 300 bar. P_1 is the lowest pressure sensor at the drill bit while the other lower pressures are located 150 m of vertical depth spacing from each other leading to lower pressures along the annulus as the mud travels back to the surface.

One of the interesting characteristics of this plot is that the increase in pressure at locations 1-5 is slightly lower relative to the other upper pressure sensors (6-10, at locations closer to the surface) at 30 *sec* of simulation time. This almost imperceptible increase in pressure is difficult

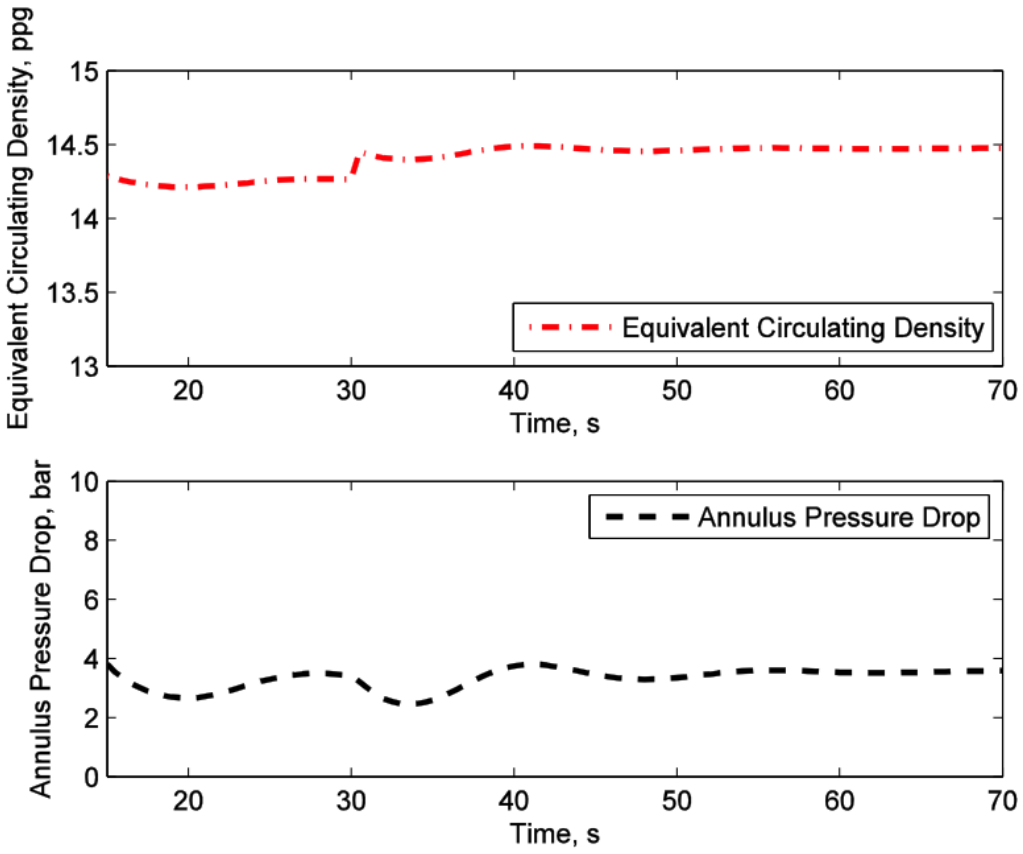

Figure 5.6: Change in equivalent circulating density and annulus pressure drop during cuttings buildup.

for an operator to identify. When density values or differential pressures are displayed, this gives a more clear notification of cuttings buildup to an operator or automatic controller.

Figure 5.8 shows the corresponding manipulated variable action necessary to adjust the bit pressure to a value of 300 bar. The change in density is detected by Moving Horizon Estimation to optimize the values of density given the time series measurements. The density estimates are fed to the predictive controller to update the underlying model used in the forward looking optimization. The pressure controller is able to adjust the pressure regardless of the change in density. In this case, the increase in pump flow rate also serves to better clean the cuttings buildup from the annulus.

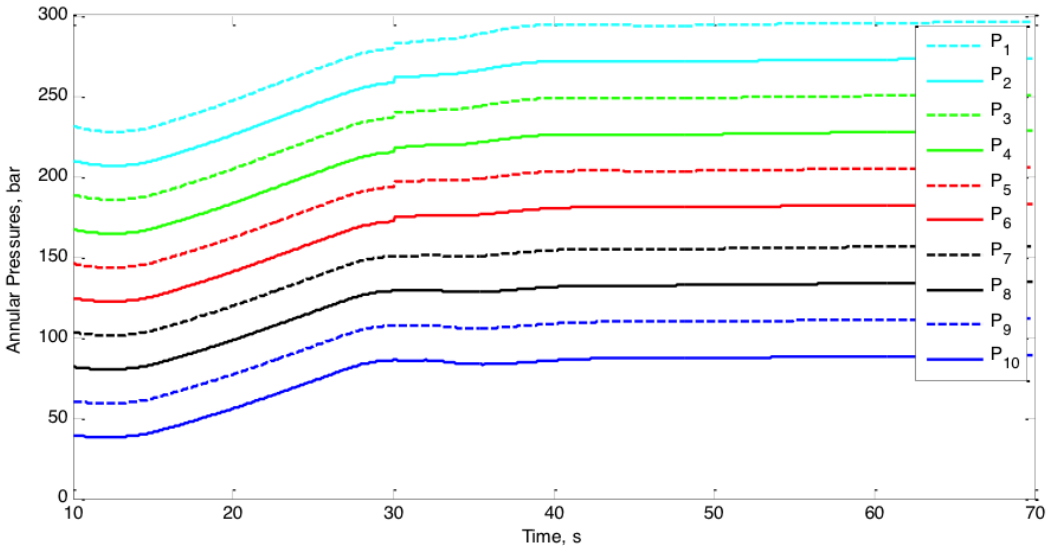

Figure 5.7: Simulation of distributed pressure sensing with along-string measurements in the annulus.

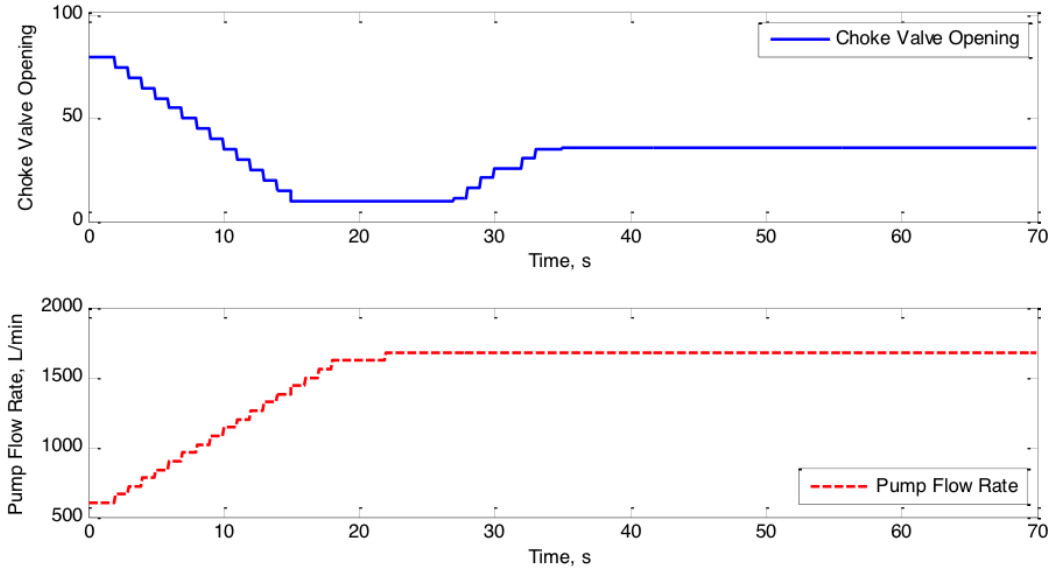

Figure 5.8: Manipulated variable action to control bit pressure to 300 bar.

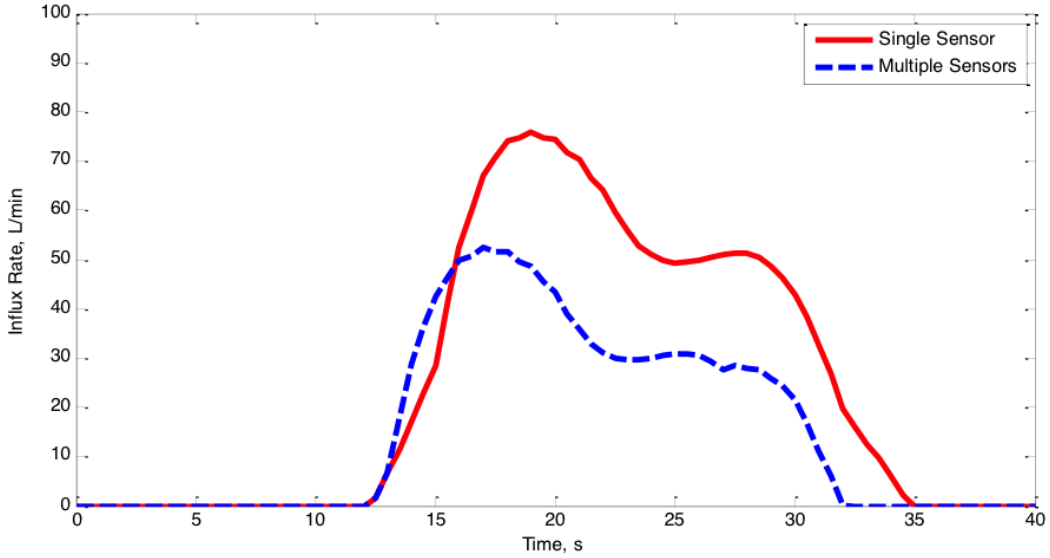

Figure 5.9: Improved kick attenuation due to availability of a sensor closer to the influx location.

5.5.4 Kick Attenuation with Distributed Pressure Measurements

The benefits of multiple sensors are evident in automatic control for kick attenuation. In this case, the kick occurs close to location 5. In the single sensor case, the only downhole sensor is at the bit location. For the multiple sensors case, the pressure sensors are located throughout the drillstring at intervals of 150 m. The simulated kick occurs at a time of 10 *sec* and the reservoir pore pressure continues to increase for 100 *sec*. Again, a reservoir pressure increase is not a plausible scenario but has a similar effect as hydrostatic head loss due to gas displacement of drilling fluid for a single phase simulation model. In the case of multiple sensors, the gas influx is less because the pressure sensor closer to the kick location is able to sense the change earlier and with a higher degree of accuracy. The comprehensive controller manipulates the RPM, pump flow, and choke valve opening simultaneously to attenuate the kick. All of these control actions are coordinated with WOB to maintain the ROP constant [96]. When there is a sufficiently large gas influx event, drilling is normally stopped to circulate out the influx. This improved rejection of unexpected gas influx is shown in Figure 5.9. This reduction in influx decreases the frequency of remedial actions such as kick circulation and periods of drilling inactivity that increase drilling costs.

5.6 Conclusion

It is clear from the results above that a comprehensive multivariate controller for ROP and pressure provides faster response time by synchronizing changes across all of the manipulated variables. Even when communication is temporarily shut off, the controller is able to attenuate the influx at constant rates without compromising ROP. The high frequency data collected by wired pipe technology or other high-speed telemetry makes this control scheme possible by frequently updating the models while implementing control actions. A substantial influence, however, on the overall performance of the controller is the availability of data during the downhole event. This argues for taking measures to ensure minimized interruption of data flow when drilling in regions where the risk of such an event is high.

Significantly, the further resolution provided by multiple sensor locations within a drill-string increases the speed of detection of a downhole influx event, providing a net improvement in the effectiveness of control over the kick and reducing the size of the influx. Further, data collected by distributed sensors is able to detect and accommodate kicks all along the drill string, not just at critical locations. Having such detailed relationships factored into the modeling process generates more consistent results that can quickly achieve target pressures and rates of penetration. These results can still be achieved during a kick event with a comprehensive controller.

The inclusion of real-world equipment characteristics and influence of cuttings loading contribute to this improved response time. Inclusion of advanced NMPC and estimators (both EKF and MHE) also help different drilling situations achieve their operational targets. This work is an ongoing study that has built off the previous results, and the future implementation of these results on actual drilling equipment will confirm the potential of automated drilling optimization.

However, there are a few problems that need to be addressed before implementing the controller,

- The controller needs to be protected against real measurement problems including data outlier and loss of signals.
- There needs to be a protective layer for controller output to make sure it always sends reasonable signals to the system.

- Transfer functions and delays of all the equipments that are connected to the controller should be considered in the controller design.

CHAPTER 6. CONCLUSION AND FUTURE WORK

Automation in the upstream oil industry is relatively undeveloped compared to other industries. Adding automation technology in this area leads to safer, more economically efficient, and environmentally friendly operations. Nonlinear model predictive control, moving horizon estimation techniques are used throughout this work. These advanced technuiques are shown to be effective for highly nonlinear and dynamic drilling systems. The advantage of ℓ_1-norm versus squared error is in its ability to reject corrupted data including data outlier, noise, and drift.

The goal of this work is to design advanced control algorithms for the upstream industry where high speed communication technology is now available. Using the techniques of Chapter 2, a nonlinear multivariate controller was designed for two main upstream industry systems including MPD process and TLP platform balancing. In order to do this high speed data communication, networks are used in both real (TLP platform) and simulated environments (TLP platform and MPD operation). Both measurement techniques are fairly new and are in the process of being fully adopted.

Monitoring system is designed based on fiber optic technology used on TLP tendons for measuring load values. The monitoring system installed on TLP tendons has high sensitivity to even small changes and can detect any load shifts. This is a breakthrough in offshore platform balancing. This monitoring system is simulated with a controller to automate the platform balancing. A MPC controller for load balancing is designed using simulated data. The results show that this leads to significant improvement in offshore platform balancing as the controller decides to either open the ballast tank discharge valve or ramp up the water pumps to maintain the balance. This automation reduces the rising and falling tide effect on the platform. These results pave the way to implement the control system on an actual offshore platform.

It is shown that automating three different drilling scenarios is feasible using a combination of model predictive control and moving horizon estimation. The controller is able to drive the pres-

sure to the desired set point (normal drilling), maintain the desired downhole pressure (connection procedure) and attenuate the unwanted gas influx (kick condition). Automated drilling process reduces drilling time and leads to reduced drilling costs. It is found that the control success is directly related to the data transfer frequency. This is achieved through a high speed wired pipe telemetry system and designing the controller based on lower order models, orthogonal collocation, efficient optimization algorithms and objective functions. With automating downhole pressure control, it is possible to maintain pressure at a lower level than the manual operation. This leads to a higher rate of penetration which is very desirable in drilling operations. At the same time it improves operator safety by attenuating kicks faster and more effectively than manual control. It is found that the drilllstring and hydraulics dynamics effect each other. Therefore for the first time a comprehensive controller is designed that considers the interactions between ROP and pressure, regulating both in a single application. This multivariate controller uses pump flow rate, choke valve opening, rotation speed and WOB as manipulated variables and seeks to maintain ROP and downhole pressure. Annulus density, friction factor, and unwanted gas influx flow rate are not directly measured during drilling and therefore are considered estimated variables. For this purpose, an MHE is designed to estimate annulus friction factor and density, and an EKF was designed to estimate unwanted gas influx flow rate.The nonlinear model predictive controller (NMPC) designed for this application uses a novel $\ell 1_1$-norm with a dead band structure in the objective function. This is known to improve robustness of the controller while rejecting data outlier, noise and drift [92]. Simulation results show that the integrated multivariate ROP and downhole pressure controller has superior performance compared to the case where each ROP and pressure have separate, independent controllers. This is because the multivariate controller has extra degrees of freedom as it is able to change the drillstring rotation speed and effect on the frictional pressure loss and therefore on the downhole pressuree in addition to the choke valve opening and mud pump flow rate. At the same time, this multivariate controller changes the downhole pressure and effect on the rate of penetration. The benefits are faster and more effective kick attenuation along with a higher ROP, leading to more efficient drilling operations. The multivariate controller is designed as follows:

During normal drillinig the goal is to maximize the ROP while maintaining the downhole pressure within a specified range. Therefore the controller calculates the required downhole RPM, WOB, and downhole pressure values that lead to highest possible ROP. Next, it manipulates the

pump flow rate and choke valve opening to regulate the downhole pressure to specified set points and changes topside WOB and RPM until the required WOB and RPM are achieved at the Bottom Hole Assembly (BHA).

During a kick event, the primary goal is to attenuate the kick while maintaining a constant ROP. First, the controller detects the kick condition through a rise in the downhole pressure and estimated unwanted gas influx value. Second, the application switches the controlled variable from downhole pressure to choke valve pressure and sets a new set point as the current value plus the desired change observed in the downhole pressure. Third, the controller calculates the optimum pump flow rate, choke valve opening and downhole RPM that leads to the new choke valve pressure set point. Finally, the controller adjusts the choke valve opening and pump flow rate and topside rotation speed to target values. This increases the pressure of the upper parts of the annulus that have not been affected by the kick and results in kick attenuation. WOB only affects ROP. Therefore, the controller also changes the topside WOB to compensate for the effect of the change in RPM to maintain a constant ROP. While attenuating the kick, the new reservoir pore pressure is estimated using the available topside and along-string measurements. When the unexpected gas influx is suppressed, the controlled variable is switched back to downhole pressure with the new set point calculated based on the new reservoir pore pressure.

Another innovation of this work is in designing a controller by considering multiple sensor measurements along the annuus. It is found that this leads to significant benefits: (1) cuttings build up can be detected early because in this case the MHE estimation results from multiple pressure sensors report different densities along the annulus and any change in the density is a sign of cuttings build up (2) kick condition is detected even earlier and attenuated faster than the single sensor case as the sensors closer to the gas influx intrusion sense an early downole pressure change, helping the controller in faster detection and attenuation of the kick.

Generally, upstream industry processes are mostly operated manually as opposed to the downstream and other energy industries. One of the main challenges in automation is the lack of a high speed data communication network and also the inherent nonlinear dynamical nature of these processes which require efficient nonlinear controllers. This study shows that it is feasible to design automation algorithms in this industry through using advanced control and estimation techniques along with the latest data measurement and communication technology.

6.1 Future Work

6.1.1 TLP Load Balancing

The MPC controller designed in this work is tested against a lower order simulation of TLP platform. For future work, a more detailed TLP simulation model should be considered with all degrees of freedom for each tendon movement. This more sophisticated model can help in designing a more efficient controller and gives a better insight on how the controller would behave in actual conditions. Also, an MPC model can be improved to better capture the TLP dynamics. It can also include the tendon length changing system as another manipulated variable.

6.1.2 Data Reconciliation and Validation for Drilling Support Centers and Automation

Automation strategies rely on a foundation of stable and reliable measurements of critical drilling parameters such as pressure and flow. When measurements are either unreliable, inaccurate, or unavailable then automation strategies may degrade in performance, require use of soft sensors (predictive models), or revert to manual control. Measurements may be available through wired drillpipe, mud pulse communication, or through stored measurement-while-drilling (MWD) tools. Some specific problems with drilling measurements are time lag, outliers, drift, and noise.

Drilling Support Centers

With increased communication capabilities to remote areas, data streaming from drilling is consolidated in drilling support centers that can advise drilling operators in real-time. One challenge is that the drilling support centers are removed from the rig and may not be aware of the remote circumstances that put the measurements into context of the overall operation. With information available from multiple measurements or model predictions, the requirement for information validation is critical for improved decision support.

Multiple Information Sources

There may be multiple sources of information that sometimes provide conflicting information. For example, mud pit level may be monitored to detect unexpected gas influx into the well

bore. A return flow meter such as a paddle wheel mud flow meter or Coriolis flow meter may also be used to predict gas influx. At times there are multiple measurements that are either redundant or exploit different technologies to measure a specific value of interest. Automatic identification of sources that are providing correct information is also critical for process automation and decision support.

Objectives

The proposed future research is to develop and apply methods to develop tiered drilling automation strategies that adapt with changing measurements and quality. As a first step, data quality is assessed to automatically indicate bad or suspect data. This is accomplished through reconciliation to lower-order models that are both computationally efficient and act as a filter to accept values that are consistent with other measurements and with predicted values. This optimization strategy is a combination of basic and advanced estimation strategies. One advanced approach is Moving Horizon Estimation (MHE) that is suitable for real-time reconciliation of measurements and model predictions as shown in Figure 1. Other advanced approaches that have been considered are the Extended Kalman Filter (EKF) and Unscented Kalman Filter (UKF).

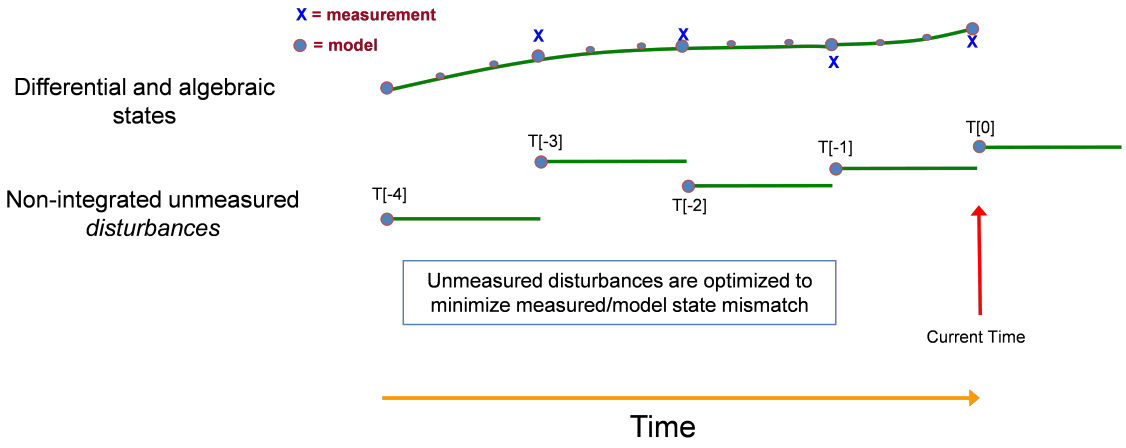

Figure 6.1: Optimized estimation over a prior time horizon of measurements.

Preliminary results with MHE demonstrate that innovative methods for data reconciliation demonstrate improved rejection of outliers, noise, and drift [5]. The lower order models are aligned

to available measurements to estimate prediction error. Stochastic or deterministic methods are used in the reconciliation process to provide specific estimates as well as probability distributions of the result. Measured values that either deviate from expected results or produce unreasonable model parameter estimates are flagged as suspect.

Automation relies on either direct measurement or soft sensors (predictions) to improve drilling operation. The specific tasks for future work include a survey of available measurements, development of automation strategies with expected combinations of available measurements, and recommendations on sensor development and requirements for improved drilling performance.

6.1.3 Using High Fidelity Simulators

The results throughout this work were based on the lower order model of the drilling process, they showed that it is possible to automate the drilling process and improve its economics and safety. The next phase of the project will be to test the controller in more realistic conditions. For this purpose, the controller can be tested using high fidelity simulator and later in a test rig. These tests can help in further improving the controller and its tuning in real conditions.

6.1.4 Kick Attenuation

There are many factors that can be indications of kick. Using only a single parameter to detect a kick risks misinterpreting the data sending the operator a false alarm. For example, sometimes a borehole expansion happens that can draw the reservoir fluid inside the annulus. This increases the downhole flow rate but it is not because of gas intrusion due to the increased reservoir pressure and can be mistaken as kick. Therefore the best way to both determine if a kick has happened and minimize false alarms is to consider the variation in all the possible sensors at the same time. For example, downhole pressure sensor along with the surface flow rate and pressures can be all considered and evaluated at the same time to determine if a kick has happened.

REFERENCES

[1] Qin, S. J., and Badgwell, T. A., 2003. "A survey of industrial model predictive control technology." *Control Engineering Practice,* **11**(7), pp. 733–764. 4, 11

[2] USGS, 2008. U.S. geological survey, July. 4, 5

[3] BP, 2013. Deepwater horizon accident and response. 5

[4] Harte Research Institute, 2013. Ixtoc I blowout and oil spill resources, August. 5

[5] Hedengren, J. D., Asgharzadeh Shishavan, R., Powell, K., and Edgar, T., 2014. "Nonlinear modeling, estimation and predictive control in APMonitor." *Computers and Chemical Engineering,* **70**(5), November, pp. 133–148. 11, 64, 81, 135

[6] Darby, M. L., and Nikolaou, M., 2012. "MPC: Current practice and challenges." *Control Engineering Practice,* **20**(4), April, pp. 328–342. 11

[7] Gyalistras, D., Pr, S., Sagerschnig, C., and Morari, M., 2011. "Modeling and identification of a large multi-zone office building." In *IEEE International Conference on Control Applications (CCA)*, Vol. 17, IEEE, pp. 55–60. 11

[8] Oldewurtel, F., Parisio, A., Jones, C., Morari, M., Gyalistras, D., Gwerder, M., Stauch, V., Lehmann, B., and Wirth, K., 2010. "Energy efficient building climate control using stochastic model predictive control and weather predictions." In *American Control Conference (ACC)*, IEEE, pp. 5100–5105. 11

[9] Nolde, K., Uhr, M., and Morari, M., 2008. "Medium term scheduling of a hydro-thermal system using stochastic model predictive control." *Automatica,* **44**(6), June, pp. 1585–1594. 11

[10] Oldewurtel, F., Jones, C. N., and Morari, M., 2008. "A tractable approximation of chance constrained stochastic MPC based on affine disturbance feedback." *2008 47th IEEE Conference on Decision and Control*, pp. 4731–4736. 11

[11] Papafotiou, G., Geyer, T., and Morari, M., 2007. "A hybrid model predictive control approach to the direct torque control problem of induction motors." *International Journal of Robust and Nonlinear Control,* **17**, November, pp. 1572–1589. 11

[12] Bemporad, A., Morari, M., Dua, V., and Pistokopoulos, E., 2002. "The explicit linear quadratic regulator for constrained systems." *Automatica,* **38**, January, pp. 3–20. 11

[13] Hedengren, J. D., and Edgar, T. F., 2008. "Approximate nonlinear model predictive control with in situ adaptive tabulation." *Computers & Chemical Engineering,* **32**(4), April, pp. 706–714. 11, 44

[14] Johansen, T. A., 2004. "Approximate explicit receding horizon control of constrained nonlinear systems." *Automatica,* **40**(2), February, pp. 293–300. 11

[15] Domahidi, A., Zeilinger, M. N., Morari, M., and Jones, C. N., 2011. "Learning a feasible and stabilizing explicit model predictive control law by robust optimization." In *Decision and Control and European Control Conference (CDC-ECC), 2011 50th IEEE Conference on*, IEEE, pp. 513–519. 11

[16] Ferreau, H. J., Bock, H. G., and Diehl, M., 2008. "An online active set strategy to overcome the limitations of explicit MPC." *International Journal of Robust and Nonlinear Control,* **18**(8), pp. 816–830. 11

[17] Pannocchia, G., Rawlings, J. B., and Wright, S. J., 2007. "Fast, large-scale model predictive control by partial enumeration." *Automatica,* **43**(5), May, pp. 852–860. 11

[18] Findeisen, R., Allgöwer, F., and Biegler, L. T., 2007. *Assessment and future directions of nonlinear model predictive control*., Vol. 358 Springer Berlin, Germany, Berlin. 12, 22

[19] Hedengren, J., 2013. Apmonitor modeling language, 7 Aug 2013. 12, 30, 44

[20] Hedengren, J., 2012. "APMonitor modeling language for mixed-integer differential algebraic systems." In *Computing Society Session on Optimization Modeling Software: Design and Applications, INFORMS National Meeting*. 12

[21] Cizniar, M., Salhi, D., Fikar, M., and Latifi, M., 2005. "A MATLAB package for orthogonal collocations on finite elements in dynamic optimisation." In *Proceedings of the 15th Int. Conference Process Control '05*, Vol. 5. 13

[22] Houska, B., Ferreau, H. J., and Diehl, M., 2011. "ACADO toolkit–an open-source framework for automatic control and dynamic optimization." *Optimal Control Applications and Methods,* **32**(3), pp. 298–312. 13

[23] Piela, P. C., Epperly, T., Westerberg, K., and Westerberg, A. W., 1991. "ASCEND: An object-oriented computer environment for modeling and analysis: The modeling language." *Computers & chemical engineering,* **15**(1), January, pp. 53–72. 13

[24] Åkesson, J., Årzén, K.-E., Gäfvert, M., Bergdahl, T., and Tummescheit, H., 2010. "Modeling and optimization with Optimica and JModelica languages and tools for solving large-scale dynamic optimization problems." *Computers & Chemical Engineering,* **34**(11), pp. 1737–1749. 13

[25] Simon, L. L., Nagy, Z. K., and Hungerbuehler, K., 2009. "Swelling constrained control of an industrial batch reactor using a dedicated nmpc environment: Optcon." In *Nonlinear Model Predictive Control*, L. M. et al., ed., Lecture Notes in Control and Information Sciences. Springer-Verlag Berlin Heidelberg, pp. 531–539. 13

[26] Nagy, Z. K., Mahn, B., Franke, R., and Allgöwer, F., 2007. "Evaluation study of an efficient output feedback nonlinear model predictive control for temperature tracking in an industrial batch reactor." *Control Engineering Practice,* **15**(7), July, pp. 839–850. 13

[27] Hedengren, J., Mojica, J., Cole, W., and Edgar, T., 2012. "APOPT: MINLP solver for differential and algebraic systems with benchmark testing." In *INFORMS National Meeting*. 13

[28] Wächter, A., and Biegler, L. T., 2006. "On the implementation of an interior-point filter line-search algorithm for large-scale nonlinear programming." *Mathematical programming,* **106**(1), pp. 25–57. 13, 18, 30

[29] Genceli, H., and Nikolaou, M., 1993. "Robust stability analysis of constrained ℓ_1-norm model predictive control." *AIChE Journal,* **39**(12), December, pp. 1954–1965. 13

[30] Garcia, C. E., Prett, D. M., and Morari, M., 1989. "Model predictive control: Theory and practice–a survey." *Automatica,* **25**(3), May, pp. 335–348. 13

[31] Nikolaou, M., 2001. "Model predictive controllers: A critical synthesis of theory and industrial needs." *Advances in Chemical Engineering,* **26**, pp. 131–204. 13

[32] Biegler, L. T., 2007. "An overview of simultaneous strategies for dynamic optimization." *Chemical Engineering and Processing: Process Intensification,* **46**(11), November, pp. 1043–1053. 15, 21

[33] Hedengren, J., 2014. Pendulum motion in the APMonitor Modeling Language URL http://APMonitor.com/wiki/index.php/Apps/PendulumMotion. 15

[34] Abu-el-zeet, Z., Roberts, P., and Becerra, V., 2002. "Enhancing model predictive control using dynamic data reconciliation." *AIChE journal,* **48**(2), pp. 324–333. 16

[35] Leibman, M., Edgar, T., and Lasdon, L., 1992. "Efficient data reconciliation and estimation for dynamic processes using nonlinear programming techniques." *Computers & chemical engineering,* **16**(10), October–November, pp. 963–986. 16, 22

[36] McBrayer, K. F., and Edgar, T. F., 1995. "Bias detection and estimation in dynamic data reconciliation." *Journal of Process Control,* **5**(4), August, pp. 285–289. 16

[37] Soderstrom, T. A., Edgar, T. F., Russo, L. P., and Young, R. E., 2000. "Industrial application of a large-scale dynamic data reconciliation strategy." *Industrial & Engineering Chemistry Research,* **39**(6), pp. 1683–1693. 16

[38] Ramamurthi, Y., Sistu, P., and Bequette, B., 1993. "Control-relevant dynamic data reconciliation and parameter estimation." *Computers & chemical engineering,* **17**(1), January, pp. 41–59. 16

[39] Albuquerque, J. S., and Biegler, L. T., 1996. "Data reconciliation and gross-error detection for dynamic systems." *AICHE Journal,* **42**(10), October, pp. 2841–2856. 16

[40] Arora, N., and Biegler, L. T., 2004. "A trust region SQP algorithm for equality constrained parameter estimation with simple parameter bounds." *Computational Optimization and Applications,* **28**(1), April, pp. 51–86. 16

[41] Biegler, L. T., and Arora, N., 2001. "Redescending estimators for data reconciliation and parameter estimation." *Computers & Chemical Engineering,* **25**(11), November, pp. 1585–1599. 16

[42] Gatzke, E. P., and Doyle Iii, F. J., 2002. "Use of multiple models and qualitative knowledge for on-line moving horizon disturbance estimation and fault diagnosis." *Journal of Process Control,* **12**(2), February, pp. 339–352. 16

[43] Mahadevan, R., and Doyle, F. J., 2004. "A partial flatness approach to nonlinear moving horizon estimation." In *American Control Conference, 2004. Proceedings of the 2004*, Vol. 1, IEEE, pp. 211–215. 16

[44] Voelker, A., Kouramas, K., and Pistikopoulos, E. N., 2013. "Moving horizon estimation: Error dynamics and bounding error sets for robust control." *Automatica,* **49**, April, pp. 943–948. 16

[45] Binder, T., Blank, L., Bock, H., Burlisch, R., Dahmen, W., Diehl, M., Kronseder, T., Marquardt, W., Schlöder, J., and Stryk, O., 2001. *Online Optimization of Large Scale Systems: State of the Art*. Springer-Verlag Berlin Heidelberg, ch. Introduction to model based optimization of chemical processes on moving horizons, pp. 295–339. 18, 21

[46] McAuley, S. W. K. A. M. T. J. H. K. B., 2011. "Selection of optimal parameter set using estimability analysis and mse-based model-selection criterion." *International Journal of Advanced Mechatronic Systems,* **3**(3), November, pp. 188–197. 18

[47] Hedengren, J., Allsford, K., and Ramlal, J., 2007. "Moving horizon estimation and control for an industrial gas phase polymerization reactor." In *Proceedings of the American Control Conference (ACC)*, IEEE, pp. 1353–1358. 18

[48] Biegler, L., Campbell, S., and Mehrmann, V., 2012. *Control and Optimization with Differential-Algebraic Constraints*. SIAM - Society for Industrial and Applied Mathematics, Philadelphia. 18

[49] Albuquerque, J. S., and Biegler, L., 1997. "Decomposition algorithms for on-line estimation with nonlinear dae models." *Computers & chemical engineering,* **21**(3), November, pp. 283–299. 18

[50] Diehl, M., Bock, H. G., Schlöder, J. P., Findeisen, R., Nagy, Z., and Allgöwer, F., 2002. "Real-time optimization and nonlinear model predictive control of processes governed by differential-algebraic equations." *Journal of Process Control,* **12**(4), June, pp. 577–585. 18

[51] Haseltine, E. L., and Rawlings, J. B., 2005. "Critical evaluation of extended kalman filtering and moving-horizon estimation." *Industrial & engineering chemistry research,* **44**(8), pp. 2451–2460. 18

[52] Odelson, B. J., Rajamani, M. R., and Rawlings, J. B., 2006. "A new autocovariance least-squares method for estimating noise covariances." *Automatica,* **42**(2), February, pp. 303–308. 18

[53] Hedengren, J., and Edgar, T., 2006. "Moving horizon estimation - the explicit solution." In *Chemical Process Control (CPC) VII Conference*. 18, 44

[54] Spivey, B., Hedengren, J., and Edgar, T., 2009. Monitoring of process fouling using first-principles modeling and moving horizon estimation. 18, 44

[55] Darby, M. L., Nikolaou, M., Jones, J., and Nicholson, D., 2011. "RTO: An overview and assessment of current practice." *Journal of Process Control,* **21**(6), July, pp. 874–884. 18

[56] Soderstrom, T., Zhang, Y., and Hedengren, J., 2010. Advanced process control in exxon-mobil chemical company: Successes and challenges, Nov 2010. 18, 44

[57] Carey, G., and Finlayson, B. A., 1975. "Orthogonal collocation on finite elements." *Chemical Engineering Science,* **30**(5), May-June, pp. 587–596. 22

[58] Albuquerque, J. S., and Biegler, L. T., 1995. "Decomposition algorithms for on-line estimation with nonlinear models." *Computers & Chemical Engineering,* **19**(10), October, pp. 1031–1039. 22

[59] Johansson, K. H., 2002. "Interaction bounds in multivariable control systems." *Automatica,* **38**(6), June, pp. 1045–1051. 27, 28

[60] Raff, T., Huber, S., Nagy, Z. K., and Allgöwer, F., 2006. "Nonlinear model predictive control of a four tank system: An experimental stability study." In *Proceedings of International Conference Control Applications*, pp. 237–242. 27

[61] Gatzke, E., Meadows, E., Wang, C., and Doyle III, F., 2000. "Model based control of a four-tank system." *Computers & Chemical Engineering,* **24**, July, pp. 1503–1509. 27

[62] Johansson, K. H., 2000. "The quadruple-tank process: A multivariable laboratory process with an adjustable zero." *Control Systems Technology, IEEE Transactions on,* **8**(3), May, pp. 456–465. 27

[63] Drca, I., 2007. "Nonlinear model predictive control of the four tank process." Master's thesis, Universidad de Sevilla. 27

[64] Mercangöz, M., and Doyle III, F. J., 2007. "Distributed model predictive control of an experimental four-tank system." *Journal of Process Control,* **17**(3), March, pp. 297–308. 27

[65] Alvarado, I., Limon, D., Muñoz de la Peña, D., Maestre, J., Ridao, M., Scheu, H., Marquardt, W., Negenborn, R., De Schutter, B., Valencia, F., et al., 2011. "A comparative analysis of distributed mpc techniques applied to the hd-mpc four-tank benchmark." *Journal of Process Control,* **21**(5), pp. 800–815. 27

[66] Biegler, L. T., 2010. *Nonlinear Programming: Concepts, Algorithms, and Applications to Chemical Processes*., Vol. 10 Society for Industrial and Applied Mathematics and the Mathematical Optimization Society. 30

[67] Rao, C., and Rawlings, J., 2000. "Linear programming and model predictive control." *Journal of Process Control,* **10**(2), pp. 283–289. 35

[68] Hedengren, J., 2014. MATLAB toolbox for the APMonitor Modeling Language URL http://APMonitor.com/wiki/index.php/Main/MATLAB. 36

[69] Hedengren, J., 2014. Python toolbox for the APMonitor Modeling Language URL http://APMonitor.com/wiki/index.php/Main/PythonApp. 36

[70] Dave, P., Willing, D. A., Kudva, G. K., Pekny, J. F., and Doyle III, F. J., 1997. "LP methods in MPC of large-scale systems: Application to paper-machine CD control." *AIChE journal,* **43**(4), April, pp. 1016–1031. 38

[71] Dave, P., Doyle III, F. J., and Pekny, J. F., 1999. "Customization strategies for the solution of linear programming problems arising from large scale model predictive control of a paper machine." *Journal of Process Control,* **9**(5), October, pp. 385–396. 38

[72] Shishavan, R. A., Brower, D., Hedengren, J. D., , and Brower, A., 2014. "New advances in post-installed subsea monitoring system for structural and flow assurance evaluation." In *Ocean, Offshore & Arctic Engineering OMAE*, no. 24300. 41, 56

[73] Brower, D., Hedengren, J., Shishivan, R. A., and Brower, A., 2013. "Advanced deepwater monitoring system." In *Ocean, Offshore & Arctic Engineering OMAE*, no. 10920. 41

[74] Kersey, A. D., 2000. "Optical fiber sensors for permanent downwell monitoring applications in the oil and gas industry." *IEICE Transactions on Electronics,* **E83-C**(3), pp. 400–404. 42

[75] Brower, D., Hedengren, J., Loegering, C., Brower, A., Witherow, K., and Winter, K., 2012. Fiber optic monitoring of subsea equipment, July. 42

[76] Kelly, J. D., and Hedengren, J. D., 2013. "A steady-state detection (ssd) algorithm to detect non-stationary drifts in processes." *Journal of Process Control,* **23**(3), pp. 326–331. 44

[77] Hedengren, J., and Brower, D., 2013. *Advanced Process Monitoring*. Springer-Verlag Berlin Heidelberg. 44

[78] Powell, K. M., Hedengren, J. D., and Edgar, T. F., 2013. Dynamic optimization of a solar thermal energy storage system over a 24 hour period using weather forecasts, June. 44

[79] Jacobsen, L. T., Spivey, B. J., and Hedengren, J. D., 2013. "Model predictive control with a rigorous model of a solid oxide fuel cell." In *American Control Conference (ACC)*, IEEE, pp. 3741–3746. 44

[80] Spivey, B., Hedengren, J., and Edgar, T., 2010. "Constrained nonlinear estimation for industrial process fouling." *Industrial & Engineering Chemistry Research,* **49**(17), May, pp. 7824–7831. 44

[81] The New York Times, 2013. In BP's record, a history of boldness and costly blunders, August. 47

[82] Asgharzadeh Shishsavan, R., Pixton, D., Eaton, A. N., Park, J., Perez, H. D., Hedengren, J., and Craig, A., 2015. "Addressing ubo and mpd challenges with wired drillpipe and model predictive control." *Submitted to SPE Journal*. 63

[83] Asgharzadeh Shishavan, R., Hubbell, C., Perez, H., Hedengren, J., and Pixton, D. S., 2014. "Combined rate of penetration and pressure regulation for drilling optimization using high speed telemetry." *Drilling and Completions Journal, Accepted for publication*. 63

[84] Pixton, D., and Craig, A., 2014. Drillstring network 2.0 - an enhanced drillstring network based on 100 wells of experience, March. 63, 64, 104

[85] Pixton, D., Asgharzadeh Shishsavan, R., Hedengren, J., and Craig, A., 2014. Addressing UBO and MPD challenges with wired drillpipe, April. 64, 95, 110

[86] Nygaard, G., and Nævdal, G., 2006. "Nonlinear model predictive control scheme for stabilizing annulus pressure during oil well drilling." *Journal of Process Control,* **16**(7), August, pp. 719–732. 65, 66, 68

[87] Siahaan, H. B., and Nygaard, G., 2008. "On modelling and observer design of fluid flow dynamics for petroleum drilling operations." In *47th IEEE Conference on Decision and Control, CDC 2008*, Proceedings of the IEEE Conference on Decision and Control, IEEE, pp. 1857–1863. 65, 66, 67

[88] Song, X., and Guan, Z., 2012. "Coupled modeling circulating temperature and pressure of gas-liquid two phase flow in deep water wells." *Journal of Petroleum Science and Engineering,* **92-93**, August, pp. 124–131. 65

[89] Oliveira, G. M. d., Franco, A. T., Negrão, C. O., Martins, A. L., and Silva, R. A., 2013. "Modeling and validation of pressure propagation in drilling fluids pumped into a closed well." *Journal of Petroleum Science and Engineering,* **103**, pp. 61–71. 65

[90] Nygaard, G., and Nævdal, G., 2005. "Modelling two-phase flow for control design in oil well drilling." In *2005 IEEE International Conference on Control Applications, CCA*, Proceedings of the IEEE International Conference on Control Applications, IEEE, Institute of Electrical and Electronics Engineers Inc., pp. 675–680. 65, 68

[91] Nygaard, G., Nvdal, G., and Mylvaganam, S., 2006. "Evaluating nonlinear kalman filters for parameter estimation in reservoirs during petroleum well drilling." In *Joint 2006 IEEE Conference on Control Applications (CCA), Computer-Aided Control Systems Design Symposium (CACSD) and International Symposium on Intelligent Control (ISIC)*, Proceedings of the IEEE International Conference on Control Applications, IEEE, Institute of Electrical and Electronics Engineers Inc., pp. 1777–1782. 65, 67

[92] Storkaas, E., Skogestad, S., and Godhavn, J. M., 2003. "A low-dimensional dynamic model of severe slugging for control design and analysis." In *11th International Conference on Multiphase 03: Extending the Boundaries of Flow Assurance*, International Conference on Multiphase: Extending the Boundaries of Flow Assurance, BHR Group Limited, pp. 117–133. 65, 132

[93] Nazari, T., Mostafavi, V., and Hareland, G., 2009. "Ukf-based estimation fusion of underbalanced drilling process using pressure sensors." In *2009 IEEE Intrumentation and*

Measurement Technology Conference, I2MTC'09, 2009 IEEE Intrumentation and Measurement Technology Conference, I2MTC 2009, IEEE Computer Society, pp. 1006–1011. 65, 66, 68

[94] Kaasa, G.-O., 2007. "A simple dynamic model of drilling for control." *StatoilHydro Research Centre, Porsgrunn, Norway*. 66

[95] Stamnes, Ø. N., 2007. "Adaptive observer for bottomhole pressure during drilling." Thesis, NTNU. 66, 71, 86

[96] Godhavn, J.-M., Pavlov, A., Kaasa, G.-O., and Rolland, N. L., 2011. "Drilling seeking automatic control solutions." In *18th IFAC World Congress*, Vol. 18 of *IFAC Proceedings Volumes (IFAC-PapersOnline)*, IFAC Secretariat, pp. 10842–10850. 66, 71, 106, 117, 127

[97] Hauge, E., Aamo, O. M., and Godhavn, J.-M., 2012. "Model-based estimation and control of in/out-flux during drilling." In *2012 American Control Conference, ACC 2012*, Proceedings of the American Control Conference, Institute of Electrical and Electronics Engineers Inc., pp. 4909–4914. 66, 69

[98] Hauge, E., Aamo, O. M., Godhavn, J. M., and Nygaard, G., 2013. "A novel model-based scheme for kick and loss mitigation during drilling." *Journal of Process Control,* **23**(4), April, pp. 463–472. 66, 67, 70, 104

[99] Yilmaz, M., Dhansri, N. R., and Mujeeb, S., 2011. "An intelligent control approach for oil drilling processes." *Procedia Computer Science,* **6**, October-November, pp. 106–111. 66, 68, 71

[100] Zhou, J., and Nygaard, G., 2011. "Nonlinear adaptive observer for managed pressure drilling system." In *2011 6th IEEE Conference on Industrial Electronics and Applications, ICIEA*, Proceedings of the 2011 6th IEEE Conference on Industrial Electronics and Applications, ICIEA 2011, IEEE Computer Society, pp. 79–84. 66, 67, 69

[101] Zhou, J., and Nygaard, G., 2011. "Automatic model-based control scheme for stabilizing pressure during dual-gradient drilling." *Journal of Process Control,* **21**(8), September, pp. 1138–1147. 66, 67, 69, 70, 104, 105

[102] Zhou, J., Stamnes, N., Aamo, O. M., and Kaasa, G. O., 2008. "Observer-based control of a managed pressure drilling system." In *Chinese Control and Decision Conference 2008, CCDC 2008*, Chinese Control and Decision Conference, 2008, CCDC 2008, IEEE, pp. 3475–3480. 66, 68, 69

[103] Stamnes, O. N., Zhou, J., Kaasa, G.-O., and Aamo, O. M., 2008. "Adaptive observer design for the bottomhole pressure of a managed pressure drilling system." In *47th IEEE Conference on Decision and Control, CDC 2008*, Proceedings of the IEEE Conference on Decision and Control, Institute of Electrical and Electronics Engineers Inc., pp. 2961–2966. 66, 68, 69, 71, 105

[104] Zhou, J., Stamnes, O. N., Aamo, O. M., and Kaasa, G.-O., 2011. "Switched control for pressure regulation and kick attenuation in a managed pressure drilling system." *IEEE Transactions on Control Systems Technology,* **19**(2), February, pp. 337–350. 66, 67, 70

[105] Stamnes, O. N., Kaasa, G.-O., and Aamo, O. M., 2011. "Adaptive estimation of downhole pressure for managed pressure drilling operations." In *Intelligent Control (ISIC), 2011 IEEE International Symposium on*, IEEE International Symposium on Intelligent Control - Proceedings, Institute of Electrical and Electronics Engineers Inc., pp. 989–995. 66, 68, 69

[106] Zhou, J., Stamnes, O. N., Aamo, O. M., and Kaasa, G.-O., 2008. "Adaptive output feedback control of a managed pressure drilling system." In *47th IEEEsd Conference on Decision and Control, CDC 2008*, Proceedings of the IEEE Conference on Decision and Control, Institute of Electrical and Electronics Engineers Inc., pp. 3008–3013. 66, 68, 69

[107] Li, Z., Hovakimyan, N., and Kaasa, G.-O., 2011. "Fast estimation and l1 adaptive control for bottomhole pressure in managed pressure drilling." In *2011 IEEE International Symposium on Intelligent Control (ISIC)*, IEEE International Symposium on Intelligent Control - Proceedings, Institute of Electrical and Electronics Engineers Inc., pp. 996–1001. 66, 68, 69

[108] Li, Z., Hovakimyan, N., Cao, C., and Kaasa, G.-O., 2009. "Integrated estimator and l1 adaptive controller for well drilling systems." In *American Control Conference (ACC),*, Proceedings of the American Control Conference, IEEE, pp. 1958–1963. 66, 68, 69

[109] Zhou, J., Stamnes, O. N., Aamo, O. M., and Kaasa, G.-O., 2009. "Pressure regulation with kick attenuation in a managed pressure drilling system." In *48th IEEE Conference on Decision and Control held jointly with 2009 28th Chinese Control Conference, CDC/CCC 2009*, Proceedings of the IEEE Conference on Decision and Control, Institute of Electrical and Electronics Engineers Inc., pp. 5586–5591. 66, 68, 70, 105

[110] Breyholtz, O., Nygaard, G., Godhavn, J.-M., and Vefring, E. H., 2009. "Evaluating control designs for co-ordinating pump rates and choke valve during managed pressure drilling operations." In *2009 IEEE International Conference on Control Applications, CCA '09*, Proceedings of the IEEE International Conference on Control Applications, Institute of Electrical and Electronics Engineers Inc., pp. 731–738. 66, 67, 68, 69

[111] Zhou, J., Nygaard, G., Godhavn, J.-M., Breyholtz, O., and Vefring, E. H., 2010. "Adaptive observer for kick detection and switched control for bottomhole pressure regulation and kick attenuation during managed pressure drilling." In *2010 American Control Conference, (ACC) 2010*, Proceedings of the 2010 American Control Conference, ACC 2010, IEEE, pp. 3765–3770. 66, 67, 69, 104, 105

[112] Zhou, L., and Nygaard, G., 2010. "Control and estimation of downhole pressure in managed pressure drilling operations." In *4th International Symposium on Communications, Control, and Signal Processing, ISCCSP-2010*, Final Program and Abstract Book - 4th International Symposium on Communications, Control, and Signal Processing, ISCCSP 2010, IEEE, pp. 1–6. 66, 67, 69, 70

[113] Nygaard, G. H., Imsland, L. S., and Johannessen, E. A., 2007. "Using nmpc based on a low-order model for controlling pressure during oil well drilling." In *8th International IFAC Symposium on Dynamics and Control of Process Systems*, pp. 6–8. 66, 67

[114] Carlsen, L. A., Nygaard, G., and Nikolaou, M., 2013. "Evaluation of control methods for drilling operations with unexpected gas influx." *Journal of Process Control,* **23**(3), pp. 306–316. 66, 70, 105

[115] Landet, I. S., Pavlov, A., Aamo, O. M., and Mahdianfar, H., 2012. "Control of heave-induced pressure fluctuations in managed pressure drilling." In *American Control Conference (ACC)*, Proceedings of the American Control Conference, Institute of Electrical and Electronics Engineers Inc., pp. 2270–2275. 66, 68

[116] Imsland, L., and Kaasa, G.-O., 2012. "Adaptive approximation-based estimation of downhole pressure in managed pressure drilling." In *2012 IEEE International Conference on Control Applications, CCA 2012*, Proceedings of the IEEE International Conference on Control Applications, Institute of Electrical and Electronics Engineers Inc., pp. 104–111. 68

[117] Stamnes, O. N., Aamo, O. M., and Kaasa, G.-O., 2011. "Adaptive redesign of nonlinear observers." *IEEE Transactions on Automatic Control,* **56**(5), May, pp. 1152–1157. 68

[118] Breyholtz, O., Nygaard, G., and Nikolaou, M., 2010. "Automatic control of managed pressure drilling." In *2010 American Control Conference, ACC 2010*, Proceedings of the 2010 American Control Conference, ACC 2010, IEEE Computer Society, pp. 442–447. 68, 70

[119] Veeningen, D., 2011. "Novel high speed telemetry system with measurements along the string mitigate drilling risk and improve drilling efficiency." In *Brazil Offshore Conference 2011*, Vol. 2 of *Society of Petroleum Engineers - Brazil Offshore Conference 2011*, Society of Petroleum Engineers, pp. 533–544. 69

[120] Vajargah, K., Miska, A., Yu, S. Z., Ozbayoglu, M., and Majidi, R., 2013. "Feasibility study of applying intelligent drill pipe in early detection of gas influx during conventional drilling." In *SPE/IADC Drilling Conference*, Society of Petroleum Engineers. 69

[121] Gravdal, F. E., Nikolaou, M., Breyholtz, Y., Carlsen, L. A., et al., 2009. "Improved kick management during mpd by real-time pore-pressure estimation." *SPE Drilling Completion,* **25**(4), October, pp. 577–584. 69

[122] Gravdal, J., Lorentzen, R., and Time, R., 2010. Wired drill pipe telemetry enables real-time evaluation of kick during managed pressure drilling. 69, 104

[123] Hargreaves, D., Jardine, S., and Jeffryes, B., 2001. "Early kick detection for deepwater drilling: New probabilistic methods applied in the field." In *Proceedings of the 2001 SPE Annual Technical Conference and Exhibition*, no. SPE-71369-MS in Proceedings - SPE Annual Technical Conference and Exhibition, Society of Petroleum Engineers (SPE), pp. 481–491. 69, 104

[124] Santos, H., Catak, E., Kinder, J., and Sonnemann, P., 2007. "Kick detection and control in oil-based mud: Real well-test results using microflux control equipment." In *SPE/IADC Drilling Conference and Exhibition 2007*, Vol. 1 of *SPE/IADC Drilling Conference, Proceedings*, Society of Petroleum Engineers (SPE), pp. 429–438. 69, 104

[125] Kamyab, M., Shadizadeh, S. R., Jazayeri-Rad, H., Dinarvand, N., et al., 2010. "Early kick detection using real time data analysis with dynamic neural network: A case study in iranian oil fields." In *2010 Nigeria Annual International Conference and Exhibition: Meeting the World's Energy Demand and Supply Mix: The Role of Africa, NAICE, July 31, 2010 - August 7, 2010*, Vol. 1 of *Society of Petroleum Engineers - Nigeria Annual International Conference and Exhibition 2010, NAICE*, Society of Petroleum Engineers, pp. 419–428. 69, 104

[126] Zhou, Q., Zhao, H., Zhan, H., Zhang, H., and Lu, C., 2013. "The application of ultrasonic based on doppler effect used in early kick detection for deep water drilling." In *2013 International Conference on Communications, Circuits and Systems, ICCCAS 2013*, Vol. 2 of *2013 International Conference on Communications, Circuits and Systems, ICCCAS 2013*, IEEE Computer Society, pp. 488–491. 69, 104

[127] Gravdal, A. E., Lorentzen, R. J., Time, R. W., et al., 2010. "Wired drill pipe telemetry enables real-time evaluation of kick during managed pressure drilling." In *SPE Asia Pacific Oil and Gas Conference and Exhibition 2010, APOGCE 2010*, Vol. 1 of *Society of Petroleum Engineers - SPE Asia Pacific Oil and Gas Conference and Exhibition 2010, APOGCE 2010*, Society of Petroleum Engineers, pp. 582–601. 70

[128] Bourgoyne, A. J., and Young, F., 1974. "A multiple regression approach to optimal drilling and abnormal pressure detection." *Society of Petroleum Engineers Journal,* **14**(SPE-4238-PA), August. viii, 70, 74

[129] Eren, T., 2010. "Real-time-optimization of drilling parameters during drilling operations." Thesis, Middle east technical university. 71, 73, 110

[130] Eren, T., and Ozbayoglu, M. E., 2010. Real time optimization of drilling parameters during drilling operations, January. 71, 107

[131] Jr., B. A., K.K., M., M.E., C., and F.S., Y., 1986. *Applied Drilling Engineering*., Vol. 1 Society of Petroleum Engineering of AIME [ie Society of Petroleum Engineers of AIME], Richardson, TX. 71

[132] Irawan, S., Abd Rahman, A. M., and Tunio, S. Q., 2012. "Optimization of weight on bit during drilling operation based on rate of penetration model." *Research Journal of Applied Sciences, Engineering and Technology,* **4**(12), pp. 1690–1695. 71, 111

[133] Arabjamaloei, R., and Karimi Dehkordi, B., 2012. "Investigation of the most efficient approach of the prediction of the rate of penetration." *Energy Sources, Part A: Recovery, Utilization and Environmental Effects,* **34**(7), February, pp. 581–590. 71, 107, 120

[134] Escudier, M. P., Oliveira, P. J., and Pinho, F. T., 2002. "Fully developed laminar flow of purely viscous non-newtonian liquids through annuli, including the effects of eccentricity and inner-cylinder rotation." *International Journal of Heat and Fluid Flow,* **23**(1), pp. 52–73. 75, 111

[135] Ahmed, R., Enfis, M., Miftah-El-Kheir, H., Laget, M., and Saasen, A., 2010. "The effect of drillstring rotation on equivalent circulation density: Modeling and analysis of field measurements." In *SPE Annual Technical Conference and Exhibition 2010, ATCE 2010*, Vol. 7

of *Proceedings - SPE Annual Technical Conference and Exhibition*, Society of Petroleum Engineers (SPE), pp. 5375–5385. 75, 111

[136] Sorgun, M., and Ozbayoglu, M. E., 2011. "Predicting frictional pressure loss during horizontal drilling for non-newtonian fluids." *Energy Sources, Part A: Recovery, Utilization and Environmental Effects,* **33**(7), pp. 631–640. 75, 111

[137] Saasen, A., 2014. "Annular frictional pressure losses during drilling-predicting the effect of drillstring rotation." *Journal of Energy Resources Technology, Transactions of the ASME,* **136**(3), March. 75, 111

[138] Olatunbosun Anifowoshe, S., 2012. "The effect of equivalent diameter definitions on frictional pressure loss estimation in an annulus with pipe rotation." In *SPE Deepwater and Completions Conference and Exhibition*, T. Galveston, ed., Society of Petroleum Engineers, Society of Petroleum Engineers. 75, 111, 112

[139] Ozbayoglu, E. M., and Sorgun, M., 2010. "Frictional pressure loss estimation of non-newtonian fluids in realistic annulus with pipe rotation." *Journal of Canadian Petroleum Technology,* **49**(12), pp. 57–64. 75, 112

[140] Johannessen, M. K., and Myrvold, T., 2010. "Stick-slip prevention of drill strings using nonlinear model reduction and nonlinear model predictive control.". 75, 116

[141] Hareland, G., Fazaelizadeh, M., and Wu, Z., 2012. Autodriller system. 76

[142] Sun, L., Castagno, J., Hedengren, J. D., and Beard, R. W. "Real-time parameter estimation for towed cable systems using moving horizon estimation." *EEE Transactions on Aerospace and Electronic Systems, in review, 2014*. 77, 81

[143] Asgharzadeh Shishavan, R., Hubbell, C., Perez, H., Hedengren, J., Pixton, D. S., Pink, A. P., et al. "Multivariate control for managed pressure drilling systems using high speed telemetry." *Submitted to SPE Journal*. 103

[144] Veeningen, D. M., 2011. "Along-string pressure evaluation enabled by broadband networked drillstring provide safety efficiency gains." *OTC Brasil*(OTC-22239-MS). 104, 123

[145] Veeningen, D. M., Pink, A. P., McRay, M., and Luthi, M., 2014. "Field premiere of along-string dynamic measurements for automated drilling optimization using downhole information." In *SPE Annual Technical Conference and Exhibition*, Society of Petroleum Engineers, Society of Petroleum Engineers. 104

[146] Craig, A. D., Teelken, R., Lindgrin, M., Stene, S. A., and Hayden, P., 2014. "Application of wired drillpipe technology used to increase drilling efficiency on north sea project." In *SPE Annual Technical Conference and Exhibition*, Society of Petroleum Engineers. 104

[147] Asgharzadeh Shishavan, R., Hubbell, C., Perez, H., Hedengren, J., and Pixton, D. S., 2014. "Combined rate of penetration and pressure regulation for drilling optimization using high speed telemetry." In *SPE Deepwater Drilling and Completions Conference*, Society of Petroleum Engineers. 105

[148] Hedengren, J., Asgharzadeh Shishavan, R., Powell, K. M., and Edgar, T., 2014. "Nonlinear modeling, estimation and predictive control in APMonitor." *Computers & Chemical Engineering,* **In Press, Accepted Manuscript**. 107

[149] Beard, R. W., and McLain, T. W., 2011. *Small Unmanned Aircraft ,Theory and Practice*. Princeton University Press, Princeton and Oxford. 115